Microengineered Responsive Platforms for Spatial and Geometrical Control of Multicellular Organizations

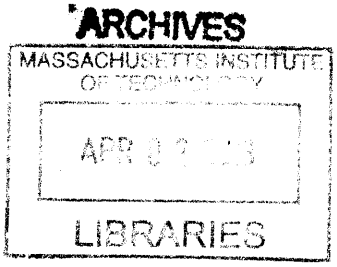

by

Halil Tekin

B.S. Control Engineering
Faculty of Electrical and Electronics Engineering
Istanbul Technical University (2005)

M.S. Control Engineering
Faculty of Electrical and Electronics Engineering
Istanbul Technical University (2007)

SUBMITTED TO THE DEPARTMENT OF ELECTRICAL ENGINEERING AND COMPUTER SCIENCE IN PARTIAL FULLFILLMENT OF THE REQUIREMENTS FOR THE DEGREE OF

DOCTOR OF PHILOSOPHY IN ELECTRICAL ENGINEERING AND COMPUTER SCIENCE

AT THE

MASSACHUSETTS INSTITUTE OF TECHNOLOGY

February 2013

Signature of Author.....
Department of Electrical Engineering and Computer Science
November 30, 2012

Certified by.....
Ali Khademhosseini
Associate Professor of Harvard-MIT Health Sciences and Technology
Harvard Medical School
Thesis Supervisor

Certified by.....
Robert Langer
Institute Professor
Massachusetts Institute of Technology
Thesis Supervisor

Accepted by.....
Leslie A. Kolodziejski
Chair, Department Committee on Graduate Students

Microengineered Responsive Platforms for Spatial and Geometrical Control of Multicellular Organizations

by

Halil Tekin

Submitted to the Department of Electrical Engineering and Computer Science on November 30, 2012 in Partial Fulfillment of the Requirements for the Degree of Doctor of Philosophy in Electrical Engineering and Computer Science

Abstract

Living systems are composed of complex multicellular organizations containing various cell types spatially distributed in defined microenvironments. The intricate cell-cell and cell-matrix interactions in these microenvironments regulate the cell fate, differentiation of the cells, and functions of the associated tissues. Recreating these complex associations *in vitro* can be highly useful for fabricating biomimetic tissues for regenerative medicine, disease models for drug discovery, and models to study embryogenesis. This thesis focused on developing microscale responsive platforms for spatial and geometrical control of multicellular organizations. The first part of the thesis describes methods to fabricate spherical and stripe microtissues of single cell types and their temperature-controlled retrieval. These microtissues were scaffold-free and can potentially produce homotypic cell-cell interactions. Microwells fabricated from poly(N-isopropylacrylamide) (PNIPAAm) responded to temperature by changing their shapes. Spherical microtissues of a single cell type were formed in responsive microwells and recovered by using shape changing properties of microwells. Elastomeric microgrooves were conformally coated with PNIPAAm to first generate stripe microtissues of a single cell type, and then harvest them by exploiting the temperature-dependent hydrophilicity and swelling change of PNIPAAm film. The second part of the thesis introduces techniques to control spatial and geometrical distribution of multiple cell types in scaffold-free and scaffold-based tissues. Shape changing properties of dynamic microwells facilitated the sequential patterning of multicompartment hydrogels. Different cell types were spatially arranged in different compartments of microgels which may lead to complex cell-matrix interactions replicating native tissues. Shape changing properties of dynamic microwells were also employed to seed different cell types at different temperatures within defined geometries to control spatial and geometrical organization of multiple cell types. Resulting scaffold-free tissues can potentially produce homotypic and heterotypic cell-cell interactions. Dynamic microstructures with different geometries could be used to recapitulate complex native tissues with controlled cell-cell and cell-matrix interactions. The techniques presented in this thesis are versatile and may potentially be useful for replicating biological complexities for a wide range of applications in tissue engineering, regenerative medicine, drug discovery, developmental biology, and cancer biology.

Thesis Supervisor: Ali Khademhosseini
Title: Associate Professor of Harvard-MIT Health Sciences and Technology and Harvard Medical School

Thesis Supervisor: Robert Langer
Title: Institute Professor of MIT

Acknowledgments

I would like to thank my supervisors Prof. Ali Khademhosseini and Prof. Robert Langer for their endless support and being great source of motivation and inspiration during my graduate studies. Although I haven't had any previous bio-lab experience, they have been very nice to get me into their labs and been very supportive throughout my doctorate. Their constant support to pursue my own ideas truly helped me to get a fantastic experience at the interface of engineering and biology and become a productive researcher with full of ideas. I'm also thankful to all members of Khademhosseini Lab and Langer Lab. I would like to acknowledge that my work was funded by the Institute for Soldier Nanotechnologies at MIT, the Draper Laboratory, the NIH, and MIT-Portugal Program.

I would also like to thank my thesis committee members Prof. Denny Freeman and Prof. M. Fatih Yanik for their guidance, motivation, and help during my doctoral studies. Their assessment of my work and mentorship helped me to complete my thesis.

I wouldn't be able to finish my studies without fantastic MIT undergraduates who worked with me. I'm truly thankful to Tonia Tsinman, Jeff Sanchez, Michael Anaya, Brianna Jones, Claire Nauman, Christian Landeros, and Karen Dubbin for their contributions to my studies. It has been a privilege working with them. Our studies together were inspired by MIT's motto "Mind and Hand".

I would like to particularly thank Prof. Terry Orlando and Janet Fischer at graduate office of EECS for their help and guidance throughout my graduate studies. I'm also grateful to my graduate counselor Prof. Roger Mark for his guidance in my graduate education.

In addition to academic side, I have had great friends at MIT who have been very helpful and supportive. I have gone through several problems in last five years. I wouldn't be able to achieve my goals without overcoming these problems which have been possible with the help of my friends. I'm grateful to Sefa Demirtas, Fatih Degirmenci, Mark Brigham, Kemal Celebi, Umit Demirbas, Selman Sakar, Burak Eskici, Osman Ahsen, Burak Dura, and Zekeriyya Gemici.

I would also like to thank professors at Istanbul Technical University for their help and guidance during my undergraduate and master studies. I'm also thankful to my friends in Turkey.

My studies and educational journey wouldn't have been possible without the constant love and support of my family. I'm very lucky and thankful to have them. My early childhood was at a village and the rest of my young ages were at a town where I attended schools before college. I haven't had so many resources as others, but I have had my family and their love which truly inspired me to achieve my goals. I dedicate this thesis to all members of my family, my dad Serafettin Tekin, my brother Fatih Tekin, my grandmother Umahan Tekin, and of course particularly to my mom Saniye Tekin, who passed away in 2004.

I hope that merging engineering principles with biology could lead us to solve all health problems on the world in the future.

Table of Contents

List of Figures

Chapter 1: Introduction and Background

1.1 Motivation

Human health care is of fundamental importance for research in life sciences. Development of drugs, therapeutics, diagnostic techniques, and new cures significantly affect people's lives and regulate industrial improvement. The success in most of the life sciences applications greatly depends on developing methods to accurately replicate physiology of human body in outside environment. Engineering principles are needed to develop required methods for recapitulating the physiological systems.

One of the fields which greatly employs engineering techniques is tissue engineering which holds a great promise for developing methods to create tissue models with the structural organization of native tissues, which could be useful for regenerative medicine and pharmaceutical research. Tissue engineering employs wide range of disciplines, such as materials science, biology, chemistry, and engineering, to fabricate physiologically relevant tissues for regenerative therapeutics and other research purposes, such as drug discovery and cancer biology. Accurate production of biomimetic tissue constructs can not only replace diseased tissues and organs but also can improve pharmaceutical industry by reducing the cost and time needed for drug discovery.

Various human diseases need to be recreated *in vitro* environment to find out the underlying pathways in disease progress and to develop new cures. One of these diseases is cancer which has its unique microenvironment depending on the organ it started. There is still so much unknown about cancer which is partially because of the lack of appropriate tumor models to study the underlying reasons in tumor formation, cancer soluble factors and to investigate disease states, such as metastasis and invasion. Most of the tumor models are produced in animal models, which take large amount of time slowing down the drug discovery process and require considerable amount of investment. These animal models also do not really mimic the tumors in human body. Thus, developing new treatment options in a fast and cost effective manner depends on accurately replicating tumor microenvironments *in vitro*.

Engineering techniques are also required to recapitulate the embryonic development *in vitro* which can be used to understand developmental stages of human embryo and control the

differentiation of embryonic stem cells. These abilities can be used to fabricate patient specific tissue constructs differentiated from adult stem cells, embryonic stem cells, and induced pluripotent stem cells. However, the current methods can not accurately replicate the native microenvironment of the embryo which changes in a dynamic manner throughout the stages of development. Mimicking these microenvironments can lead to a better understanding of developmental biology and new applications in regenerative medicine directly using stem cells.

Various microengineered platforms such as microfluidics[1-3] and microchannels/wells[4-6] have been employed to recapitulate the native tissue architectures. Microfabrication methods, such as soft lithography[7, 8] and photolithography,[9, 10] have also been used to fabricate physiologically relevant tissues. However, each of these techniques has limitations. There is still a need for dynamic microstructures which can change their configuration and surface properties for different applications. Dynamic microstructures could better recapitulate the native human tissues *in vitro* which could enable various applications in life sciences.

This chapter first gives an overview about the importance of geometry and spatial distribution of cells in multicellular organizations while the second part discusses the cell-cell and cell-matrix interactions. The third part reviews previously developed techniques to fabricate cell constructs and the fourth part describes the thermoresponsive platforms for cell culture applications. Finally, this chapter ends by giving the scope of the thesis.

1.2 Importance of geometry and spatial distribution of cells in multicellular systems

From early developmental stages of human embryo to functional organs, it can be observed that the various cells are spatially distributed in defined microenvironments. These distributions regulate the specific tasks of the multicellular community. These tasks could be either the differentiation of cells into different forms or the synthesis of proteins and secretions of the tissues. This part highlights the importance of tissue geometry and spatial distribution of cells for different multicellular communities, such as embryo, cardiac and liver tissues, and tumor tissues.

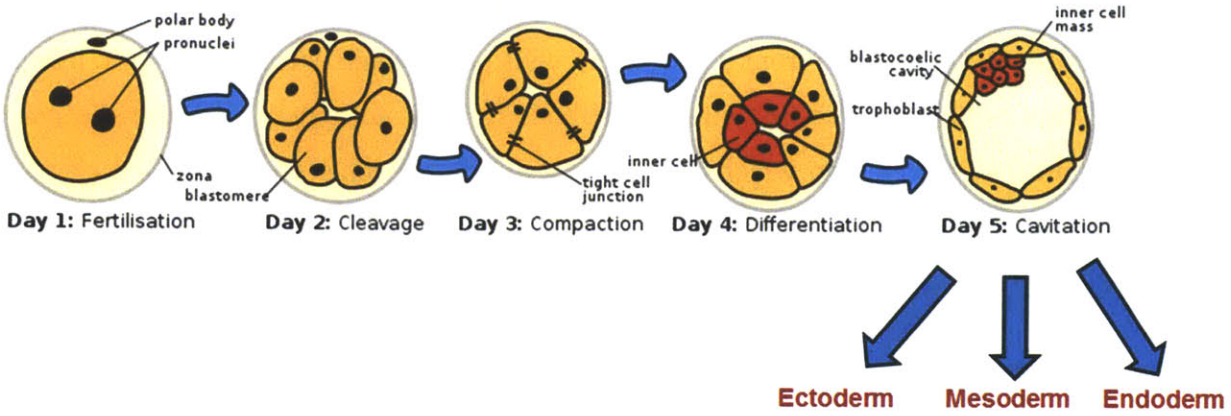

Figure 1.1. Schematic of early stages of human embryonic development.[11] Following the fertilization, zygote splits into multiple cell types which are totipotent. These cells form tight cell-cell junctions. The intricate interactions between cells and the geometry of surrounding microenvironment regulate the differentiation of cells. The embryo locates in one side of the extraembryonic tissue. The interplay between cells in the embryo and the microenvironmental cues control the formation of three germ layers, ectoderm, mesoderm, and endoderm. The picture used here is adapted under the Creative Commons Attribution-Share Alike 3.0 Unported license.[12]

After fertilization, zygote which is totipotent divides into multiple cells in a sphere shape (**Figure 1.1**).[13] Distribution of these cells in this geometry and their interactions each other form different cell types. At blastocyst stage, the inner cell mass, also called embryo, locates in one side of the extraembryonic tissue.[13] Cells in the embryo are pluripotent and form three germ layers, endoderm, mesoderm, and ectoderm. The shape of the embryo and the shape of the extraembryonic tissue change overtime, regulating the distribution of various cell types and their interactions.[13] These associations direct cells to differentiate into different phenotypes throughout development. Controlling the dynamic geometry of embryogenesis and the arrangements of various cell types can enable us to first understand the developmental stages and control the differentiation of embryonic stem cells into particular cell types.

All tissues in human body have their own multicellular complexities. For example, liver can be considered as made of repeating units of lobule which is a well-defined microarchitecture of various spatially distributed cell types.[14-16] Hepatocytes are in contact and located in hepatic units

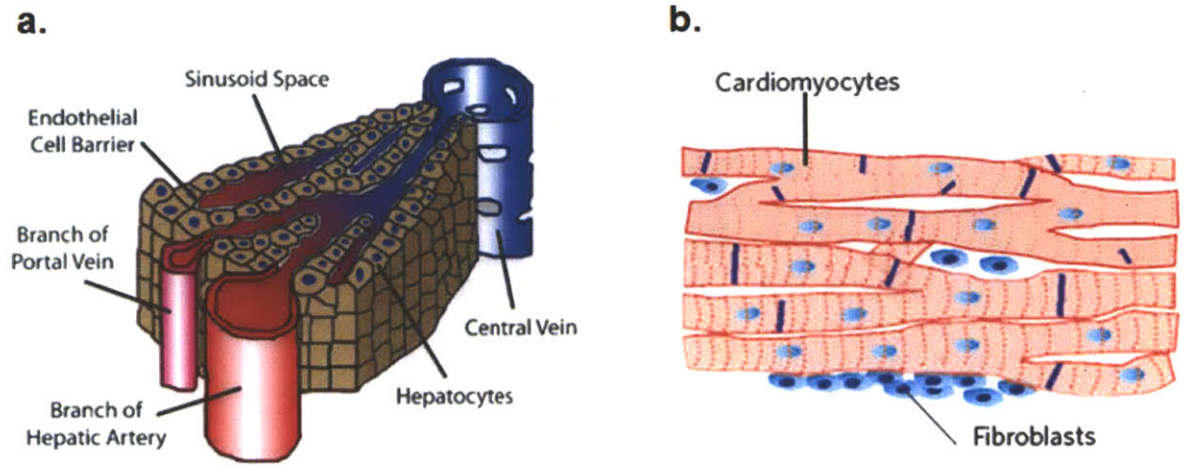

Figure 1.2. Schematics of microenvironments of liver tissue and cardiac tissue. a) Microenvironment of liver tissue. Blood is supplied to sinusoids from portal vein and hepatic arteries. It leaves the sinusoids via central vein. Hepatocytes are in contact with tight junction producing homotypic cell-cell interactions. There is an endothelial cell barrier between sinusoid space and hepatocytes. Used with kind permission from P. J. Lee et al. An artificial liver sinusoid with a microfluidic endothelial-like barrier for primary hepatocyte culture. Biotechnology and Bioengineering 97 (5): 1340-6 (2007). Copyright (2007) Wiley. Adapted with permission from Wiley. b) Microenvironment of cardiac tissue. Cardiomyocytes are elongated and aligned. Blood vessels are interwoven cardiac fibers. Tight Junctions between cardiomyocytes and interactions between cardiomyocytes and fibroblasts regulate electrical and contractile properties of cardiac tissues. Used with kind permission from T. Dvir et al. Nanotechnological strategies for engineering complex tissues. Nature Nanotechnology 6 (1): 13-22 (2011). Adapted by permission from Macmillan Publishers Ltd., copyright (2011).

of the lobule (**Figure 1.2a**). Blood is supplied to the lobules through sinusoids. Sinusoidal endothelial cells are aligned on the walls of the sinusoid. There is a space between hepatocytes and endothelial cells where there is extracellular matrix (ECM).[17] Thus, liver is made of structurally well-organized complex architecture of various cell types. The intricate interactions between various spatially organized cell types in a three-dimensional (3D) liver tissue regulate liver-specific functions like albumin production, urea synthesis, and metabolism.[14, 15] The multicellular complexity can also be found in cardiac microenvironment. Cardiac tissue contains various cell types, such as cardiomyocytes, fibroblasts, and endothelial cells which are

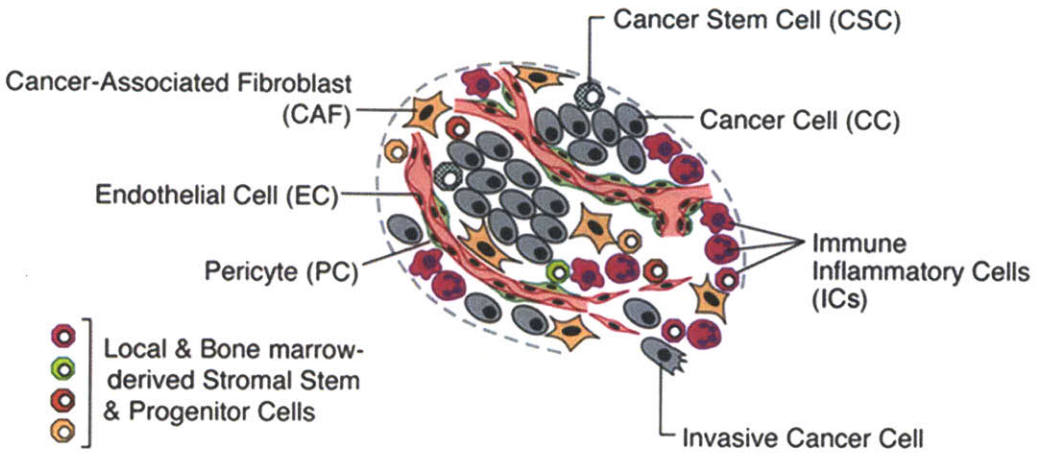

Figure 1.3. Schematic of the tumor microenvironment. Various cell types are spatially distributed in a defined microenvironment. The complex interactions between these cell types and the cell-ECM interactions regulate the tumor growth, metastasis, and angiogenesis. Used with kind permission from D. Hanahan et al. Hallmarks of cancer: the next generation. Cell 144 (5): 646-74 (2011). Copyright (2011). Adapted with permission from Elsevier.

distributed in a spatially organized manner and alignment (**Figure 1.2b**).[16, 18] Cardiomyocytes are elongated in one direction trapped in collagen fibers.[16] Blood vessels interweave these muscle fibers.[16] Spatial organization of multiple cell types in a 3D matrix and their interplay with each other regulate the propagation of electrical signals through the muscle tissue and the contractile properties of the heart. Recreating these complexities in vitro requires particular engineering methodologies which can lead to functional biomimetic tissues. The complexity in multicellular organizations can also be exemplified by the tumor microenvironment which contains many different cell types, such as cancer cells, fibroblasts, cancer stem cells, endothelial cells, as well as immune inflammatory cells (**Figure 1.3**).[19] These various cell types are spatially distributed in a 3D geometry which controls their interactions with neighboring cells and the ECM. These associations regulate the synthesis of cancer related soluble factors and the different states of the cancer, such as angiogenesis, metastasis, and invasion.[19] Tumor models mimicking the native tumor microenvironment can be used to study disease progress and test drug candidates in a high-throughput manner. To recapitulate such diseases *in vitro*, new engineered tools need to be employed.

1.3 Cell-cell and cell-matrix interactions

In addition to the spatial distribution of multiple cells in a 3D matrix, their interactions with each other and with the surrounding ECM are of importance in regulating the differentiation, migration, fate of the cells and the functions of tissues and organs. For example, in liver, homotypic (between hepatocyte and hepatocyte) and heterotypic (between hepatocyte and non-parenchymal) cell-cell interactions control the secretion of liver associated proteins and the phenotype of the hepatocytes. Heterotypic interactions maintain the long term hepatocyte vitality and improve their functionality, such as albumin secretion and urea production.[15] This also depends on the population of hepatocytes and non-parenchymal cells, such as fibroblasts and endothelial cells, and their distribution in a defined microenvironment. Homotypic interactions can also improve the functionality of the hepatocytes and induce the generation of bile canaliculi and cell-cell junctions.[15, 20] In addition to cell-cell interactions, cell-matrix interactions regulate the functionality of the liver tissue.[21] Some ECM molecules, such as laminin, fibronectin, and collagens I, II, III, IV, V, VI, are present in the liver microenvironment.[17] Some cellular processes, such as cell signaling and gene expression, depend on the interactions between ECM and integrins of the cells.[22] Cell-ECM interactions are also important in development and regeneration of the liver and regulating its functions.

Cell-cell and cell-ECM interactions are also key modulators of functions of the heart. Due to the main purpose of the heart as a pump, its structure is made of highly elastic and mechanically stiff collagen-based ECM.[18] Its mechanical properties through cell-ECM interactions support its electrical and contractile properties.[18] Tight junctions between cardiomyocytes and cardiomyocytes-fibroblasts help the propagation of electrical signals between cells which all control the contractile properties of cardiac tissue.[18] Continuous electrical excitation and mechanical stretch affect the cellular processes of various cell types and their interactions with each other in cardiac microenvironment. Given these, different organs have different structural and functional complexities which all depend on cell-cell and cell-ECM interactions in a 3D microenvironment.

Cell-cell and cell-ECM interactions also play an important role in development. After the fertilization, zygote divides into numerous new cells which form tight cell junctions.[13] The interplay between these cells form differentiated cell types forming the inner cell mass. Starting

in early developmental stages, cells interact with the surrounding microenvironment through cell-ECM interactions and with the neighboring cells through cell-cell interactions both of which affect cell-signaling pathways.[13, 23] These associations regulate the differentiation of the pluripotent cells in embryo into new phenotypes and the formation of three germ layers, which are endoderm, mesoderm, and ectoderm. The interplay between mesenchymal (derived from mesoderm) and epithelial (derived from endoderm) layers manages the differentiation of the cells, the tissue morphogenesis, and the development of organ specific functions.[23] The microenvironment not only affects the development and tissue morphogenesis but also is influenced by the consequences of these developmental stages.[23] Growth factors, hormones, and cytokines also play important roles in development and differentiation.[23] Embryonic development is a structurally and functionally complex process. Controlling the cell-cell and cell-ECM interactions in biomimetic microenvironments could bring new developmental models and be used to form specific tissues.

Tumor microenvironment is highly controlled by complex interactions between various cell types and their interactions with surrounding ECM. There are a number of cell types in tumor microenvironment, such as the cancer cells, fibroblasts, cancer stem cells, endothelial cells, immune inflammatory cells, and stromal cells, all of which generate homotypic and heterotypic cell-cell interactions resulting in regulation of complex cell-signaling circuitry in tumor microenvironment and stages of cancer.[19] Cancer cells and cancer stem cells are origins of tumor existence which carry cancer related genes. These cells can induce tumors in their associated tissues and support its progression.[19] Stromal cells can enhance tumor invasion in healthy tissue and its further progress towards metastasis.[19] Macrophages can contribute to that invasion by providing some proteases.[19] Another contribution to the cellular heterogeneity in tumor microenvironment comes from endothelial cells which form tumor vasculature through angiogenesis.[19] Pericytes support endothelial cells in tumor microenvironment. Immune inflammatory cells are also present in tumor microenvironment which can act either as tumor-promoters or tumor-suppressors.[19] There are also cancer associated fibroblasts which have two types; one type is mostly like normal fibroblasts which structurally contribute to the epithelial tissues, and the other type is myofibroblast which can support angiogenesis, tumor growth, invasion, and metastasis.[19] The interactions in tumor microenvironment resulting from various cell types and their surrounding ECM are complex. For example, ECM can induce differentiation

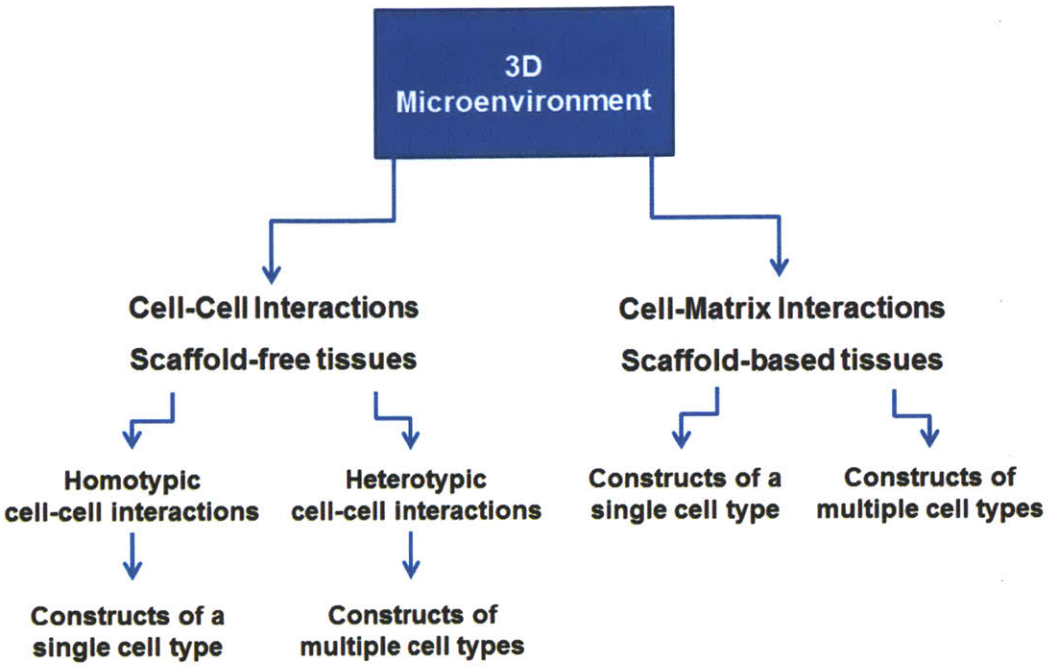

Figure 1.4. Schematic of classification of replicating 3D microenvironment of native tissues in scaffold-based and scaffold-free tissues. Scaffold-free tissues can be formed to generate homotypic and heterotypic cell-cell interactions. Scaffold-based tissues generate cell-matrix interactions.

and proliferation of cancer cells and cancer-associated fibroblasts by supporting them with a cytokine, the transforming growth factor beta (TGF-β), which can promote tumor growth.[19] These associations can also initiate angiogenesis through vascular endothelial growth factor (VEGF) which can be provided by ECM and tumor-promoting inflammatory cells.[19] ECM can be affected by proteases resulting from its interactions with cancer cells and tumor-promoting inflammatory cells.[19] There are still unknowns about the exact underlying signaling circuits which are due to the lack of right tumor models to study. New engineering tools could resolve this problem by replicating the tumor tissues in vitro in a 3D microenvironment.

1.4 Previous attempts to replicate native multicellular organizations

Various engineering methods have been previously employed to fabricate biomimetic tissues. As native tissue microenvironment is 3D, the targeted tissue structures are 3D in vitro which can

better replicate native ones. Because two dimensional tissue constructs lack of physiological relevance and they cannot satisfy the needs in regenerative medicine and drug discovery. Furthermore, 3D microenvironments *in vitro* can better recapitulate in vivo organizations of embryonic development and the tumor vasculature. The 3D microenvironment can be captured in a scaffold with cells or just cells without scaffold (**Figure 1.4**). Scaffold-free tissues can promote homotypic and heterotypic cell-cell interactions, and cells can produce their own ECM. Scaffold-based tissue constructs are fabricated by encapsulating cells within either natural polymers or synthetic materials which result in cell-ECM interactions. This part will first review the previous methods to fabricate constructs of a single cell type, and then will describe the techniques to generate constructs of multiple cell types.

1.4.1 Constructs of a single cell type

Depending on the applications, constructs of a single cell type can be fabricated either with or without scaffold. Scaffold-free tissues are generated by using microfabricated templates made of hydrogels[4] or elastic polymers.[5, 6] These templates can be fabricated in different shapes. Circular and square microwells can be used to form 3D spherical and cubic microtissues. Cells are first seeded on these platforms, and then they produce their own natural ECM over time. If these cells are the same type, their interactions will be homotypic. For example, microwells have been employed to fabricate embryonic bodies to control stem cell differentiation based on the size of 3D spheroid tissues and cell-cell interactions in a defined microenvironment.[4] At initial stage the interactions between embryonic stem cells in microwells are homotypic, but cells differentiate overtime and their interactions become heterotypic. Spheroid tissues made of different cell types, such as hepatocytes and mesenchymal cells, could also be useful for applications in tissue engineering and regenerative medicine. Also, microtextured substrates have been used to generate stripe tissues[5] which can mimic the native muscle and cardiac tissues. Similar to microwells, the interplay between cells in microgrooves is homotypic and cells form the natural ECM. Microfluidic methods have also been utilized to pattern single type cells to form microtissues.[1, 2] Most of these microfabricated templates can be coated with functional polymers which can initiate the retrieval of tissues from the substrates which will be reviewed further in this chapter.

Natural or synthetic polymers can be used to encapsulate cells of a single type. These polymers can give mechanical strength and elasticity to the tissues which could mimic the native ones in a better way. Microscale polymers can be fabricated by using micromolding,[7, 8] photolithographic,[9] and microfluidic techniques[24] in different patterned shapes, such as cubic, cylindrical, and striped. Physically crosslinkable or photocrosslinkable materials are first seeded with cells then can be shaped by using a micromolding technique. Micromolds can be made of synthetic or natural polymers which preferably should not interact with the cell encapsulating material. Photolithography is only applicable to photocrosslinkable materials. For this purpose, a photomask is required. By using these techniques, cell encapsulating polymers can be fabricated with various shapes, such as cylindrical, cubic, and striped.

1.4.2 Constructs of multiple cell types

As native tissues have multicellular complexity, different applications in life sciences may require 3D arrangements of multiple cell types. These arrangements can be generated in a scaffold or without a scaffold. Scaffold-free tissues produce homotypic interactions between same cell types which can be parenchymal to parenchymal and non-parenchymal to non-parenchymal and heterotypic interactions between different cell types which can be parenchymal to non-parenchymal. These associations can enhance the organotypic functions of tissue constructs made of multiple cell types and can better mimic the embryonic development and tumor microenvironment. However, it is challenging to fabricate tissue constructs containing multiple spatially organized cell types. Because the conventional microfabricated templates are static inhibiting the subsequent patterning of more cell types after the initially seeded one. Microfluidic platforms have been used to fabricate multi-layered cell patterns, but the device fabrication and cell patterning process are cumbersome which prevent high-throughput production.[3, 25] Stencils have also been employed to generate these patterns.[26] One stencil is used to pattern the first cell type and another stencil needs to be aligned on the first pattern to pattern the second cell type, which is tedious. It is also challenging to align the stencils and generate different shapes. Micromechanical substrates have been used to form patterns containing two different cell types, requiring the manipulation of substrates at each step as well.[27] Similar to stencils, it remains a challenge to generate various patterned shapes by using this method. In another study, cell membranes have been engineered to promote the attachment to the other cells which can be used to assemble cell constructs.[28] However, the method is quite tedious and hard

to form different patterns both of which limit the high-throughput production. Thus, there is still a need for a straightforward and versatile method to generate tissue constructs of spatially organized multiple cell types.

To replicate the mechanical stiffness of natural tissues and the interactions of different cell types with ECM, multiple cell types can be sequentially encapsulated into photocrosslinkable materials by using photolithography.[10] Multiple cell types can be spatially arranged into microscale hydrogels having various shapes like cylindrical, cubic, and striped by using this method. Mechanical stiffness and elasticity of native tissues can be mimicked by changing the prepolymer concentrations and crosslinking conditions. However, this technique is not applicable to non-photocrosslinkable synthetic or natural polymers. Conventional micromolds are also static limiting the sequential patterning of biomaterials. The lack of a desired method limits the use of various materials in recapitulating native tissues for a wide range of applications in tissue engineering, regenerative medicine, and drug discovery.

1.5 Thermoresponsive platforms for cell culture applications

Native tissues contain different cell types, with each cell type having its own unique 3D ECM environment, and mechanical properties. To recreate such complexity in engineered tissues various approaches have been used. Each of the previously developed techniques has their own limitations. For example, photolithography is only applicable to photocrosslinkable materials,[29] whereas most soft lithographic methods rely on static microstructures, that limit the range of microgel shapes that can be fabricated.[29] Also, the pattern geometries and surface properties of static microstructures cannot be changed. These static features may be limited in creating biomimetic micro-tissues and the retrieval of tissues from these platforms in a controlled manner.

Dynamic microstructures with controllable features and switchable surface properties are emerging as useful tools for creating biomimetic and retrievable modular tissues. Poly(N-isopropylacrylamide) (PNIPAAm) is a well-known stimuli-responsive polymer, which responds to temperature by changing its hydrophilicity and swelling.[30-32] Properties of PNIPAAm make it favorable to fabricate dynamic platforms to overcome the static features of previous technologies. This part of the chapter will review the current developments in PNIPAAm-based thermoresponsive platforms for cell culture applications. The content of the part 1.5 has been published in the following journal article: H. Tekin, J.G. Sanchez, T. Tsinman, R. Langer, A.

Khademhosseini. Thermoresponsive platforms for tissue engineering and regenerative medicine. *AIChE Journal*, 2011, 57 (12): 3249–3258.

1.5.1 Characteristics of PNIPAAm and its derivatives

Stimuli-responsive polymers show great potential in several fields, including tissue engineering and drug delivery, due to their controllable hydrogel properties, such as swelling/deswelling and surface energy. PNIPAAm is one such polymer with a lower critical solution temperature (LCST) of ~32 °C.[30, 31] It shrinks and becomes hydrophobic at temperatures above its LCST, and turns into swollen and hydrophilic state below its LCST.[30] The entropic gain of the system produces this responsive behavior by segregating water molecules from isopropyl chains at temperatures above the phase temperature (LCST).[30] The entropic gain of the system in aqueous environment is higher than the enthalpic gain of the bonds between water molecules and PNIPAAm chains at this phase transition.[30]

The LCST of PNIPAAm can be tailored by incorporating hydrophilic or hydrophobic co-monomers into the polymer structure.[30] For example, phase temperature can be adjusted to around physiological temperature (37 °C) to tailor its use for biological applications.[30] To alter the LCST of PNIPAAm, hydrophilic co-monomers, such as Acrylamide (AAm), N-methyl-N-vinylacetamide (MVA), N-vinylacetamide (NVA), and N-vinyl-2-pyrrolidinone (VPL), have been crosslinked with N-isopropylacrylamide (NIPAAm) via free radical polymerization.[33] At lower concentrations of these co-monomers, LCST point has been adjusted to between 32 °C and 37 °C.[33] Incorporation of slight amounts of ionic co-monomers in PNIPAAm hydrogels can raise the LCST.[34, 35] Copolymers of PNIPAAm with two distinct LCSTs can be fabricated by using oligomers, such as carboxy-terminated oligo NIPAAm, oligo(N-vinylcaprolactam) (VCL) and a random co-oligomer of NIPAAm and AAm.[36] These modifications on PNIPAAm hydrogels can be useful for controlled release applications in drug delivery and tissue engineering.

PNIPAAm-based hydrogels can be utilized for temperature-controlled drug delivery, in two ways. In the first approach, drugs can be released from the hydrogel structure as a result of PNIPAAm shrinking at temperatures above LCST.[37] In the second approach, drugs can be dissociated from swollen polymer network by decreasing the temperature below LCST.[37] Incorporation of hydrophilic co-monomers within PNIPAAm structure could speed up the deswelling kinetics of the hydrogels.[38] Acrylic acid (AAc) or methacrylic acid (MAAc) can be

crosslinked with NIPAAm to generate hydrogels with rapid thermoresponsiveness.[38] Faster release kinetics can also be achieved by synthesizing a comb-type PNIPAAm hydrogel network, which has been demonstrated to have faster deswelling kinetics than linear type PNIPAAm hydrogel networks.[39, 40]

Additional functionalities, such as pH responsiveness and partial degradability, can be given to PNIPAAm hydrogels by incorporating co-monomers and proteins into the polymer network. For example, temperature and pH responsive hydrogels were generated by copolymerizing NIPAAm with AAc.[41] Crosslinked and random copolymers of NIPAAm and MAAc also showcase the temperature and pH responsiveness.[42, 43] Graft copolymers of these configurations demonstrate higher temperature- and pH-dependent swelling kinetics than random copolymers.[32, 41] Furthermore, biodegradable materials, such as zein protein[44] and alginate[45], were incorporated within PNIPAAm networks while maintaining thermoresponsiveness. In addition, gelatin was used to generate interpenetrating networks with PNIPAAm without chemical crosslinking.[46]

Due to its switchable hydrophilicity and tunable hydrogel properties, PNIPAAm is highly favorable for use in cell culture platforms.[32, 47] Hydrophobic surfaces, such as polystyrene culture dishes and elastomeric templates, are attractive for protein adhesion and subsequent cell attachment.[32] However, detachment of cells and tissues from these templates requires either enzymatic reaction or physical scraping, both of which can damage cells and cell-ECM interactions.[48, 49] Cell culture platforms have been increasingly functionalized with PNIPAAm to first induce cell attachment at temperatures above LCST, and then trigger controlled cell detachment from the surface by decreasing the temperature below LCST. Micro- and nano-fabrication techniques have also been utilized to create PNIPAAm-based platforms for tissue engineering applications.

1.5.2 Two-dimensional thermoresponsive platforms

Cell sheet engineering has been a growing approach to generate functional tissues for biomedical applications. In this approach cell are initially induced to form a monolayer upon adhesion to hydrophobic surfaces, such as polystyrene culture dishes and elastomeric substrates. The resulting monolayers, also called cell sheets, can be removed from the substrates to generate functional tissues.

Thermoresponsive surfaces are useful for controlling the cell attachment and detachment to produce intact cell sheets. A pioneering study on thermoresponsive surfaces was published in 1990 which demonstrated the use of PNIPAAm grafted culture substrates for temperature dependent detachment of cell sheets.[50] Cells adhered to these substrates at 37 °C since PNIPAAm was hydrophobic at these temperatures.[51] Enzymatic recovery damages cell-cell junction proteins and cell-ECM interactions, preventing retrieval of monolayer tissues.[51] To maintain intact structure, detachment of tissues was induced at ambient temperatures as the substrate becomes hydrophilic, inhibiting cell adhesion.[51] Cell sheets generated using this process have been used for various tissue engineering applications, including cardiac,[51, 52] hepatic,[53] skin,[54] kidney,[55] and corneal.[56] Here we review some of these studies.

1.5.2.1 PNIPAAm coating on cell culture substrates

Various methods have been used to create PNIPAAm coated substrates.[31, 48, 49, 57] Some of these surfaces were successfully used to generate cell sheets. However, some PNIPAAm coated surfaces were not suitable for the formation of tissue monolayers as they inhibit cell attachment at temperatures above LCST.[58, 59]

The most common method to coat cell culture substrates with PNIPAAm is by the use of electron-beam (e-beam) irradiation.[51-56, 58] Controlled cell adhesion and further tissue retrieval were reported for limited grafting densities of 1.4-2 $\mu g/cm^2$ and for limited PNIPAAm thicknesses ranging from 15 to 20 nm.[53, 54, 58] Increasing PNIPAAm thickness above 30 nm did not allow cell attachment on these surfaces for grafting densities of 2.9-3 $\mu g/cm^2$.[58, 59]

Plasma polymerization was also employed to induce covalent bonding of NIPAAm on cell culture substrates.[49, 60] Plasma coating of PNIPAAm showed similar properties of crosslinked polymers as it maintained its NIPAAm structure and phase transition behavior.[61] Cell attachment and detachment process showed similar trends for different plasma-coated PNIPAAm surfaces with different PNIPAAm thicknesses.[49, 60] Cell adhesion and detachment for plasma-coated PNIPAAm substrates was shown to be independent from PNIPAAm thickness.[31]

Ultraviolet (UV) irradiation has also been used to coat cell culture substrates with a copolymer of PNIPAAm.[62] Cell attachment and detachment process for these substrates were independent from copolymer thickness for grafting densities in the range of 2.4-6.9 $\mu g/cm^2$.[62] Photo-

polymerization was also utilized to form micropatterns of thermoresponsive polymer on substrates.[63, 64] Cells were selectively attached on the thermoresponsive micropatterns, and disassociated from these regions at 10 °C.[63, 64] These micropatterned thermoresponsive surfaces could be useful for co-culture of different cell types with controlled spatial distribution.[31]

1.5.2.2 Cell adhesion on thermoresponsive substrates and controlled detachment of tissues

Even though many thermoresponsive cell culture surfaces have been generated using different methods, only some of these are suitable for cell adhesion,[51-56, 58] in contrast many others have failed to be cell adhesive even above their LCST.[58, 59] For example, cells did not adhere to PNIPAAm coated surfaces with a thickness over 30 nm,[58, 59] methylenebis(acrylamide) (MBAAm) crosslinked PNIPAAm hydrogels,[58, 59] and non-crosslinked PNIPAAm hydrogels.[50] Adsorption of serum proteins, such as fibronectin, on the substrates can promote further cell attachment,[31] however fibronectin was not able to adsorb significantly on e-beam polymerized PNIPAAm with the highest density or on crosslinked PNIPAAm polymers.[58, 59]

Static water contact angle measurements of polymer based surfaces were used to explain cell adhesion properties. As expected, the contact angle suitable for cell attachment was found to be ~70°.[65] Cell repellent behavior of MBAAm crosslinked PNIPAAm hydrogels was correlated with low static water contact angles of these hydrogels.[58] Although similar contact angles were reported for surfaces with plasma polymerized PNIPAAm,[61, 66] these surfaces were suitable for cell attachment and detachment.[61] These findings suggest that in addition to surface wettability there are other factors, such as grafting density and polymer thickness, which influence cell adhesion for different PNIPAAm polymerization methods. For example, increasing the thickness of e-beam polymerized PNIPAAm did not change the contact angles of the substrates, though cell attachment on these surfaces decreased significantly compared to low thicknesses.[31] This shows that cell adhesion depends on the PNIPAAm thickness for surfaces coated with e-beam irradiation. Furthermore, for e-beam deposited PNIPAAm surfaces, although high grafting densities (2.9 $\mu g/cm^2$) demonstrated similar contact values with low grafting densities (1.4 $\mu g/cm^2$ and 1.6 $\mu g/cm^2$), cell attachment significantly decreased for high grafting densities,[58] suggesting cell adhesion also depends on the grafting density of the PNIPAAm.

Swelling ratio and molecular mobility of the polymer films can also affect the cell adhesion behavior of the surfaces.[31, 67] Crosslinking PNIPAAm on a surface affects its chain mobility and swelling properties.[31, 67] Decreasing the grafting thickness decreases the swelling ratio of e-beam grafted PNIPAAm films.[31, 58] PNIPAAm chains are less independent at the interface of the substrate due to the high hydrophobic interactions, resulting in a dehydrated and aggregated layer at the inner most layer of the film.[67] Above this aggregated layer, there is somewhat hydrated and hydrophobic layer, supporting cell adhesion and detachment. It was reported that the thickness of this cell adhesive layer can be between 15 nm and 20 nm.[67] At the outermost layer of e-beam grafted PNIPAAm films, chains have more mobility and are dehydrated, which were reported as non-supportive for cell adhesion.[67] Cells cannot adhere to PNIPAAm chains for e-beam grafted surfaces with a film thickness of above 30 nm.[58, 59] Thus, cell adhesion on PNIPAAm coated surfaces depends on various factors, including chain mobility, grafting density, swelling ratio, and wettability.[31]

Adhered cells spread and proliferate on thermoresponsive surfaces at physiological temperatures.[67] Adhesion and further cell morphology on the substrate require metabolic activities, such as ATP synthesis.[67, 68] High cell confluence leads to the formation of monolayers of tissues on the substrates. Mechanical or enzymatic removal of these tissues can destroy cell-cell interactions and subsequently the intact structure of the tissue. Cell sheets can be dissociated from the surface by decreasing the temperature below LCST, facilitating the hydration of the PNIPAAm layer.[67] Different cell types require different retrieval temperatures, such as 10 °C for hepatocytes and 20 °C for endothelial cells.[67, 69] Detachment process can be suppressed by treating cells with an ATP synthesis inhibitor or with a tyrosine kinase inhibitor, suggesting that cell retrieval process depends on cell metabolic activities.[67, 68]

Temperature controlled cell detachment method maintains the intact structure of the tissue with its natural ECM. The content of the ECM depends on the cultured cell types as different cell types produce different ECM proteins.[31, 67] Also, previously deposited proteins on the substrate, such as fibronectin, can be detached with cell sheets from the thermoresponsive surface at low temperatures.[70] Recovered tissues leave a small amount of ECM proteins on the surface after the retrieval process.[49, 60] This may be due to weak interactions between cells and remaining ECM

proteins on the surface.[49] As the amount of remaining protein is small, the resulting monolayer tissues retain their intact structure.

1.5.2.3 Patterned co-culture platforms

Control of the spatial distribution of different cell types in close proximity can be used to replicate native tissues *in vitro*. Patterned co-cultures of different cell types can generate functional tissue constructs. Merging patterning techniques with thermoresponsive substrates can provide not only tissue retrieval but also controlled co-culture platforms. To develop a platform to generate cell sheets with multiple cell types, masked e-beam irradiation was utilized to create circular PNIPAAm domains on polystyrene dishes.[71, 72] The first cell type was attached on cell culture dishes at 37 °C. As the temperature was decreased to 20 °C, cells on PNIPAAm domains were detached due to the hydration of PNIPAAm, but cells on polystyrene parts remained attached. PNIPAAm domains were then used to culture another cell type. This patterning technique controlled spatial arrangements of two different cell types in a co-culture platform.[71, 72] In another approach, cell culture substrates with dual thermoresponsiveness were fabricated with e-beam irradiation to culture different cell types in a spatial arrangement.[67, 73] The LCST can be reduced by copolymerization of n-butyl-methacrylate (BMA), a hydrophobic monomer, on PNIPAAm grafted surfaces with e-beam polymerization.[74] Micropatterns of BMA were grafted on PNIPAAm coated culture dishes, producing a dual thermoresponsive substrate.[73] Hepatocytes and endothelial cells were cultured on micropatterned dual thermoresponsive substrates to fabricate co-cultured cell sheets.[73]

1.5.2.4 Cell sheet technology

Thermoresponsive platforms have been successfully employed to generate intact monolayers of tissues. Cell sheets can be easily recovered with their natural ECM from the substrates by exploiting the hydration property of PNIPAAm at temperatures below LCST.[67] As this method does not require the use of enzymes, tissues preserve their structural integrity. This gives additional mechanical strength to cell sheets, enabling further manipulation of tissues.[52-55] As a cell sheet is transferred to another substrate or a physiological environment, the ECM proteins induce its attachment to the new environment.[70]

Cell sheets can be implanted *in vivo* and attach to the new tissue through ECM proteins, eliminating the use of sutures.[75] Cell sheets also do not require any scaffolding material, which

may minimize inflammation and immune rejection *in vivo*.[31] Larger tissue constructs can be fabricated by stacking cell sheets.[76] For example, seeding endothelial cells between two layers of cell sheets leads to the formation of vessels, resulting in prevascularized tissues.[76] Cell sheet technology has been utilized to fabricate different types of tissues, such as myocardial and hepatic.

Attaining tight cell-cell connections is important for engineering cardiac tissues with functional features *in vitro*.[67] Thermoresponsive platforms have been used to fabricate cardiac cell sheets with an electrical functionality. In this approach, cardiomyocytes were cultured on thermoresponsive surfaces, producing an intact cardiac cell sheet with tight cell-cell junctions.[51, 52] These junctions are critical for electrical communication between cardiomyocytes, facilitating the contraction and beating of the monolayer tissues.[67] Three-dimensional cardiac tissues were also fabricated by stacking cardiac cell sheets.[51, 52, 77] The gap junctions between stacked cardiac cell sheets produced an electrical communication between layered monolayer tissues.[67]

To assess the functionality of the cell sheet cardiac tissue, stacked monolayers of co-cultured cardiac cells with endothelial cells were implanted into nude rats.[51, 52] It was observed that the implanted tissues formed a vascular connection with the host tissue,[78] facilitating the connection with the native microenvironment.[51, 52, 78] Cell sheet technology also enables the recovery of intact cardiac cell sheets with their own ECM and high cell-cell interactions.[67] Vascular network and cardiac functionalities result from these tight cell-cell interactions and secreted proteins within the stacked cardiac tissues.[51, 52, 67] Controlling the cell-cell interactions within the cardiac cell sheets can lead to functional vascularized cardiac tissues,[67] which could be useful for in vitro studies and to treat impaired hearts.

Cardiac cell sheets were also used to fabricate cell-based components of microdevices. For example, cardiac cell sheet based micropumps were integrated on chip for flow control applications.[79] A micro-spherical heart-like pump was also fabricated from monolayer cardiac tissues with contractile properties.[80] These cell-sheet based applications could lead to self-actuated microdevices. Furthermore, myocardial tubes were fabricated by rolling cardiac cell sheets around a thoracic aorta of an adult rat, which were then implanted into nude rats for a circulatory assist.[81] Implanted tubes exhibited integration with the native tissue within four

weeks after the procedure.[81] Given these results, engineering cardiac cell sheets shows promise for regenerative therapies and in vitro studies.

Hepatic tissue engineering attempts to create liver-like tissue constructs for use either in regenerative therapies or *in vitro* studies, such as drug toxicity screening. Some of the previous approaches encapsulated hepatocytes within ECM proteins[82] or biodegradable scaffolds[83] to fabricate implantable liver tissues. As an alternative approach, scaffold-free liver tissues were also generated by culturing hepatocytes on thermoresponsive culture dishes to form monolayers of hepatic tissues, which were then recovered with a temperature change.[84] Hepatic cell sheets that were implanted into the subcutaneous spaces of mice maintained their functionality for more than 200 days.[84] In other experiments, hepatic cell sheets were also layered to form thick hepatic tissues.[84]

Heterotypic cell-cell interactions play an important role to produce hepatic tissues with improved functionalities.[73] To meet this demand, dual thermoresponsive surfaces were fabricated for co-culture of hepatocytes and endothelial cells.[73] Copolymerization of BMA with PNIPAAm was used to reduce the LCST.[74] Micropatterns of BMA were grafted on PNIPAAm coated substrate, resulting in a dual thermoresponsive surface.[73] Hepatocytes attached on hydrophobic BMA grafted domains on the surface at 27 °C.[85] Endothelial cells were placed on hydrophobic PNIPAAm coated regions at 37 °C, producing co-cultured hepatic cell sheets.[85] Intact hepatic cell sheets were successfully recovered from the substrates at 20 °C.[85] Co-culture of hepatocytes with endothelial cells demonstrated improved functionalities, such as albumin synthesis and ammonium metabolism.[73, 85] Furthermore, endothelial cell sheets were placed on top of hepatic cell sheets to generate layered co-cultured hepatic tissues.[53] These studies show that thermoresponsive cell culture surfaces were successfully employed to produce mono-cultured or co-cultured hepatic tissue sheets for transplantation and *in vitro* use.

1.5.3 Three-dimensional thermoresponsive platforms

Thermoresponsive templates have also been used to directly generate 3D tissue structures which can mimic native tissues. Structural organization of cells is a critical issue in the formation of functional tissues. Micropatterned substrates can be used to control the alignment and elongation of cells to induce cytoskeletal organization of the cells which can lead to physiologically active modular tissues. These microstructures can be fabricated from various materials, such as

poly(dimethylsiloxane) (PDMS) and polystyrene. However, these surfaces demonstrate constant hydrophobicity, preventing controlled detachment of tissues from the substrates. To overcome this problem, microtextured surfaces were coated with PNIPAAm, generating a temperature dependent switchable surface.[86-88] Microtextured polystyrene templates were coated with a thin film of PNIPAAm by employing e-beam irradiation.[86] Smooth muscle cells were seeded on PNIPAAm coated microtextured substrates and non-patterned polystyrene surfaces. Cell orientations on patterned substrates were significantly higher compared to non-textured surfaces.[86] Hydration of the PNIPAAm film at 20 °C allowed for the retrieval of tissues with an intact structure.[86] These functional microtextured templates enabled not only the cytoskeletal organization of cells but also the controlled detachment of tissues.

Controlled capillary formation is important to fabricate vascularized micro-tissues, which can overcome oxygen and diffusion limitations.[87] Micropatterned surfaces have been shown to trigger capillary formation.[89] PNIPAAm coated microtextured substrates were also employed to induce capillary network formation.[87] Microgroove patterns of poly(urethane acrylate) were generated with soft lithographic methods by using photoresist patterned silicon wafers as molding templates.[87] PNIPAAm was covalently grafted on these patterns by using e-beam polymerization. The ridges demonstrated rounded shapes and the aggregation of PNIPAAm coating has been observed in the grooves.[87] As the thick PNIPAAm graft in the grooves prevents cell adhesion, endothelial cells moved through to top of the ridges and formed capillary networks within 3 weeks. Tubular endothelial networks were easily recovered from the groove substrates after reducing the temperature to 20 °C.[87]

Previous coating methods employed liquid phase polymerization, which may not easily coat all the surfaces of a microfabricated platform. Non-conformal coatings can change the shapes of the device patterns, which can affect the structural organization of tissues.

1.6 Scope of this thesis

Controlling multicellular organization in a 3D geometry can give us an ability to replicate native tissue microenvironments which could be highly useful for applications in life sciences. The goal of this thesis is to develop effective methods based on microengineered thermoresponsive platforms for spatial and geometrical control of multicellular communities. Multicellular organizations can be made of cells of a single type or multiple types. Cells can either be

encapsulated within a biomaterial or form scaffold-free tissues. First two chapters of this thesis will describe methods to form geometrically controlled scaffold-free tissues made of single cell types and control the retrieval of tissues from the templates for further use. Later two chapters will cover techniques to control spatial and geometrical distribution of multiple cell types either in a microgel to obtain a suitable microenvironment for cell-matrix interactions, or without a scaffold to obtain cell-cell interactions.

Chapter 2 describes a method to form spheroids of a single cell type which can be beneficial for various applications ranging from biotechnology to regenerative therapies. Microwells have previously been demonstrated as a potentially useful method for generating controlled-size cell aggregates. In addition to controlling cell aggregate size and homogeneity, the ability to confine cell aggregates on glass adhesive substrates and subsequently retrieve aggregates from microwells for further experimentation and analysis could be beneficial for various applications. However, it was often difficult to retrieve cell aggregates from previously developed glass-bottomed microwells without the use of digestive enzymes. Chapter 2 demonstrates the stable formation of cell aggregates in responsive microwells with adhesive substrates and their further retrieval in a temperature dependent manner by exploiting the stimuli responsiveness of these microwells. This approach can be potentially integrated into high-throughput systems and may become a versatile tool for various applications that require single cell type aggregate formation and experimentation.

Chapter 3 demonstrates the fabrication of a thermoresponsive platform and its use for the formation of striped tissues and their further retrieval in a temperature dependent manner. Striped tissues made of a single cell type could be biomimetic models of cardiac and muscle tissues. Microfabricated templates, such as made of PDMS, have been previously utilized to generate these tissues, however it has been difficult to harvest them from the substrates without digestive enzymes. Liquid based polymerization methods were used to coat the platforms with responsive polymers to initiate the retrieval of the striped tissues. However, conformal coating of complex devices prepared by standard microfabrication techniques with desired chemical functionality is challenging. Chapter 3 describes the conformal coating of PDMS microgrooves with PNIPAAm by using initiated chemical vapor deposition (iCVD). These microgrooves guided the formation of striped tissue constructs of a single cell type that could be retrieved by the temperature

dependent swelling property and hydrophilicity change of the PNIPAAm. The resulting striped tissues were the same size as the grooves and could be used in further applications.

Chapter 4 showcases a method to spatially organize multiple cell types into geometrically controlled multicompartment hydrogels. Photolithographic methods are the most common way to pattern microscale hydrogels, but are limited to photocrosslinkable polymers. So far, conventional micromolding approaches use static molds to fabricate structures, limiting the resulting shapes that can be generated. Chapter 4 describes a dynamic micromolding technique to fabricate sequentially patterned hydrogel microstructures by exploiting the thermo-responsiveness of PNIPAAm-based micromolds. These responsive micromolds can be used to immobilize various cell types into different compartments of hydrogel microstructures in a biomimetic manner to recapitulate both multicellular organization and cell-matrix interactions of native tissues.

Chapter 5 describes a simple method to control spatial organizations of multiple cell types in predefined geometries by using PNIPAAm-based dynamic microwells. The pattern areas of these microwells change at different temperatures due to the thermoresponsiveness of PNIPAAm. Dynamic microwells were used to pattern two different cell types in a spatially controlled manner by exploiting their shape changing properties at two different temperatures. Both spatial organization of two different cell types and control of pattern geometry were achieved with circular and square dynamic microwells. This method can replicate different biological complexities with controlled heterotypic and homotypic cell-cell interactions.

Finally, Chapter 6 gives concluding remarks of this thesis and directions for future studies.

1.7 References

[1] D. T. Chiu, N. L. Jeon, S. Huang, R. S. Kane, C. J. Wargo, I. S. Choi, D. E. Ingber, G. M. Whitesides, Proceedings of the National Academy of Sciences of the United States of America 2000, 97, 2408.

[2] A. Khademhosseini, G. Eng, J. Yeh, P. A. Kucharczyk, R. Langer, G. Vunjak-Novakovic, M. Radisic, Biomedical Microdevices 2007, 9, 149.

[3] Y.-s. Torisawa, B. Mosadegh, G. D. Luker, M. Morell, K. S. O'Shea, S. Takayama, Integrative Biology 2009, 1, 649.

[4] H.-C. Moeller, M. K. Mian, S. Shrivastava, B. G. Chung, A. Khademhosseini, Biomaterials 2008, 29, 752.

[5] D. Motlagh, T. J. Hartman, T. A. Desai, B. Russell, Journal of Biomedical Materials Research Part A 2003, 67A, 148.

[6] K. Nakazawa, Y. Izumi, J. Fukuda, T. Yasuda, Journal of Biomaterials Science-Polymer Edition 2006, 17, 859.

[7] G. T. Franzesi, B. Ni, Y. Ling, A. Khademhosseini, Journal of the American Chemical Society 2006, 128, 15064.

[8] J. Yeh, Y. Ling, J. M. Karp, J. Gantz, A. Chandawarkar, G. Eng, J. Blumling, III, R. Langer, A. Khademhosseini, Biomaterials 2006, 27, 5391.

[9] V. A. Liu, S. N. Bhatia, Biomedical Microdevices 2002, 4, 257.

[10] Y. A. Du, M. Ghodousi, H. Qi, N. Haas, W. Q. Xiao, A. Khademhosseini, Biotechnol. Bioeng. 2011, 108, 1693.

[11] http://en.wikipedia.org/wiki/File:HumanEmbryogenesis.svg, Accessed September 29, 2012.

[12] http://creativecommons.org/licenses/by-sa/3.0/deed.en.

[13] A. M. Wobus, K. R. Boheler, Physiological Reviews 2005, 85, 635.

[14] D. Sasse, U. M. Spornitz, I. P. Maly, Enzyme 1992, 46, 8.

[15] S. N. Bhatia, U. J. Balis, M. L. Yarmush, M. Toner, Faseb Journal 1999, 13, 1883.

[16] A. Khademhosseini, J. P. Vacanti, R. Langer, Scientific American 2009, 300, 64.

[17] L. M. Reid, A. S. Fiorino, S. H. Sigal, S. Brill, P. A. Holst, Hepatology 1992, 15, 1198.

[18] G. Vunjak-Novakovic, N. Tandon, A. Godier, R. Maidhof, A. Marsano, T. P. Martens, M. Radisic, Tissue Engineering Part B-Reviews 2010, 16, 169.

[19] D. Hanahan, R. A. Weinberg, Cell 2011, 144, 646.

[20] J. Landry, D. Bernier, C. Ouellet, R. Goyette, N. Marceau, Journal of Cell Biology 1985, 101, 914.

[21] P. V. Moghe, F. Berthiaume, R. M. Ezzell, M. Toner, R. G. Tompkins, M. L. Yarmush, Biomaterials 1996, 17, 373.

[22] S. Klein, A. R. de Fougerolles, P. Blaikie, L. Khan, A. Pepe, C. D. Green, V. Koteliansky, F. G. Giancotti, Molecular and Cellular Biology 2002, 22, 5912.

[23] C. M. Nelson, M. J. Bissell, in *Annual Review of Cell and Developmental Biology*, Vol. 22, 2006, 287.

[24] K. Liu, H.-J. Ding, J. Liu, Y. Chen, X.-Z. Zhao, Langmuir 2006, 22, 9453.

[25] J. Tien, C. M. Nelson, C. S. Chen, Proceedings of the National Academy of Sciences of the United States of America 2002, 99, 1758.

[26] Y.-C. Toh, K. Blagovic, H. Yu, J. Voldman, Integrative Biology 2011, 3, 1179.

[27] E. E. Hui, S. N. Bhatia, Proceedings of the National Academy of Sciences of the United States of America 2007, 104, 5722.

[28] Z. J. Gartner, C. R. Bertozzi, Proceedings of the National Academy of Sciences of the United States of America 2009, 106, 4606.

[29] H. Tekin, T. Tsinman, J. G. Sanchez, B. J. Jones, G. Camci-Unal, J. W. Nichol, R. Langer, A. Khademhosseini, Journal of the American Chemical Society 2011, 133, 12944.

[30] C. D. H. Alarcon, S. Pennadam, C. Alexander, Chemical Society Reviews 2005, 34, 276.

[31] R. M. P. Da Silva, J. F. Mano, R. L. Reis, Trends in Biotechnology 2007, 25, 577.

[32] N. A. Peppas, P. Bures, W. Leobandung, H. Ichikawa, European Journal of Pharmaceutics and Biopharmaceutics 2000, 50, 27.

[33] F. Eeckman, A. J. Moes, K. Amighi, European Polymer Journal 2004, 40, 873.

[34] S. Hirotsu, Y. Hirokawa, T. Tanaka, Journal of Chemical Physics 1987, 87, 1392.

[35] S. Beltran, J. P. Baker, H. H. Hooper, H. W. Blanch, J. M. Prausnitz, Macromolecules 1991, 24, 549.

[36] T. Inoue, G. H. Chen, K. Nakamae, A. S. Hoffman, Polymer Gels and Networks 1997, 5, 561.

[37] H. Allan S, Journal of Controlled Release 1987, 6, 297.

[38] Y. Kaneko, S. Nakamura, K. Sakai, T. Aoyagi, A. Kikuchi, Y. Sakurai, T. Okano, Macromolecules 1998, 31, 6099.

[39] R. Yoshida, K. Uchida, Y. Kaneko, K. Sakai, A. Kikuchi, Y. Sakurai, T. Okano, Nature 1995, 374, 240.

[40] Y. Kaneko, S. Nakamura, K. Sakai, A. Kikuchi, T. Aoyagi, Y. Sakurai, T. Okano, Polymer Gels and Networks 1998, 6, 333.

[41] G. H. Chen, A. S. Hoffman, Nature 1995, 373, 49.

[42] E. Diez-Pena, I. Quijada-Garrido, J. M. Barrales-Rienda, Polymer 2002, 43, 4341.

[43] E. Diez-Pena, I. Quijada-Garrido, P. Frutos, J. M. Barrales-Rienda, Macromolecules 2002, 35, 2667.

[44] L. Bromberg, Journal of Physical Chemistry B 1997, 101, 504.

[45] H. K. Ju, S. Y. Kim, Y. M. Lee, Polymer 2001, 42, 6851.

[46] D. Dhara, G. V. N. Rathna, P. R. Chatterji, Langmuir 2000, 16, 2424.

[47] E. S. Gil, S. M. Hudson, Progress in Polymer Science 2004, 29, 1173.

[48] N. Yamada, T. Okano, H. Sakai, F. Karikusa, Y. Sawasaki, Y. Sakurai, Makromolekulare Chemie-Rapid Communications 1990, 11, 571.

[49] H. E. Canavan, X. H. Cheng, D. J. Graham, B. D. Ratner, D. G. Castner, Journal of Biomedical Materials Research Part A 2005, 75A, 1.

[50] T. Takezawa, Y. Mori, K. Yoshizato, Bio-Technology 1990, 8, 854.

[51] T. Shimizu, M. Yamato, A. Kikuchi, T. Okano, Biomaterials 2003, 24, 2309.

[52] T. Shimizu, M. Yamato, Y. Isoi, T. Akutsu, T. Setomaru, K. Abe, A. Kikuchi, M. Umezu, T. Okano, Circulation Research 2002, 90, E40.

[53] M. Harimoto, M. Yamato, M. Hirose, C. Takahashi, Y. Isoi, A. Kikuchi, T. Okano, Journal of Biomedical Materials Research 2002, 62, 464.

[54] M. Yamato, M. Utsumi, A. Kushida, C. Konno, A. Kikuchi, T. Okano, Tissue Engineering 2001, 7, 473.

[55] A. Kushida, M. Yamato, A. Kikuchi, T. Okano, Journal of Biomedical Materials Research 2001, 54, 37.

[56] K. Nishida, M. Yamato, Y. Hayashida, K. Watanabe, N. Maeda, H. Watanabe, K. Yamamoto, S. Nagai, A. Kikuchi, Y. Tano, T. Okano, Transplantation 2004, 77, 379.

[57] L. K. Ista, S. Mendez, V. H. Perez-Luna, G. P. Lopez, Langmuir 2001, 17, 2552.

[58] Y. Akiyama, A. Kikuchi, M. Yamato, T. Okano, Langmuir 2004, 20, 5506.

[59] M. Yamato, C. Konno, S. Koike, Y. Isoi, T. Shimizu, A. Kikuchi, K. Makino, T. Okano, Journal of Biomedical Materials Research Part A 2003, 67A, 1065.

[60] H. E. Canavan, X. H. Cheng, D. J. Graham, B. D. Ratner, D. G. Castner, Langmuir 2005, 21, 1949.

[61] X. H. Cheng, H. E. Canavan, M. J. Stein, J. R. Hull, S. J. Kweskin, M. S. Wagner, G. A. Somorjai, D. G. Castner, B. D. Ratner, Langmuir 2005, 21, 7833.

[62] H. A. von Recum, S. W. Kim, A. Kikuchi, M. Okuhara, Y. Sakurai, T. Okano, Journal of Biomedical Materials Research 1998, 40, 631.

[63] G. P. Chen, Y. Imanishi, Y. Ito, Journal of Biomedical Materials Research 1998, 42, 38.

[64] Y. Ito, G. P. Chen, Y. Q. Guan, Y. Imanishi, Langmuir 1997, 13, 2756.

[65] Y. Tamada, Y. Ikada, Journal of Biomedical Materials Research 1994, 28, 783.

[66] N. A. Bullett, R. A. Talib, R. D. Short, S. L. McArthur, A. G. Shard, Surface and Interface Analysis 2006, 38, 1109.

[67] N. Matsuda, T. Shimizu, M. Yamato, T. Okano, Advanced Materials 2007, 19, 3089.

[68] M. Yamato, M. Okuhara, F. Karikusa, A. Kikuchi, Y. Sakurai, T. Okano, Journal of Biomedical Materials Research 1999, 44, 44.

[69] T. Okano, N. Yamada, M. Okuhara, H. Sakai, Y. Sakurai, Biomaterials 1995, 16, 297.

[70] A. Kushida, M. Yamato, C. Konno, A. Kikuchi, Y. Sakurai, T. Okano, Journal of Biomedical Materials Research 1999, 45, 355.

[71] M. Yamato, C. Konno, M. Utsumi, A. Kikuchi, T. Okano, Biomaterials 2002, 23, 561.

[72] M. Yamato, O. H. Kwon, M. Hirose, A. Kikuchi, T. Okano, Journal of Biomedical Materials Research 2001, 55, 137.

[73] Y. Tsuda, A. Kikuchi, M. Yamato, A. Nakao, Y. Sakurai, M. Umezu, T. Okano, Biomaterials 2005, 26, 1885.

[74] Y. Tsuda, A. Kikuchi, M. Yamato, Y. Sakurai, M. Umezu, T. Okano, Journal of Biomedical Materials Research Part A 2004, 69A, 70.

[75] K. Nishida, M. Yamato, Y. Hayashida, K. Watanabe, K. Yamamoto, E. Adachi, S. Nagai, A. Kikuchi, N. Maeda, H. Watanabe, T. Okano, Y. Tano, New England Journal of Medicine 2004, 351, 1187.

[76] T. Sasagawa, T. Shimizu, S. Sekiya, Y. Haraguchi, M. Yamato, Y. Sawa, T. Okano, Biomaterials 2010, 31, 1646.

[77] T. Shimizu, M. Yamato, T. Akutsu, T. Shibata, Y. Isoi, A. Kikuchi, M. Umezu, T. Okano, Journal of Biomedical Materials Research 2002, 60, 110.

[78] S. Sekiya, T. Shimizu, M. Yamato, A. Kikuchi, T. Okano, Biochem. Biophys. Res. Commun. 2006, 341, 573.

[79] Y. Tanaka, K. Morishima, T. Shimizu, A. Kikuchi, M. Yamato, T. Okano, T. Kitamori, Lab on a Chip 2006, 6, 362.

[80] Y. Tanaka, K. Sato, T. Shimizu, M. Yamato, T. Okano, T. Kitamori, Lab on a Chip 2007, 7, 207.

[81] H. Sekine, T. Shimizu, J. Yang, E. Kobayashi, T. Okano, Circulation 2006, 114, I87.

[82] T. Yokoyama, K. Ohashi, H. Kuge, H. Kanehiro, H. Iwata, M. Yamato, Y. Nakajima, Am. J. Transplant. 2006, 6, 50.

[83] H. M. Lee, R. A. Cusick, H. Utsunomiya, P. X. Ma, R. Langer, J. P. Vacanti, Tissue Engineering 2003, 9, 1227.

[84] K. Ohashi, T. Yokoyama, M. Yamato, H. Kuge, H. Kanehiro, M. Tsutsumi, T. Amanuma, H. Iwata, J. Yang, T. Okano, Y. Nakajima, Nature Medicine 2007, 13, 880.

[85] Y. Tsuda, A. Kikuchi, M. Yamato, G. P. Chen, T. Okano, Biochem. Biophys. Res. Commun. 2006, 348, 937.

[86] B. C. Isenberg, Y. Tsuda, C. Williams, T. Shimizu, M. Yamato, T. Okano, J. Y. Wong, Biomaterials 2008, 29, 2565.

[87] Y. Tsuda, M. Yamato, A. Kikuchi, M. Watanabe, G. Chen, Y. Takahashi, T. Okano, Advanced Materials 2007, 19, 3633.

[88] H. Tekin, G. Ozaydin-Ince, T. Tsinman, K. K. Gleason, R. Langer, A. Khademhosseini, M. C. Demirel, Langmuir 2011, 27, 5671.

[89] C. C. Co, Y. C. Wang, C. C. Ho, Journal of the American Chemical Society 2005, 127, 1598.

Chapter 2: Stimuli-responsive microwells for formation and retrieval of microtissues of a single cell type

The content of this chapter has been published in the following journal article: H. Tekin, M. Anaya, M. Brigham, C. Nauman, R. Langer, A. Khademhosseini. Stimuli-responsive microwells for formation and retrieval of cell aggregates. *Lab on a Chip*, 2010, 10 (18): 2411-2418.

2.1 Introduction

Control of the cell microenvironment is important to better mimic native tissues by providing the appropriate conditions for cellular dynamics such as migration, spreading, differentiation, and proliferation. Microscale engineering approaches have been shown to be useful in controlling cellular behavior *in vitro* to fabricate modular tissues, to direct stem cell differentiation into desired cell types, and to perform high-throughput assays for drug toxicity and metabolism screening.[1, 2]

Controlling the size and shape of cell aggregates can be used to form functional tissue units or to trigger embryonic stem (ES) cell differentiation.[3-5] Particular cell types like hepatocytes and pancreatic cells require three dimensional (3D) environments to maintain their function.[6-8] For example, hepatocyte spheroids drive bile canaliculi formation and enhance cell-cell interactions by increasing the degree of cell-cell contact.[9-12] Furthermore, these spheroids better maintain hepatic activities such as production of albumin, urea and metabolic enzymes.[9, 13-15] Cell aggregates of differentiating ES cells, known as embryoid bodies (EBs) have also been shown to control the differentiation of ES cells.[16-21] Formation of EBs with homogenous sizes and shapes is one approach to regulate ES cell differentiation.[5, 22] Suspension culture methods have been used to form EBs,[20] but high rotation speeds generate shear forces which may influence ES cell proliferation, viability, and agglomeration[23]. Another approach for EB formation is by the hanging drop method,[21, 24] though this method is cumbersome for generating large number of EBs and cannot be easily merged with high-throughput testing systems.

Microengineering systems have been used to form cellular aggregates and control the resulting microenvironmental signals. In one of these approaches, microwell structures have been fabricated from photocrosslinkable poly(ethylene glycol) (PEG) hydrogels[5, 25] by using soft lithography[26, 27]. The surface of PEG hydrogels is resistant to cell adhesion which enhances subsequent aggregate formation within the microwells.[25] PEG microwells have also been used to form size and shape controlled EBs to direct the differentiation of ES cells[5, 28], and to immobilize stem cells within microfluidic devices[29]. Microwells have also been used to generate controlled 3D co-cultures to control and analyze the interactions between of multiple cell types.[2] All of these microwells have static environments such that their diameters and hydrogel properties cannot be controlled with external stimuli. To better mimic the temporally regulated aspects of the cellular microenvironment in the body, it may be important to fabricate microstructures with dynamic features like controllable microwell diameters and surface properties. Furthermore, aggregate harvesting from microwell arrays is a prerequisite for further encapsulation[30] and biological analysis[5, 31]. In PEG bottomed arrays,[22] the non-adhesive surface results in aggregates which do not attach to the substrate. These aggregates may be retrievable via agitation, gravitational forces or flow[28]. The relative ease with which aggregates may be removed from non-adhesive, PEG bottomed arrays makes these systems non-ideal for high-throughput applications involving fluid flow or other agitations. On the other hand, aggregate retrieval is particularly difficult in experiments in which the underlying substrate is exposed (i.e. glass bottomed microwells),[25] where cell aggregates often firmly adhere to the base of the microwells. Although an electrochemical method has been previously developed to harvest spheroids from microcavities, the technique requires a complicated substrate fabrication process and the need for applied electrical potential.[32]

To develop a method to form cell aggregates of a single cell type on adhesive substrates for high-throughput experimentation and to retrieve the resulting cell aggregates in a dynamic manner, we fabricated stimuli-responsive microwells with adhesive bottoms from photocrosslinkable poly(N-isopropyl-acrylamide) (PNIPAAm) by using soft lithography. PNIPAAm is a well-known stimuli responsive polymer which switches from hydrophobic to hydrophilic, and thus swells, under temperatures below its Lower Critical Solution Temperature (LCST) of 32 °C.[33] Because of its temperature dependent switchable surface properties, PNIPAAm has been used in cell sheet tissue engineering,[34-36] capillary network

formation,[37] drug delivery,[38, 39] and fabrication of hydrogel microstructures[40-42]. Here dynamic microwells were fabricated with either shape varying or shape constant properties and were used to form cell aggregates. Furthermore, we used the temperature dependent properties of the microwells to drive retrieval of the aggregates. Given its tunable stimuli-responsive features, this microwell array system can be potentially useful in the formation and analysis of cell aggregates and can be integrated within high-throughput screening devices.

2.2 Materials and Methods

Materials

N-isopropylacrylamide (NIPAAm), N,N-methylene-bis-acrylamide (MBAAm), dimethyl sulfoxide (DMSO), photo-initiator 2-hydroxy-2-methylpropiophenone (PI), 3-(tri-methoxysilyl)propyl-methacrylate (TMSPMA), and sodium Hydroxide (NaOH) were purchased from Sigma-Aldrich Chemical Company (St. Louis, MO). Poly(ethylene glycol) dimethacrylate (*PEGDMA* MW = 1000) was purchased from Polysciences Company (Warrington, PA). Irgacure-2959 was purchased from Ciba Specialty Chemical Corporation (Tarrytown, NY). Ethanol was purchased from Fisher Scientific (Fair Lawn, NJ). Silicon elastomer and curing agent were purchased from Dow Corning Corporation (Midland, MI). Dulbecco's phosphate buffered saline (PBS), calcein-AM and ethidium homodimer, Dulbecco's modified eagle medium (DMEM), fetal bovine serum (FBS), and penicillin streptomycin (Pen-strep) were purchased from Gibco Invitrogen (Carlsbad, CA).

PDMS molds and glass substrates

Silicon masters with 150 μm diameter cylindrical patterns were fabricated with SU-8 photolithography and used as templates to form poly(dimethylsiloxane) (PDMS) replicas. A mixture of 10:1 silicon elastomer and curing agent was cured at 70 °C for 2 h to generate PDMS stamps which were then detached from silicon masters. The resulting PDMS molds had cylindrical protruding patterns which were used to fabricate microwell structures of PNIPAAm and PEG.

Glass slides were first cleaned with 10 wt.% NaOH in deionized water for 12 h, and then

rinsed with deionized water and ethanol 3 times. After drying at ambient temperature, glass slides were treated with TMSPMA at 70 °C for 24 h. Subsequently, glass substrates were washed with ethanol 3 times and dried at room temperature for further usage.

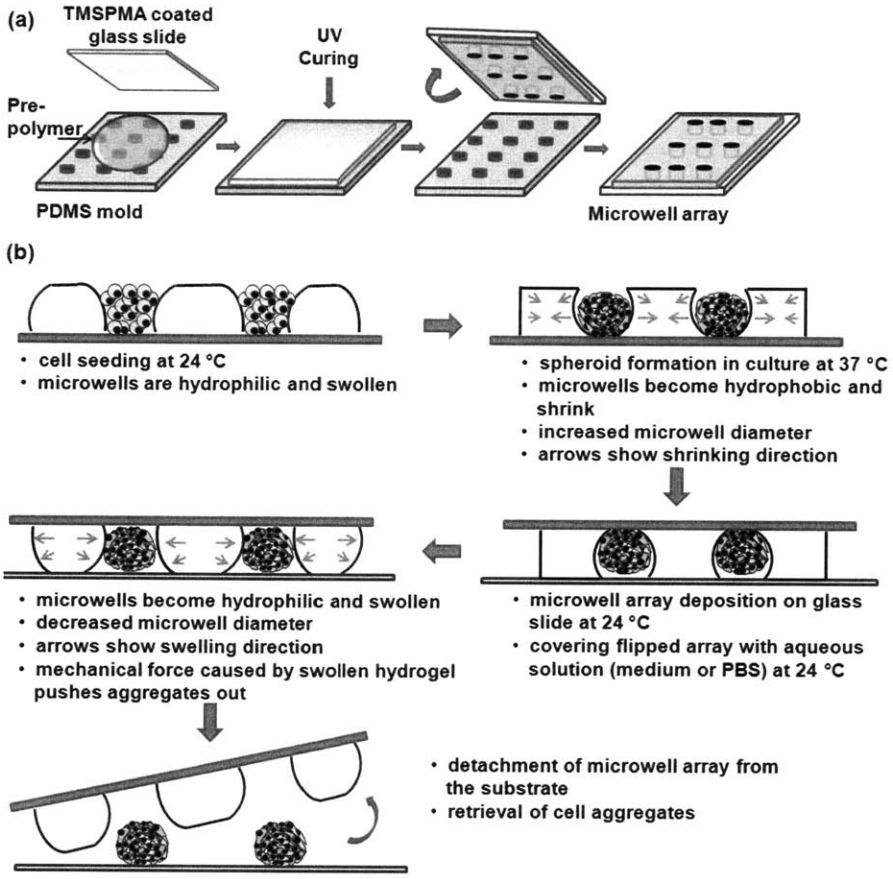

Figure 2.1. Schematics of (a) soft-lithographic fabrication of temperature responsive microwells and (b) the steps of cell seeding, aggregate formation and retrieval from glass bottomed temperature responsive microwells.

Fabrication of PNIPAAm and PEG microwells

Prepolymer solutions to fabricate shape varying (PNIPAAm-1) and shape constant (PNIPAAm-2) microwell structures were prepared by mixing NIPAAm, MBAAm, DMSO, deionized water, and PI in the weight ratios of 1.3:0.04:1.87:1:0.09 and 2.18:0.12:3:1:0.15, respectively. The weight ratios of PNIPAAm-2 solution were previously used in the fabrication of adaptive liquid microlenses.[43] The recipe of PNIPAAm-1 solution was designed with greater water and lower crosslinker (MBAAm) content than PNIPAAm-2 with

the intention of creating a less densely crosslinked hydrogel. The PEG prepolymer solution was a mixture of PEGDMA-1000 and Irgacure as photoinitiator with weight ratios of 20 wt.% and 1 wt.%, respectively, dissolved in PBS.

Desired volumes of PNIPAAm prepolymer solutions were stirred overnight at ambient temperature and photoinitiator was added to prepolymer solutions immediately before the photocrosslinking step. PEG prepolymer solutions were prepared on the day of fabrication. Microwell structures with glass bottom surfaces were fabricated with a micromolding approach by using PDMS mold substrates as shown in **Figure 2.1a**. Prepolymer solution was put on a PDMS mold and a TMSPMA coated glass slide was gently placed on the PDMS substrate, then exposed to ultraviolet (UV) light to form microstructures. Both PNIPAAm-1 and PNIPAAm-2 microwells were crosslinked by UV light of 320-500 nm at an intensity of 4 mW cm^{-2} for 30 s using the OmniCure Series 2000 (EXFO, Mississauga, Canada). PEG microwells were formed by exposure to the same UV light source at an intensity of 52 mW cm^{-2} for 30 s. The depth and thickness of the microwells were adjusted to ~150 μm. Fabricated microwells were immersed in 70% ethanol solution to clean unreacted chemicals within the hydrogel structure, washed with PBS and then kept in PBS until further experimentation.

Responsiveness tests for fabricated microwells

Responsiveness tests for all microwell arrays were conducted in ambient and cell-culture conditions to observe and quantify microwell behaviors under temperature stimuli. Microwells were washed with 70% ethanol solution and PBS to rinse off unreacted chemicals and kept in PBS. Time lapse images were taken with an inverted microscope (Nikon Eclipse TE2000-U) for all microwells at 24 °C with 1 h time intervals for 3 h. Arrays were subsequently moved to 37 °C and kept for 6 h; time-lapse images were taken every 1 h. Finally, all microwell arrays were moved back to 24 °C for 6 h and time-lapse images were taken every 1 h. There were 3 samples for each microwell type (n=3) and 6 single microwells per microscope image taken on each sample. To quantify dynamic behavior under different temperatures, the approximate top-view surface area of each microwell was measured by Spot Advanced software. The responsiveness of each microwell type at corresponding time points was represented by a mean value and standard deviation.

Scanning Electron Microscopy

To remove the water, PNIPAAm microwells were dried at room temperature for 24 h. The samples were subsequently mounted onto aluminum stages, sputter coated with gold and analyzed under scanning electron microscopy (SEM) (JEOL JSM 6060) at a working distance of 20 mm.

Cell culture and cell seeding on the microwells

Human hepatoblastoma cells, HepG2, were cultured at 37 °C in a 5% CO_2 humidified incubator in culture medium containing 89% DMEM, 10% FBS, and 1% Pen-strep.

All microwell types were placed in 6 well culture plates after fabrication, rinsed with ethanol, and kept in PBS until cell seeding. HepG2 cells were trypsinized and prepared in culture medium at a density of $4x10^6$ cells/mL. PNIPAAm microwells were kept at room temperature for at least 1 h to make the hydrogel surface hydrophilic for a better cell-seeding condition at 24 °C. PEG microwells were also subjected to the same conditions. After aspirating PBS from each 6 well plate, 200 μL of a solution containing $4x10^6$ cells/mL was seeded on each microwell array and kept at ambient temperature for 20 min to drive spreading of the cell suspension on the hydrophilic microwell array surface. Subsequently, microwell arrays were gently washed with PBS to remove cells on the hydrogel surface and immersed in fresh culture medium **(Figure 2.1b).** Cell seeding onto PNIPAAm-1 arrays was also performed at physiological temperature (37 °C) while microwells were open to their full capacity. Seeded microwell arrays were kept in a 5% CO_2 humidified incubator at 37 °C for 3 days. Microscope images were taken daily to analyze aggregate formation in the microwell structures.

Cell aggregate retrieval from the microwells

After culturing cell-seeded microwell arrays for 3 days, cell aggregates were retrieved from the microwells by deposition of the arrays on glass slides as shown in **Figure 2.1b**. For release experiments at 24 °C, microwell arrays were gently placed on a glass slide and immersed in 24 °C PBS with the wells facing down. Control experiments with the same method were conducted at 37 °C to test whether the temperature was the main driving force

in releasing the aggregates from the microwells. For control experiments at 37 °C, microwells were covered with 37 °C PBS. The duration at the experimental temperature while wells were face down was defined as the retrieval time. Different retrieval times (5, 10, and 15 min) were tested in order to analyze the controlled release behavior of responsive microwells. Release experiments with the same retrieval times at 24 °C and 37 °C were also done for PEG microwells to compare the aggregate release characteristics of static microwells with those of dynamic microwell arrays. Three samples of each microwell type (n=3) were analyzed for each retrieval time and incubation temperature. Retrieved aggregates from each sample were counted with Image-J software after taking low magnification (2x) pictures from 3 different parts of each glass slide. The percentage of aggregates that were released per array was calculated by dividing the total number of aggregates released from one microwell array by the total number of microwells on the array. Approximate diameters of retrieved aggregates were measured with Spot Advanced software to determine the frequency of diameters of aggregates formed within dynamic microstructures.

Live/Dead staining

Live/dead assay was prepared from 2 μM of calcein-AM and 4 μM of ethidium homodimer in PBS. For live and dead evaluation, each microwell array was placed in live/dead solution during deposition on glass substrate for a maximum of 15 min at 24 °C or 37 °C. Calcein AM stained live cells with fluorescent green color while homodimer caused fluorescent red staining in dead cells. Cells were visualized under an inverted microscope (Nikon Eclipse TE2000-U).

Statistical Analysis

Data was shown as the mean and ± standard deviation (± sd). Statistical analysis was performed with unpaired student's t-test and $p<0.05$ was considered as significant.

2.3 Results and Discussion

Fabrication of temperature responsive microwells

Microwells were fabricated by micromolding of photocrosslinkable hydrogels as illustrated in **Figure 2.1a**. Two distinct types of dynamic microwell structures were formed with shape

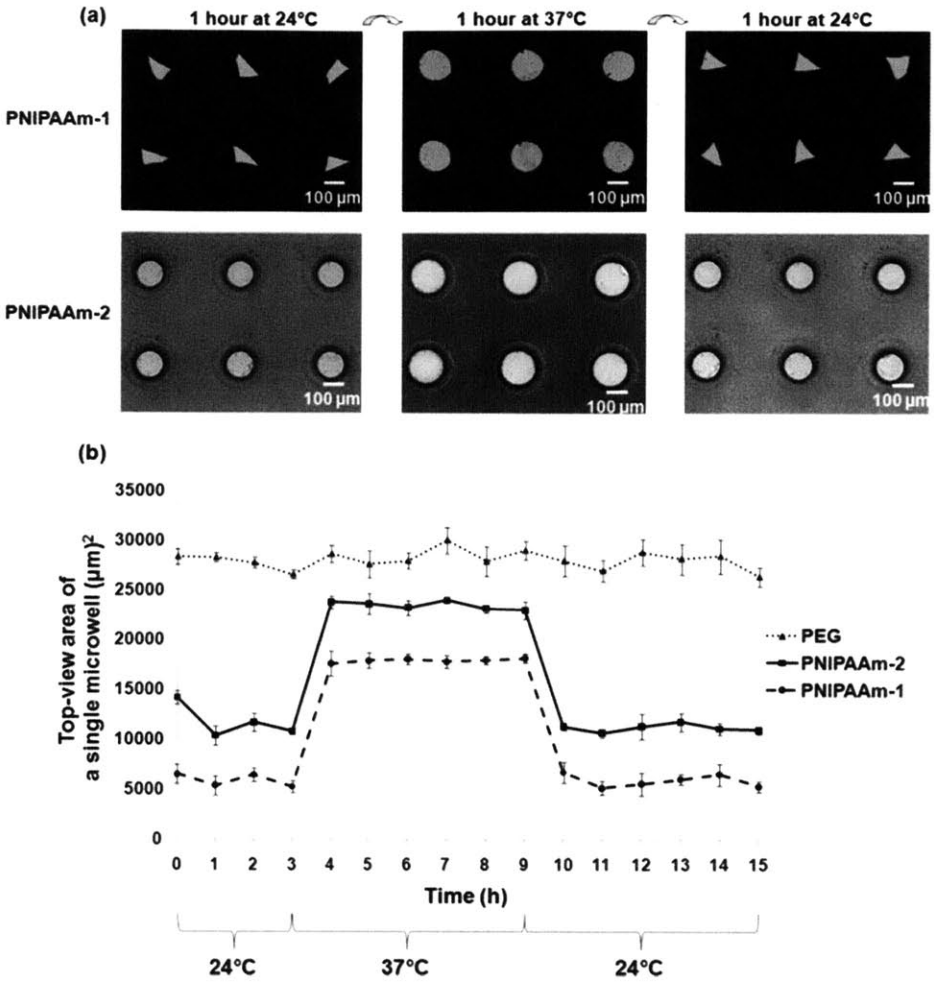

Figure 2.2. Temperature responsiveness of shape varying (PNIPAAm-1) and shape constant (PNIPAAm-2) microwells. (a) Time lapse images for both microwell types were taken in 1h time intervals at 24°C and 37°C. (b) Responsiveness of different microwell types was analyzed by measuring the top-view area of a single microwell. The microwells were initially kept at 24°C for 3 hours, then at 37°C and 24°C for 6 hours each. Data represents average ±sd for n=3 samples.

varying (PNIPAAm-1) and shape constant (PNIPAAm-2) properties. The diameter of both types of PNIPAAm microwells changed in a temperature dependent manner by swelling or shrinking (**Figure 2.2a**). Within 1h after being placed at 24 °C, PNIPAAm-1 microwells not only changed their diameter but also changed their shape whereas PNIPAAm-2 microwells maintained their rounded shape and only changed their diameter. The shape varying feature of PNIPAAm-1 microwells may be a result of less chemical crosslinker (MBAAm)

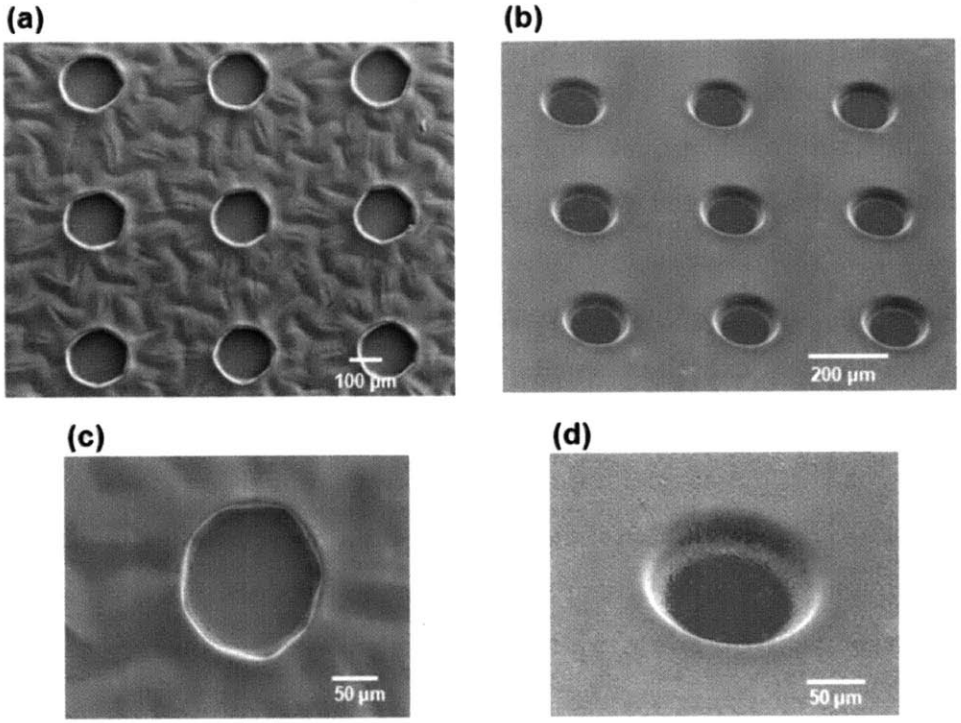

Figure 2.3. Scanning electron micrographs of fabricated PNIPAAm-1 (a, c) and PNIPAAm-2 (b, d) microwells. High resolution images of single microwells for PNIPAAm-1 (c) and PNIPAAm-2 (d).

concentration in the prepolymer solution. In contrast, PNIPAAm-2 prepolymer solution has a higher amount of crosslinker, resulting in more controlled shape structures. Interestingly, PNIPAAm-1 structures changed their microwell diameters non-uniformly under temperature variation, whereas PNIPAAm-2 structures responded to external stimuli by changing their diameters uniformly (**Figure 2.2a**). PNIPAAm-2 structures were also more transparent than those made of PNIPAAm-1. Furthermore, SEM images and time-lapse microscopy of microwell array swelling show that PNIPAAm-2 microwells (**Figure 2.3b,d)** were smooth in comparison to PNIPAAm-1 (**Figure 2.3a,c**) which qualitatively suggests that the higher crosslinker ratio in PNIPAAm-2 solution results in higher pattern transfer fidelity. It is important to note that the microwells were dehydrated for SEM analysis.

Temperature responsiveness test for microwell arrays

To quantify the dynamics of responsive microwells, we kept arrays at ambient (24 °C) and physiological (37 °C) temperatures for different time intervals. **Figure 2.2b** shows a plot of

the average microwell area as a function of time, for all microwell types. Within 1 h after changing the temperature from 24 °C to 37 °C, the free space of the PNIPAAm microwells expanded as a result of hydrogel contraction, presumably caused by the increase in temperature above the expected LCST point (~32 °C) of PNIPAAm. Microwell areas returned to their initial values within 1 h when temperature was decreased to 24 °C, demonstrating that both microwell types possess reversible shape changing property. PNIPAAm-1 microwells exhibited smaller initial microwell areas as a result of lower crosslinker to monomer ratio compared to PNIPAAm-2. Interestingly, the absolute change in microwell areas due to the temperature transition was similar for both PNIPAAm-1 and PNIPAAm-2 microwells. Control experiments with PEG microwells demonstrated that PEG microwells were non-responsive to temperature stimuli. Thus, PNIPAAm microwells have a potential advantage over PEG arrays with their tunable thermo-responsive characteristics.

Cell-seeding and formation of cell aggregates within microwells

Microwell arrays were previously shown to be useful tools for 3D cell culture and aggregate formation.[2, 11, 22, 25, 28, 29] The responsive microwell structures exhibit switchable swelling properties, a potentially useful feature in controlling the microwell surface adhesiveness for cell aggregation and retrieval. After fabrication, microwells were usually kept at room temperature for 1 h to form a swollen gel and a smaller exposed area before cell-seeding at 24 °C. In some cases, PNIPAAm-1 arrays were kept at 37 °C until microwells were in an open state with a maximum area of ~18000 μm^2. HepG2 cells were used as the model cell type due to their relevance in drug discovery and their ability to form spheroids. To generate cell aggregates in the microwells, a suspension of HepG2 cells was pipetted onto a glass slide containing microwells at a density of ~2.7×10^5 cells cm^{-2}. After 20 min, arrays were gently washed to remove cells that were not in the microwells. Cell seeded microwell arrays were kept in the incubator for 3 days to form cell aggregates. **Figure 2.4** illustrates that cell-seeding efficiency and spheroid formation in responsive microwells were comparable to those formed in glass-bottomed PEG microwells (all samples were seeded with cells at 24 °C). After one day, cell aggregates could be observed in many microwells and by day 3 tightly packed cell clusters were visible in majority of the wells. At 37 °C, the microwells were hydrophobic which may increase the level of protein adsorption from the serum and

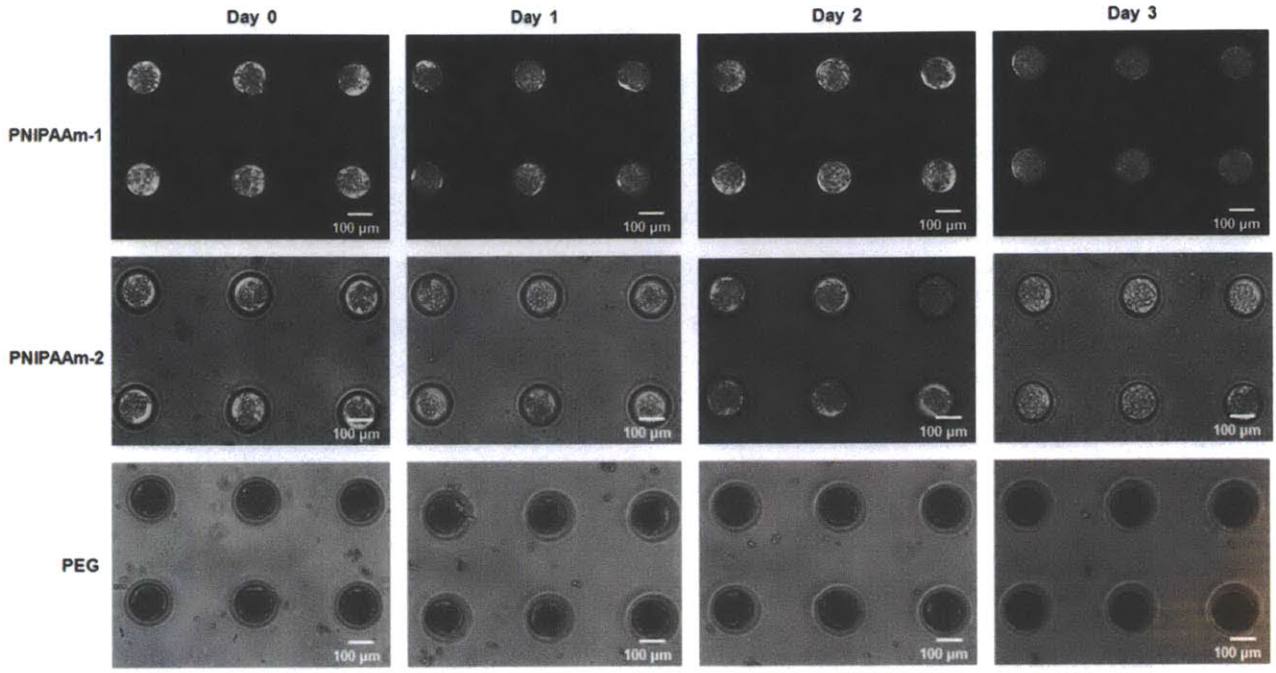

Figure 2.4. Light-microscopy images of spheroid formation within PNIPAAm-1, PNIPAAm-2 and PEG microwells over a 3 day incubation period.

subsequent cell adhesion. Thus after several days, some aggregates in PNIPAAm microwells appeared to adhere to the surrounding hydrogel matrix (**Figure 2.4**). This contact may increase the stability of cell aggregates in the PNIPAAm microwells in comparison to their PEG counterparts.

To further analyze the effect of stimuli-responsiveness of microstructures on aggregates, microwells were removed from 37 °C and placed at 24 °C for 1 h. We observed that the diameter change of responsive microwells applied mechanical force on aggregates formed in PNIPAAm-1 and PNIPAAm-2 microwells. Taken together our cell seeding and aggregate formation experiments demonstrate that responsive microwell structures are potentially useful templates for 3D culture conditions and, with their switchable and tunable properties, offer potential advantages over static microstructures.

Controlled retrieval of spheroids from microwell arrays

Aggregate retrieval with high-efficiency is a desirable property of microwell array culture systems. Successful retrieval allows for further experimentation, such as molecular biology

analysis of EBs[5, 31] or encapsulation of spheroids within biomaterials[30] for developing functional tissue constructs. We developed a temperature responsive strategy for aggregate harvesting from microfabricated stimuli-responsive devices by exploiting the switchable swelling/deswelling properties of PNIPAAm-1. PNIPAAm-2 microwells were not tested due to the frequent detachment of the array from the TMSPMA coated surface during long-term culture. For aggregate retrieval, bare glass slides were gently placed on the microwell arrays, and the entire structures were inverted to initiate the release of cell aggregates, as shown in **Figure 2.1b**. To keep the microwells in an aqueous environment, inverted microwell arrays were covered with PBS. The experiment was performed at 24 °C and 37 °C for PNIPAAm-1 and PEG microwells. Here we defined the retrieval time as the duration in which microwell arrays were face down on a glass slide at a particular temperature. Aggregate release experiments were conducted with 3 different retrieval times of 5, 10, and 15 min. After the retrieval period, excess solution was removed from the periphery and the microwell array was gently detached from the deposition surface as shown in **Figure 2.1b**.

When the aggregate retrieval experiment was performed at 37 °C, with the PNIPAAm-1 arrays in a hydrophobic/contracted state, limited aggregate release was observed for both the PNIPAAm-1 and PEG microwells (**Figure 2.5a,c**). However, when the procedure was conducted at 24 °C, the PNIPAAm microwells demonstrated a dramatic increase in aggregate release, while the PEG microwells showed no change (**Figure 2.5b,d**). Time course experiments for PNIPAAm-1 at 24 °C showed a moderate increase in aggregate retrieval at 5 min, followed by a significantly greater increase at 10 min (**Figure 2.5e**). Furthermore, we observed high cell viability levels based on live/dead staining images for all time points in the PNIPAAm-1 experiments (**Figure 2.5e**), qualitatively suggesting that the PNIPAAm-1 microwells did not adversely affect the vitality of the cells. Due to the potential lack of dye penetration into cell aggregates, cell viability was not estimated quantitatively.

Qualitative aggregate release efficiencies were confirmed by quantification of the percentage of aggregates that were released from a microwell array (**Figure 2.5f**). PEG microwells exhibited a maximum aggregate release of 15.4±3.8% for any time point or temperature. Similarly, we observed PNIPAAm-1 microwells at 37 °C to have a maximum aggregate release of 19.7±4%. Alternatively, PNIPAAm-1 microwells at 24 °C showed a marked

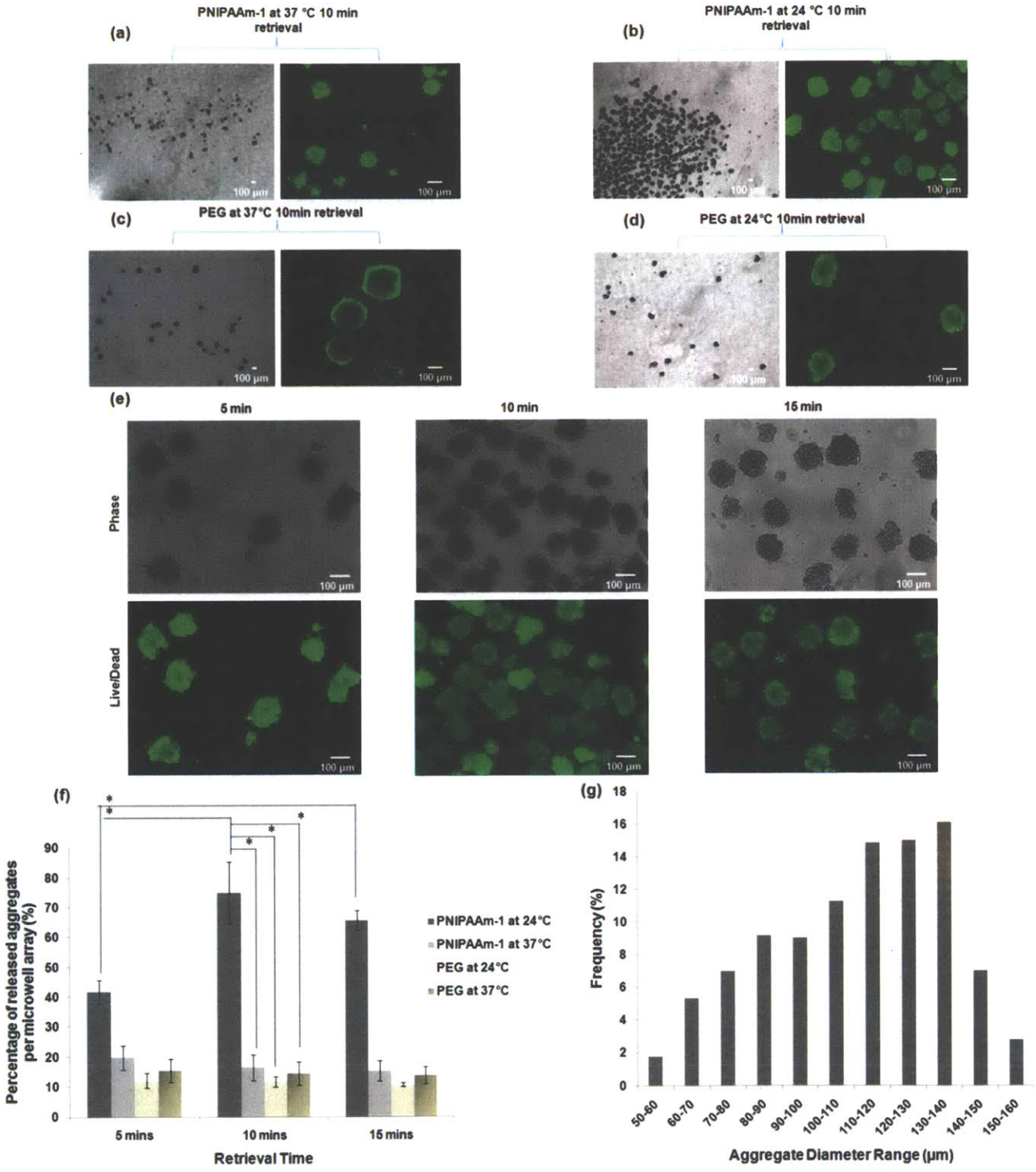

Figure 2.5. Aggregate retrieval from PNIPAAm-1 and PEG microwells and quantification of retrieval efficiency and diameter ranges of aggregates recovered from PNIPAAm-1 microwells. Phase contrast and fluorescent images of released aggregates from (a) PNIPAAm-1 microwells at 37 °C for 10 min retrieval time (control experiment) (b)

PNIPAAm-1 microwells at 24 °C for 10 min retrieval time (c) PEG microwells at 37 °C for 10 min retrieval time (d) PEG microwells at 24 °C for 10 min retrieval time (e) PNIPAAm-1 microwells at 24 °C for 5, 10, and 15 min retrieval times. Retrieval efficiency from microwells and size distribution of released cell aggregates. (f) Cell aggregates were formed within microwells in 3 days. On day 3, microwell arrays were inverted on the glass slides with the wells facing down for 5, 10, and 15 min time scales to release the aggregates in controlled manner. PNIPAAm-1 microwells were tested at 24 °C to show aggregate release percentage is more than previously developed PEG microwells and gravity is less effective in the retrieval. Release experiments were also conducted at 37 °C as control experiments to show that temperature is the main driving force for the aggregate release from the stimuli-responsive microwells. Data for percentage aggregate release per microwell array were shown with average ± sd for n=3 experiments. * shows statistically significant difference in variance ($p<0.05$). (g) Frequency of spheroid diameter was shown here for total released aggregates from PNIPAAm-1 microwells at 24 °C for 5, 10, and 15 min retrieval times.

increase in aggregate release at 5 min (41.7±3.8%) and a maximal aggregate release at 10 min (74.8±10.4%). No further significant increase in aggregate retrieval was observed at 15 min compared to 10 min ($p>0.1$), suggesting that 10 min at 24 °C is sufficient to achieve the maximum recovery of cell aggregates from PNIPAAm-1 microwell arrays.

Comparing the results of control experiments at 37 °C for PNIPAAm-1 microwells with the results of release experiments at 24 °C for PNIPAAm-1 microwells, we infer that temperature is the main triggering force in aggregate retrieval in a controlled manner from PNIPAAm-1 microwell arrays. We hypothesize that the swollen state of these temperature responsive PNIPAAm-1 microwells in an aqueous environment at 24 °C generates mechanical force on the aggregates which drives their release from the microwells. Static PEG microwells provided no mechanical force to overcome the adhesion of cell aggregate to the glass bottomed substrate.

Aggregate retrieval from previously developed static PEG bottomed microwells has been achieved by flowing an aqueous solution over the microwell arrays or by agitation of the

arrays[22, 28] both of which may lead to damage of the spheroids. The significant improvement in aggregate retrieval in the PNIPAAm-1 arrays suggests an obvious advantage compared to their static PEG array counterparts. Furthermore, the use of enzymes to detach the aggregates from substrates also disrupts cell-cell contacts and may not be suitable for these applications.

It should be noted that all microwell arrays in our experiments had glass bottoms which after the adhesion of the serum proteins provide adhesive regions for the cells[25] making the

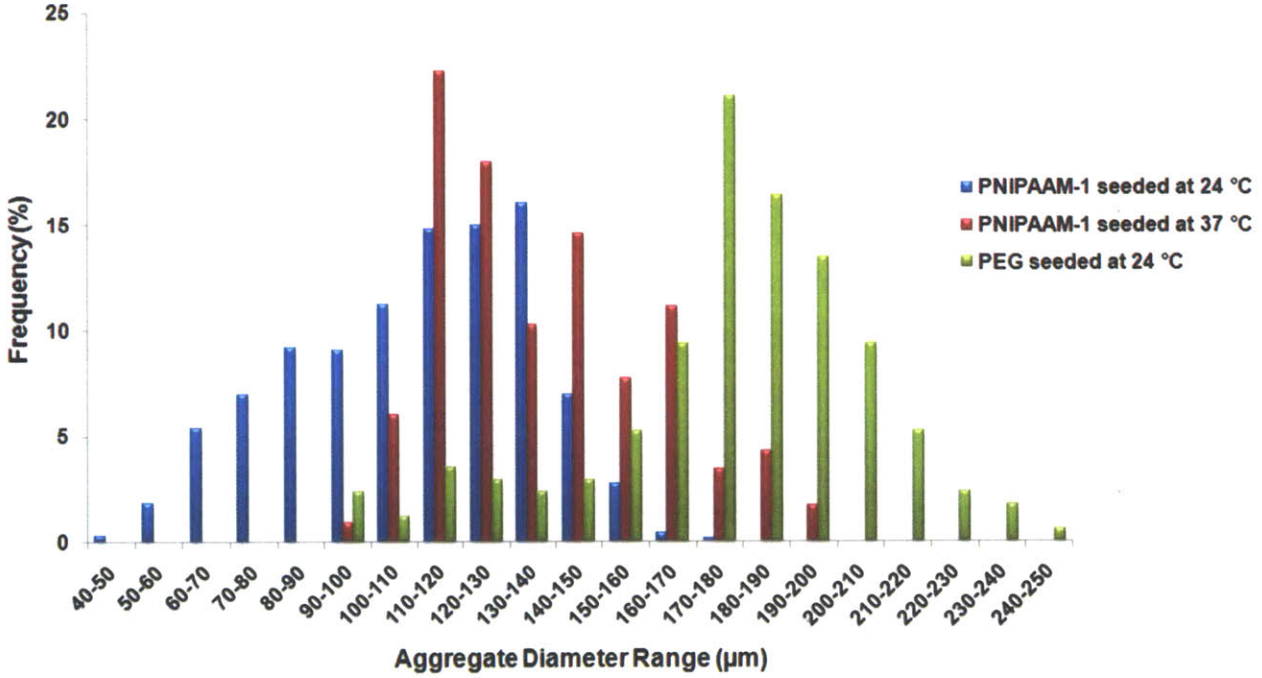

Figure 2.6. The frequency of diameter ranges for aggregates retrieved from PNIPAAm-1 microwells seeded at 24 °C, PNIPAAm-1 microwells seeded at 37 °C and PEG microwells seeded at 24 °C. It should be noted that this is not necessarily a good comparison because aggregate release from PNIPAAm-1 microwells seeded at 37 °C was less than 10% for any retrieval time or temperature and a maximum aggregate release of 15.4±3.8% from PEG microwells was shown for any time point or temperature, whereas PNIPAAm-1 microwells seeded at 24 °C exhibited a maximum aggregate release of 74.8±10.4%. The shifted distributions of aggregate diameter ranges for 3 different experimental conditions may have resulted from the fact that PNIPAAm-1 microwells had a maximum microwell area of ~6000 μm^2 at 24 °C and a maximum area of ~18000 μm^2 at 37 °C whereas PEG microwells held a maximum exposed area of ~28000 μm^2 at 24 °C.

mechanical force caused by the swollen state of the responsive microwells more effective than gravity in aggregate retrieval. Thus, stimuli-responsive microwells possess a prominent advantage over previous aggregate retrieval methods from static microwell structures[22, 28] with their controllable aggregate release property. However, it should be noted that although live/dead images suggest that mechanical detachment of cell aggregates from the glass bottomed microwells did not adversely affect cell viability, the possibility of undesirable stress-induced effects resulting from forced detachment from the glass surface has not been ruled out.

To characterize the uniformity of the retrieved aggregates, the diameters of released aggregates from PNIPAAm-1 microwells at 24 °C were quantified. As shown in **Figure 2.5g**, a wide distribution in the frequency of aggregate diameter ranges was observed. This may be due to the effects of mechanical forces from the swelling of the microwell walls. Another reason could be the decreased diameters of PNIPAAm-1 microwells during cell seeding at 24 °C, prevented the high initial number of cells to dock in the microwells. As shown in **Figure 2.2b**, during the cell seeding process at 24 °C, PNIPAAm-1 microwells held a maximum area of ~6000 μm^2 whereas PEG microwells had a maximum area of ~28000 μm^2. This may explain the fact that spheroids formed in PEG microwells appeared to be more packed than those formed in PNIPAAm microwells as shown in **Figure 2.4**. We also seeded cells onto PNIPAAm-1 arrays at 37 °C while microwells were open state with a maximum area of ~18000 μm^2. It was shown that spheroids formed in PNIPAAm-1 microwells were larger than those formed when cell seeding was performed at 24 °C (**Figure 2.6**). However, aggregate release was less than 10% for any retrieval time or temperature (data not shown). In further studies, it may be possible to form homogenous aggregates with more shape constant dynamic microwells or by better controlling cell-seeding efficiency on the responsive microwells. We also observed that removing the responsive microwells from the glass surface after aggregate retrieval sometimes led to detachment from TMSPMA surfaces at 24 °C, which may also cause aggregate deformation if the microwell array is not removed gently from the deposition surface. In further investigations, applying new surface chemistry methods on glass substrates may alleviate stability limitations of temperature responsive microwell structures in a variety of aqueous conditions.

2.4 Conclusions

Here we show that microfabricated PNIPAAm based microwell arrays with different shape changing characteristics can be used to form cell aggregates on adhesive glass substrates and enable their subsequent release in a controllable manner. These dynamic microwells have potential advantages over static microwell structures due to their high aggregate retrieval efficiency and tunable stimuli-responsiveness. These microwells may also be used to generate EBs and direct ES cell differentiation in a controllable manner, generate micro tissues, and can easily be integrated into high-throughput screening systems.

2.5 References

[1] A. Khademhosseini, R. Langer, J. Borenstein, J. P. Vacanti, Proceedings of the National Academy of Sciences of the United States of America 2006, 103, 2480.

[2] J. Fukuda, A. Khademhosseini, Y. Yeo, X. Y. Yang, J. Yeh, G. Eng, J. Blumling, C. F. Wang, D. S. Kohane, R. Langer, Biomaterials 2006, 27, 5259.

[3] J. C. Mohr, J. J. de Pablo, S. P. Palecek, Biomaterials 2006, 27, 6032.

[4] J. C. Mohr, J. Zhang, S. M. Azarin, A. G. Soerens, J. J. de Pablo, J. A. Thomson, G. E. Lyons, S. P. Palecek, T. J. Kamp, Biomaterials, 31, 1885.

[5] Y. S. Hwang, B. G. Chung, D. Ortmann, N. Hattori, H. C. Moeller, A. Khademhosseini, Proceedings of the National Academy of Sciences of the United States of America 2009, 106, 16978.

[6] N. Koide, T. Shinji, T. Tanabe, K. Asano, M. Kawaguchi, K. Sakaguchi, Y. Koide, M. Mori, T. Tsuji, Biochemical and Biophysical Research Communications 1989, 161, 385.

[7] J. Fukuda, H. Mizumoto, K. Nakazawa, T. Kajiwara, K. Funatsu, International Journal of Artificial Organs 2004, 27, 1091.

[8] C. Hober, P. Y. Benhamou, P. C. Watt, Y. Watanabe, Y. Nomura, E. Stein, F. C. Brunicardi, Y. Mullen, Pancreas 1997, 14, 199.

[9] N. Koide, K. Sakaguchi, Y. Koide, K. Asano, M. Kawaguchi, H. Matsushima, T. Takenami, T. Shinji, M. Mori, T. Tsuji, Experimental Cell Research 1990, 186, 227.

[10] S. F. Abu-Absi, J. R. Friend, L. K. Hansen, W. S. Hu, Experimental Cell Research 2002, 274, 56.

[11] J. Fukuda, Y. Sakai, K. Nakazawa, Biomaterials 2006, 27, 1061.

[12] P. J. Lee, P. J. Hung, L. P. Lee, Biotechnology and Bioengineering 2007, 97, 1340.

[13] J. Fukuda, K. Okamura, K. Nakazawa, H. Ijima, Y. Yamashita, M. Shimada, K. Shirabe, E. Tsujita, K. Sugimachi, K. Funatsu, Cell Transplantation 2003, 12, 51.

[14] T. Matsushita, H. Ijima, N. Koide, K. Funatsu, Applied Microbiology and Biotechnology 1991, 36, 324.

[15] F. J. Wu, J. R. Friend, R. P. Remmel, F. B. Cerra, W. S. Hu, Cell Transplantation 1999, 8, 233.

[16] F. M. Watt, B. L. M. Hogan, Science 2000, 287, 1427.

[17] D. Falconnet, G. Csucs, H. M. Grandin, M. Textor, Biomaterials 2006, 27, 3044.

[18] E. S. Ng, R. P. Davis, L. Azzola, E. G. Stanley, A. G. Elefanty, Blood 2005, 106, 1601.

[19] T. C. Doetschman, H. Eistetter, M. Katz, W. Schmidt, R. Kemler, Journal of Embryology and Experimental Morphology 1985, 87, 27.

[20] J. Itskovitz-Eldor, M. Schuldiner, D. Karsenti, A. Eden, O. Yanuka, M. Amit, H. Soreq, N. Benvenisty, Molecular Medicine 2000, 6, 88.

[21] G. M. Keller, Current Opinion in Cell Biology 1995, 7, 862.

[22] H. C. Moeller, M. K. Mian, S. Shrivastava, B. G. Chung, A. Khademhosseini, Biomaterials 2008, 29, 752.

[23] M. Schroeder, S. Niebruegge, A. Werner, E. Willbold, M. Burg, M. Ruediger, L. J. Field, J. Lehmann, R. Zweigerdt, Biotechnology and Bioengineering 2005, 92, 920.

[24] T. Yamada, M. Yoshikawa, S. Kanda, Y. Kato, Y. Nakajima, S. Ishizaka, Y. Tsunoda, Stem Cells 2002, 20, 146.

[25] A. Khademhosseini, J. Yeh, S. Jon, G. Eng, K. Y. Suh, J. A. Burdick, R. Langer, Lab on a Chip 2004, 4, 425.

[26] A. Revzin, K. Sekine, A. Sin, R. G. Tompkins, M. Toner, Lab on a Chip 2005, 5, 30.

[27] Y. S. Kim, K. Y. Suh, H. H. Lee, Applied Physics Letters 2001, 79, 2285.

[28] J. M. Karp, J. Yeh, G. Eng, J. Fukuda, J. Blumling, K. Y. Suh, J. Cheng, A. Mahdavi, J. Borenstein, R. Langer, A. Khademhosseini, Lab on a Chip 2007, 7, 786.

[29] A. Khademhosseini, J. Yeh, G. Eng, J. Karp, H. Kaji, J. Borenstein, O. C. Farokhzad, R. Langer, Lab on a Chip 2005, 5, 1380.

[30] S. M. Chia, K. W. Leong, J. Li, X. Xu, K. Y. Zeng, P. N. Er, S. J. Gao, H. Yu, Tissue Engineering 2000, 6, 481.

[31] R. L. Carpenedo, C. Y. Sargent, T. C. McDevitt, Stem Cells 2007, 25, 2224.

[32] R. Inaba, A. Khademhosseini, H. Suzuki, J. Fukuda, Biomaterials 2009, 30, 3573.

[33] C. D. H. Alarcon, S. Pennadam, C. Alexander, Chemical Society Reviews 2005, 34, 276.

[34] H. Shimizu, K. Ohashi, R. Utoh, K. Ise, M. Gotoh, M. Yamato, T. Okano, Biomaterials 2009, 30, 5943.

[35] Y. Tsuda, A. Kikuchi, M. Yamato, A. Nakao, Y. Sakurai, M. Umezu, T. Okano, Biomaterials 2005, 26, 1885.

[36] N. Matsuda, T. Shimizu, M. Yamato, T. Okano, Advanced Materials 2007, 19, 3089.

[37] Y. Tsuda, M. Yamato, A. Kikuchi, M. Watanabe, G. P. Chen, Y. Takahashi, T. Okano, Advanced Materials 2007, 19, 3633.

[38] G. H. Hsiue, S. H. Hsu, C. C. Yang, S. H. Lee, I. K. Yang, Biomaterials 2002, 23, 457.

[39] D. Schmaljohann, Advanced Drug Delivery Reviews 2006, 58, 1655.

[40] H. van der Linden, W. Olthuis, P. Bergveld, Lab on a Chip 2004, 4, 619.

[41] S. R. Sershen, G. A. Mensing, M. Ng, N. J. Halas, D. J. Beebe, J. L. West, Advanced Materials 2005, 17, 1366.

[42] D. Kim, D. J. Beebe, Lab on a Chip 2007, 7, 193.

[43] L. Dong, A. K. Agarwal, D. J. Beebe, H. R. Jiang, Nature 2006, 442, 551.

Chapter 3: Conformally coated thermoresponsive microgrooves for formation of harvestable micro-constructs of a single cell type

The content of this chapter has been published in the following journal article: H. Tekin, G.O. Ince, T. Tsinman, K.K. Gleason, R. Langer, A. Khademhosseini, M.C. Demirel. Responsive microgrooves for the formation of harvestable tissue constructs. *Langmuir*, 2011, 27 (9): 5671–5679.

3.1 Introduction

Chapter-2 has introduced a generic technique to form spherical microtissues. Native tissues can also possess stripe geometries, such as cardiac and muscular tissues. This chapter describes a versatile method to fabricate stripe microtissues of a single cell type by using poly(dimethylsiloxane) (PDMS) based thermoresponsive microgrooves.

PDMS is widely used for fabrication of complex 3D or high aspect ratio microstructures and devices due to its physicochemical properties. Elasticity, ease of processing, biocompatibility, and mechanical stability of PDMS[1] makes it a desirable substrate to fabricate microdevices for biomedical applications such as cell culture[2, 3] and drug toxicity and metabolism screening[4]. Recently, PDMS has been also been used as a stretchable "organ-on-a-chip" device,[5] which could potentially replace expensive animal testing.

PDMS possesses high gas and liquid permeability coefficients due to its large free volume, and low selectivity.[1] Although this may be advantageous for a range of applications, the ability to control the permeability of PDMS surfaces is desirable to prevent the leakage of hydrophobic drugs or metabolites in drug toxicity and metabolism screening. In addition, the ability to reversibly change PDMS substrate properties may be of interest for a range of cell culture applications. Therefore, simple approaches of modifying PDMS substrates while maintaining its mechanical and optical properties are desirable.[6] Strategies for coating pores or microchannels involve vapor phase deposition of crystalline (e.g. parylene[7, 8]) or amorphous polymers (e.g. pHEMA[9]). A crystalline polymer provides a perfect high barrier for molecular penetration but it

has limited mechanical properties (e.g. stretchability) due to its high modulus (i.e. elastic modulus of 1-10 GPa). An amorphous polymer, on the other hand, is typically used on stretchable devices to complement the low modulus (i.e. 1-100 MPa) of PDMS but the molecular pores of the amorphous phase should be engineered to gain high barrier properties for moisture as well as chemicals. The latter could be achieved easily, in vapor phase coatings, by adjusting the crosslinker density of the polymer.[10]

A few studies have been conducted to fabricate tissue constructs (e.g. cell detachment,[11] mechanical conditioning and cell detachment[12]) using PNIPAAm grafted PDMS[12]. PNIPAAm is a stimuli-response polymer that undergoes a dramatic change in surface energy at its lower critical solution temperature (LCST) of approximately 32 °C. At temperatures above the LCST, PNIPAAm dehydrates, changes its conformation to a collapsed form,[13] which is suitable for cell adhesion and culture at 37 °C. Below LCST, it swells and hydrates in aqueous solution,[13] which drives cell detachment with conditioned ECM from the culture surface without disturbing cell-cell and cell-ECM interactions[14-17]. Surface-grafted PNIPAAm was also used for temperature controlled release of biofilms from the substrates.[18] Thermo-responsive substrates with microgroove patterns were fabricated to form harvestable cell sheets[19] or capillary networks[20]. Microgroove patterns can be potentially useful to align the cells along the channel direction and initiate cytoskeletal organization to form physiologically active modular tissue constructs. In these studies PNIPAAm was grafted in liquid phase on microgrooves to tune surface energy. However, conformal grafting of PNIPAAm in liquid phase was difficult to achieve. Recently, PNIPAAm based hydrogel microstructures were fabricated using a soft lithographic approach, however these microstructures exhibit temperature dependent shape changes which applies mechanical forces on the resulting tissue constructs and may deform the final aggregate shapes.[21]

Microtextured surfaces were previously coated with PNIPAAm using electron-beam polymerization in liquid phase.[20] This method has led PNIPAAm to agglomerate non-uniformly in groove patterns and caused rounded shape ridges. Overall process has produced a non-uniform PNIPAAm coating on the substrates which can adversely affect cell orientation and tissue formation within grooves. Herein, we created conformal PNIPAAm coating on PDMS using iCVD technique. iCVD is a free radical polymerization technique to produce structurally well-defined conformal polymer coatings, and therefore offers a high degree of control over the

geometry and thickness of the polymer.[10] While traditional grafting approaches require substrates that possess specific functional groups and produce films of limited thickness, the iCVD method can be applied to virtually any substrate and can result in film thicknesses ranging from a few nm to a few microns.[10, 22] The iCVD process occurs in a single step and growth rates can exceed 100 nm/min.[22] We used a growth rate of ~6 nm/min to create ~300 nm conformal PNIPAAm coating on PDMS substrates.

We showed that the conformal coating of PDMS microgrooves with PNIPAAm by using iCVD can be used to form geometrically controlled longitudinal tissue constructs and enable their further retrieval in a temperature dependent manner by exploiting the swelling/deswelling property and tunable hydrophilicity of the responsive polymer. This stimuli-responsive template can be useful in fabricating modular tissue units for tissue engineering applications and potentially integrated within microfluidic devices.

3.2 Materials and Methods

Materials

Silicon elastomer and curing agent were purchased from Dow Corning Corporation (Midland, MI). Dulbecco's phosphate buffered saline (PBS), calcein-AM and ethidium homodimer, Dulbecco's modified eagle medium (DMEM), fetal bovine serum (FBS), and penicillin-streptomycin (Pen-strep), Alexa-Fluor 594 Phalloidin were all purchased from Invitrogen (Carlsbad, CA). Glass slides and ethanol were purchased from Fisher Scientific (Fair Lawn, NJ). The monomer, N-isopropylacrylamide (NIPAAm) (97%), the initiator, Tert-butyl peroxide (TBPO) (98%, Aldrich), trichlorovinylsilane, fluorescein isothiocyanate conjugated bovine serum albumin (FITC-BSA), bovine serum albumin (BSA), TritonX-100 were all purchased from Sigma-Aldrich Chemical Company (St. Louis, MO). Paraformaldehyde was purchased from Electron Microscopy Sciences (Hatfield, PA). The crosslinker, ethylene glycol diacrylate (EGDA) (98%) was purchased from Polysciences Company (Warrington, PA). Silicon (Si) wafers were purchased from University Wafer (Boston, MA).

Fabrication of PDMS microgrooves

Silicon masters with longitudinal patterns were developed with SU-8 photolithography and used as templates to fabricate PDMS replicas. PDMS microgrooves were formed by curing a mixture of 10:1 silicon elastomer and curing agent at 70 °C for 2 h and then detached from silicon masters. The channel depth and width of the resulting PDMS microgrooves were adjusted to ~150 μm. The space between two channels was ~150 μm.

PNIPAAm coating with iCVD

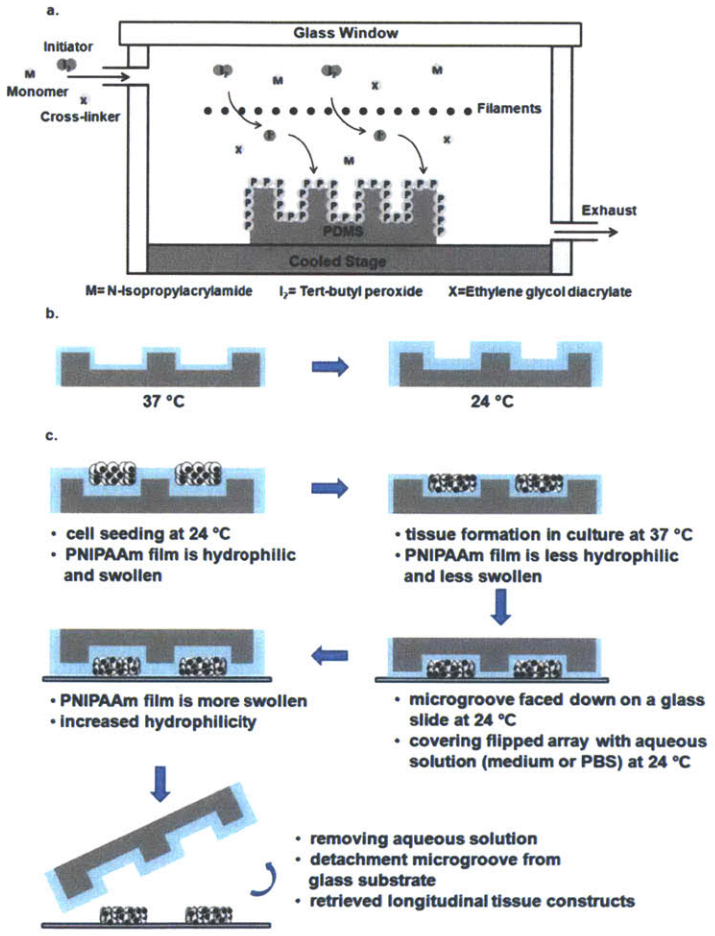

Figure 3.1. Schematic of a) PNIPAAm coating on PDMS microgrooves by chemical vapor deposition, b) swelling of PNIPAAm film on PDMS microgrooves at physiological (37 °C) and ambient temperature (24 °C), and c) formation and retrieval process of longitudinal tissue constructs.

PDMS substrates were treated before iCVD to provide covalent bonding of PNIPAAm to the surface. The PDMS surfaces were first treated with oxygen plasma for 30 seconds. After the plasma treatment the PDMS surfaces were immediately placed in an oven at 40 °C together with 5ml of Trichlorovinylsilane. The samples were kept in the oven for 4 minutes giving them sufficient time to react with silane. Following this treatment the samples were directly placed in the iCVD reactor for deposition. The iCVD of PNIPAAm were performed in a custom built deposition reactor with a base pressure of 1 mTorr as illustrated in **Figure 3.1a**. The monomer and the crosslinker were heated in separate glass jars to 75 °C and 80 °C separately and delivered into the reactor using needle valves. The initiator was kept at room temperature and delivery into the reactor was achieved by using a mass flow controller. Nitrogen gas was used as a patch flow. A filament array of 14 parallel chrome alloy filaments was used for thermal decomposition of the initiator molecules. A back-side cooled sample stage kept the temperature of the sample constant. The thickness of the deposited films was monitored in real-time using a He-Ne laser interferometry set-up, in which the laser beam entered the reactor from the top quartz window and reflected from the sample surface. The thickness measurements were performed on Si-wafers that were located next to PDMS samples in the reactor. The thickness of the film was calculated from the beam intensity oscillations. The iCVD deposition of 300 nm thick PNIPAAm was performed at 100 mTorr pressure and the sample and filament temperatures were kept constant at 30 °C and 250 °C, respectively. The flow rates of NIPAAm, EGDA, TBPO and N_2 were maintained at 5, 1, 1, 1 sccm respectively. At these conditions the growth rate was ~6 nm/min. PNIPAAm reacts with the vinyl bonds of the silane on PDMS surface. Without silane treatment, PNIPAAm can form a conformal thin film without covalent bonding which has weaker adhesion compared to the silanized surface.

Characterization

Surface modification of PNIPAAm deposited PDMS surface was analyzed by Fourier Transform Infrared Spectroscopy with attenuated total reflection (FTIR-ATR). The spectra were recorded by using a Bruker Alpha FTIR. Uncoated PDMS surface was used as control. Chemical characterization of the deposited films on Si-wafer was done using a Nexus 870 FTIR (Thermo Nicolet) equipped with a DTGS-TEC detector. The spectra were acquired at 4 cm^{-1} resolution

and the number of scans was kept at 128. The spectrum of a bare Si wafer was used as the background.

Scanning electron microscopy

PNIPAAm coated microgrooves were dried at room temperature. The samples were subsequently mounted onto aluminum stages, sputter coated with gold and analyzed under scanning electron microscopy (SEM) (JEOL JSM 6060) at a working distance of 4 mm.

Atomic Force Microscopy

Surface topography of uncoated and PNIPAAm coated PDMS samples was determined by using an atomic force microscope (AFM) (Nanoscope V, Veeco Inc.). AFM images were obtained in tapping mode using rectangular shaped silicon nitride cantilevers. The root mean square (rms) value of the surface roughness for flattened images was quantified by using the software equipped with Nanoscope V.

Contact angle measurement and swelling test

Static contact angle measurements was performed with deionized water (10 μl droplet) using a contact angle measuring instrument (FTA 1000B, First Ten Angstroms Inc. Portsmouth, VA). To analyze the swelling properties, Si wafers were coated with ~300 nm PNIPAAm; water swelling of the PNIPAAm films was then monitored in real-time using an interferometry set-up (J.A. Woollam Inc., Lincoln, NE).

Cell culture

NIH-3T3 fibroblasts were cultured in medium containing 89% DMEM, 10% FBS, and 1% Penicillin-Streptomycin and passaged every 3 days. Cells were maintained at 37 °C in a 5% CO_2 humidified incubator.

Cell adhesion and protein adsorption on PNIPAAm coated PDMS surfaces

PNIPAAm coated PDMS surfaces, bare PDMS surface, and bare glass slide were rinsed with ethanol, and kept in PBS until cell seeding. NIH-3T3 fibroblasts were trypsinized and prepared

in culture medium. All samples were immersed in 6 mL of a cell solution containing 2.5 x 10^5 cells/mL. Cell adhesion on PNIPAAm coated surfaces were performed at 37 °C for 2 h and 24 °C for 2 h while bare PDMS surface and glass slide were only subjected to 37 °C for 2 h. After incubation at experimental temperatures, all samples were dipped into PBS to remove non-adherent cells. Samples were visualized with an inverted microscope (Nikon Eclipse TE2000-U) and adherent cells were counted.

FITC-BSA was dissolved in PBS at a density of 25 μg/ml. To test the protein adsorption to PNIPAAm coated PDMS surfaces, bare PDMS surface, and bare glass slide, 200 μL of the protein solution was evenly distributed on the surfaces. PNIPAAm coated surfaces were incubated at 37 °C for 2 h and 24 °C for 2 h while bare PDMS surface and glass slide were only subjected to 37 °C for 2 h. After incubation, samples were washed with PBS and analyzed under an inverted fluorescent microscope (Nikon Eclipse TE2000-U). Fluorescent images were analyzed using ImageJ software.

Cell seeding on microgrooves and formation of longitudinal tissues

PNIPAAm coated microgrooves were placed in 6 well culture plates after fabrication, rinsed with ethanol, and kept in PBS until cell seeding. NIH-3T3 fibroblasts were trypsinized and prepared in culture medium. Microgrooves were kept at room temperature for at least 30 min to make the surface hydrophilic for a better cell-seeding condition at 24 °C. After aspirating PBS from each 6 well plate, a suspension of NIH-3T3 fibroblasts was seeded on each microgroove array at a density of ~2.7 x 10^5 cells/cm^2 and kept at ambient temperature for 20 min to drive spreading of the cell suspension on the surface. Subsequently, microgroove arrays were gently washed with PBS to remove undocked cells on the microgroove surface and immersed in fresh culture medium. Seeded microgroove arrays were kept in a 5% CO_2 humidified incubator at 37 °C for 3 days. Microscope images were taken daily to analyze longitudinal tissue formation in the microgrooves.

To analyze cytoskeletal organization in microgrooves after 3 days of incubation, F-actin fibrils in the cells within formed tissue constructs were stained with phalloidin. Samples were first fixed with 4% paraformaldehyde for 10 min at room temperature and then rinsed two times with PBS. Cells were permeabilized with 0.1% TritonX-100 for 5 min at room temperature and washed two

times with PBS. Samples were then incubated in a PBS solution containing 1% BSA and Alexa-Fluor 594 Phalloidin (1:40 dilution in PBS after dissolving stock powder in 1.5 mL methanol) for 1 h at room temperature. Samples were finally washed three times with PBS and visualized under an inverted fluorescent microscope (Nikon Eclipse TE2000-U).

Live/dead staining

Live/dead solution was prepared with 2 mM of calcein-AM and 4 mM of ethidium homodimer in PBS. For live and dead evaluation, each microgroove was placed in live/dead solution during deposition on a glass substrate for a maximum of 30 min at 24 °C or 37 °C. Live cells were stained by Calcein AM with fluorescent green color while homodimer stained dead cells with fluorescent red color. Cells were analyzed under an inverted microscope (Nikon Eclipse TE2000-U).

Retrieval of modular longitudinal tissue constructs

After culturing cell-seeded microgroove arrays for 3 days, longitudinal tissue constructs were retrieved from the microgrooves by deposition of the arrays on glass slides as shown in **Figure 3.1c**. For release experiments at 24 °C, microgroove arrays (n=3) were gently placed on a glass slide and immersed in 24 °C PBS for 30 min with the grooves facing down. Control experiments for microgroove arrays (n=3) with the same method were performed at 37 °C for 30 min to test whether the temperature was the main driving force in releasing the tissue constructs from the microgrooves. For control experiments at 37 °C, microgrooves were covered with 37 °C PBS. Phase images for each sample were taken using an inverted microscope (Nikon Eclipse TE2000-U). Approximate lengths of retrieved tissue constructs were measured with Spot Advanced software to determine the frequency of tissue lengths for released modular tissue constructs from PNIPAAm coated microgrooves at 24 °C.

Statistical analysis

Data was shown as the mean and ± standard deviation (±sd). Statistical analysis was performed with an unpaired student's t-test and $p < 0.05$ was considered as significant.

3.3 Results and Discussion

PNIPAAm coating on PDMS substrates

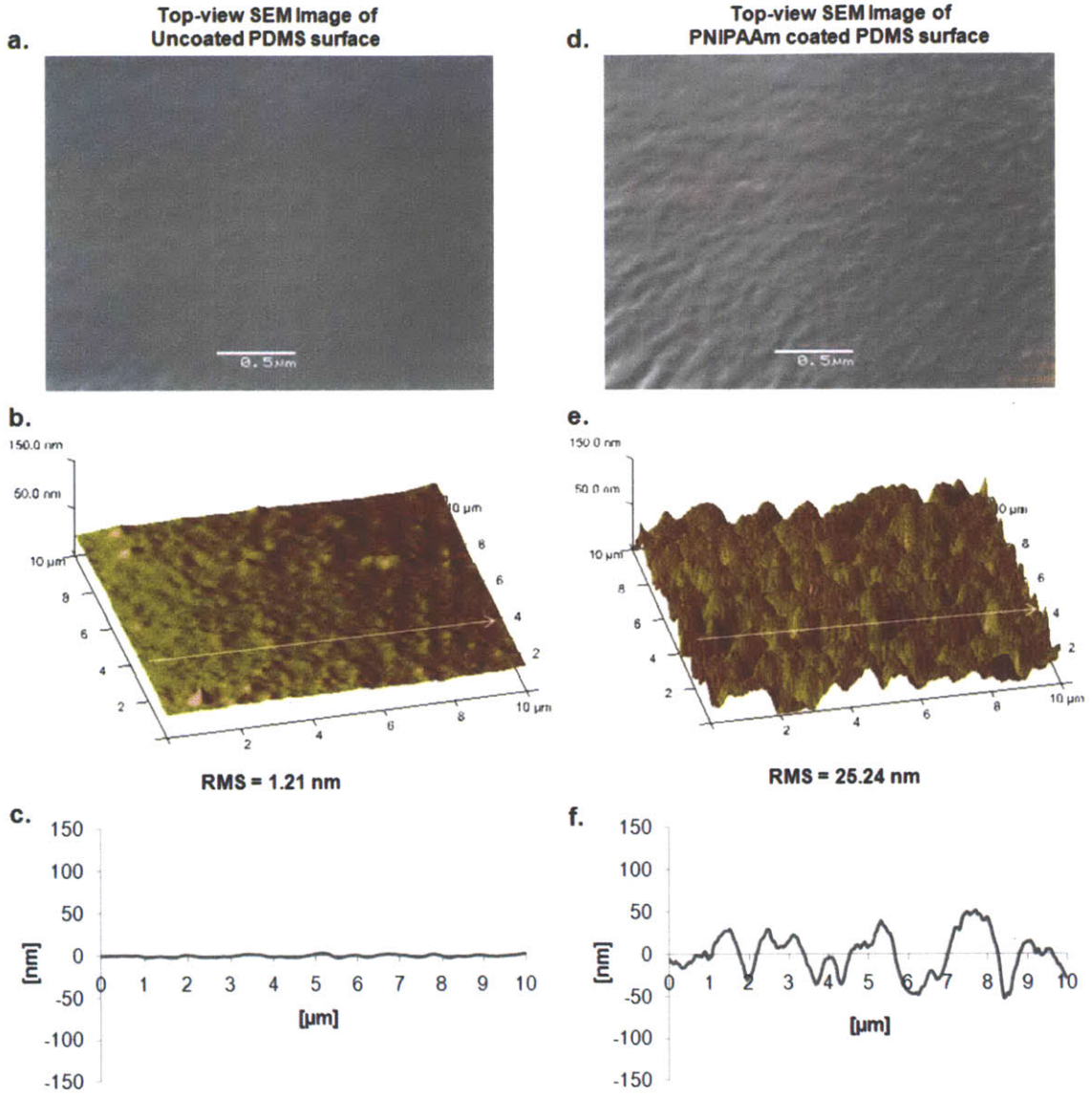

Figure 3.2. SEM and AFM images of coated and uncoated PDMS surfaces and their surface analysis. a) SEM image and b) AFM image showing surface topography of uncoated PDMS surface. Surface analysis for flattened AFM image of bare PDMS surface gives RMS value of 1.21 nm. c) Height change for uncoated PDMS surface through arrow direction. d) Scanning electron microscopy image and e) AFM image showing surface topography of PNIPAAm coated PDMS surface. Surface analysis for PNIPAAm coated PDMS surface exhibits RMS value of 25.24 nm. f) Height change over the topography of PNIPAAm coated PDMS surface through arrow direction.

PNIPAAm coating on PDMS substrates with iCVD method was performed in a custom built deposition reactor as illustrated in **Figure 3.1a**. The as-deposited thickness of the responsive film was adjusted to be ~300 nm. The coating thickness on the samples varied ±10 nm, while thickness variation among 4 samples was ± 20 nm. The swelling of the responsive film was observed as illustrated in **Figure 3.1b**. To observe the effect of PNIPAAm coating on surface roughness, SEM and tapping mode AFM images were taken for bare PDMS surface (**Figure 3.2a-b**) and PNIPAAm coated PDMS surface (**Figure 3.2d-e**). Top-view SEM images, AFM images and plots of corresponding height change (**Figure 3.2c and 3.2f**) showing surface topographies demonstrated that PNIPAAm coating on the surface caused increased roughness. RMS values reveal the degree of surface roughness. RMS value of PNIPAAm coated PDMS surface (25.24 nm) is significantly higher than bare PDMS surface (1.21 nm), suggesting that PNIPAAm coating on PDMS surfaces were more rough compared to bare PDMS substrates.

We also analyzed the chemical properties of PNIPAAm deposition using FTIR characterization. **Figure 3.3a** shows the FTIR spectra of the PNIPAAm coated PDMS surfaces as well as non-coated PDMS substrates. FTIR peaks for the PNIPAAm coated surfaces show O-H stretching at 3700-3050 cm^{-1} for NIPAAm as well as C=O stretching 1750-1690 cm^{-1} for EGDA. **Figure 3.3b** shows the FTIR spectra of PNIPAAm deposited Si-wafer. We note that the absence of peaks in **Figure 3.3b** due to unsaturated carbon at 1640-1660 cm^{-1} for PNIPAM indicates the complete reaction of the vinyl bonds, thus complete polymerization.

To test the changes in surface energy under temperature transformation from 24 °C and 37 °C, static contact angle measurements were performed for PNIPAAm coated substrates. Interestingly, contact angle at 24 °C was measured to be 30° ± 2, while it was 50° ± 1 at 37 °C. Also, contact angle for bare PDMS surface at 24 °C was measured to be 96° ± 4. It was previously shown that contact angle values for bare PDMS do not change significantly between ambient and physiological temperatures.[23] We also tested the repeatability of temperature dependent wettability of PNIPAAm films at 24 °C and 37 °C. The results showed a substantial reversibility for 3 cycles of quick temperature transformations between 24 °C and 37 °C (**Figure 3.3c**). Furthermore, we observed that volumetric swelling of PNIPAAm film at 24 °C was approximately three times greater than at 37 °C. This observation correlates with recent experiments in which it was shown that PNIPAAm coated Si-wafer with iCVD exhibited 3 times

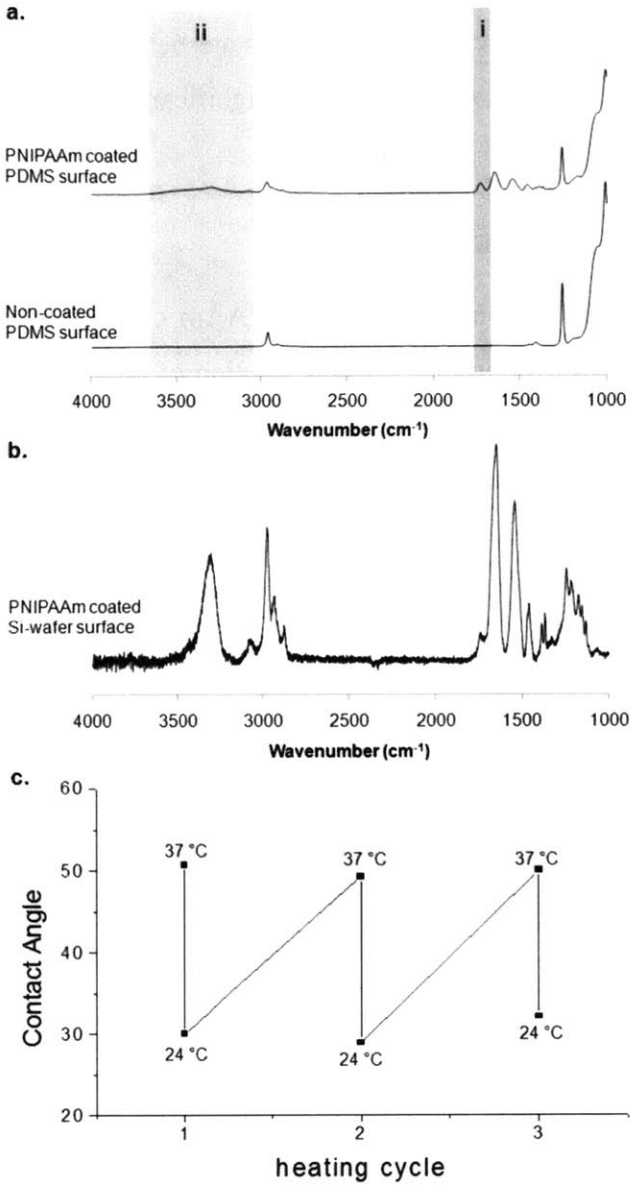

Figure 3.3. Chemical characterization and contact angle measurements for PNIPAAm coating. a) The FTIR spectra for iCVD PNIPAAm on PDMS (top) and bare PDMS (bottom). The shaded regions correspond to (i) C=O stretching at 1750-1690 cm^{-1} for EGDA and (ii) O-H stretching at 3700-3050 cm^{-1} for NIPAAm. Additionally, the amide I (~1660 cm^{-1}) and amide II (~1530 cm^{-1}) bands are visible in both iCVD coated PDMS and in b) FTIR spectra for iCVD PNIPAAm on a Si-wafer substrate. The absence of peaks due to unsaturated carbon at 1640-1660 cm^{-1} for PNIPAM shows the complete reaction of the vinyl bonds. c) Contact angle results for PNIPAAm film for 3 cycles of quick temperature changes between 24 °C and 37 °C.

thickness change in swollen state compared to dry state below LCST.[22] Conformal PNIPAAm coating on silicon based substrates demonstrated a significant swelling change and an increased hydrophilicity at room temperature.

Cell adhesion and protein adsorption

To test the cell adhesion on various surfaces, PNIPAAm coated PDMS surfaces, bare PDMS surface, and bare glass slide were immersed in a solution of NIH-3T3 fibroblasts containing 2.5 x 10^5 cells/mL. Cells adhesion on PNIPAAm coated PDMS surface at 24 °C was significantly less than the control experiments with the same surface and bare PDMS at 37 °C (**Figure 3.4a**).

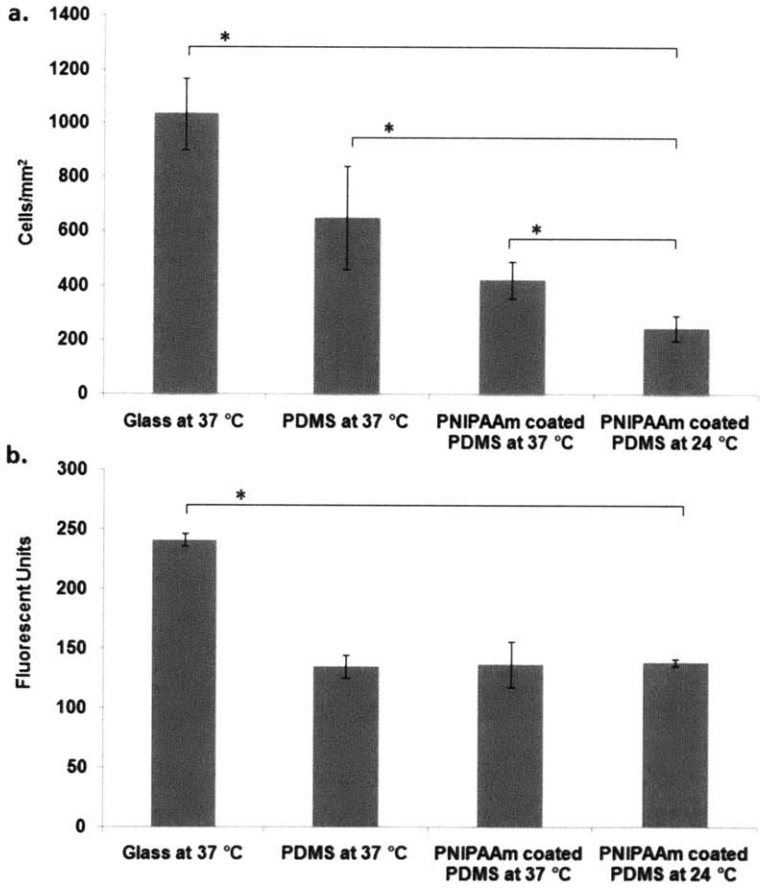

Figure 3.4. Characterization of a) cell adhesion and b) protein adsorption on 300 nm of PNIPAAm coated 2D PDMS surfaces for 2h incubation at 37 °C and at 24 °C and comparison with adhesion on bare PDMS and glass surfaces. * shows statistically significant difference in variance ($p < 0.05$).

Contact angle results indicate that PNIPAAm coated PDMS surfaces had a higher degree of hydrophilicity at 24 °C, which may contribute to a lower level of cell adhesion. It was also previously shown that hydrophilic PNIPAAm surfaces drove the cell detachment from the substrate.[14-17] Another contributing factor to a lower degree of cell adhesion may be due to the increased swelling of the PNIPAAm film on the surface at 24 °C compared to 37 °C. Interestingly, no significant difference was observed between the number of adhered cells to PNIPAAm coated or non-coated PDMS substrates at 37 °C. Both surfaces were hydrophobic at this temperature. Hydrophobic substrates are attractive for protein adsorption and subsequent cell adhesion.[24-29] We hypothesize that the adsorption of proteins such as fibronectin from FBS on hydrophobic surfaces may have caused the same tendency of cell adhesion on these substrates. In addition, cells adhered to glass surface at 37 °C at significantly higher values than all other surfaces.

The protein adsorption on PNIPAAm coated PDMS surfaces, bare PDMS surface, and bare glass slide was analyzed by quantifying the fluorescent expression of these surfaces after exposure to fluorescently labeled protein. As shown in **Figure 3.4b**, no significant difference was observed between the degrees of FITC-BSA adsorption on PNIPAAm coated PDMS surface at 24 °C and at 37 °C, although swelling of PNIPAAm film on PDMS surface at 24 °C was more than 37 °C. This suggests that proteins adsorbed on PNIPAAm coatings at both temperatures. Interestingly, protein adsorption at 37 °C on bare PDMS surface was similar to PNIPAAm coated PDMS surface. It was previously reported that proteins may physically adsorb on PDMS with hydrophobic interactions between the protein and PDMS surface.[23] In this study, PNIPAAm film was somewhat swollen at 37 °C. We hypothesize that, for adhesion on PDMS at 37 °C, proteins may have physically adsorbed on PDMS with hydrophobic interactions and in the case of PNIPAAm coated PDMS, proteins may have diffused into PNIPAAm coated PDMS through the somewhat hydrated PNIPAAm chains at 37 °C and adsorbed on PDMS substrate with hydrophobic interactions. We also hypothesize that proteins may have diffused into swollen PNIPAAm film at 24 °C and physically adsorbed onto PDMS layer through hydrophobic interactions. In addition, the fluorescent expression of glass slide at 37 °C was significantly higher than all other substrates.

Cell seeding and formation of longitudinal tissue constructs within PNIPAAm deposited microgrooves

Microfabricated platforms were previously shown to be useful for 3D cell culture with controlled alignment and longitudinal tissue formation.[30-35] This study shows PDMS microgroove patterns functionalized with the deposition of a thermo-responsive polymer and their use in harvestable modular tissue formation. Thermo-responsive films on the microgroove arrays exhibited swelling/deswelling property and had a tunable hydrophilicity that could be useful in controlling the microgroove surface adhesiveness for tissue formation and retrieval. Cell seeding process plays an important role to immobilize cells inside the grooves and prevent cell growth on the ridges. After fabrication, microgroove arrays were kept at room temperature for 30 min to form a swollen polymer film with increased hydrophilicity before cell seeding at 24 °C to prevent cell

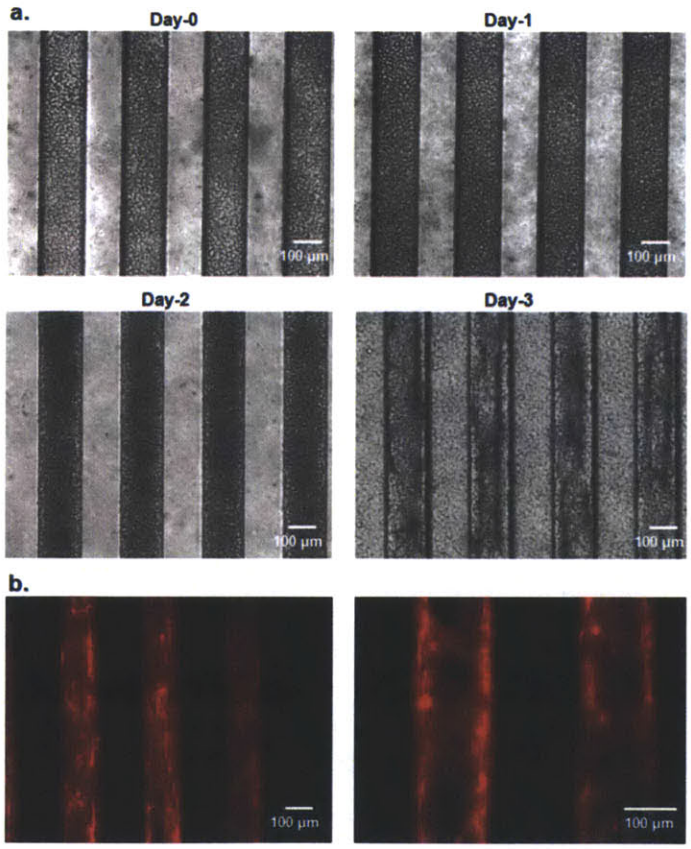

Figure 3.5. a) Seeding NIH-3T3 cells onto PNIPAAm coated microgrooves and formation of longitudinal tissue constructs. b) Phalloidin staining to visualize F-actin in tissue constructs formed within PNIPAAm coated microgrooves by day 3.

adhesion on microgroove surfaces. NIH-3T3 fibroblasts were used as the model cell type to form longitudinal tissues in the channels. To generate tissue constructs in the microgrooves, a suspension of NIH-3T3 fibroblasts were pipetted onto microgroove arrays at a density of ~2.7 x 10^5 cells/cm^2 at 24 °C. After 20 min incubation at room temperature to drive spreading of cell suspension on microgroove surfaces, arrays were gently rinsed to remove the non-adhered cells that were not inside the microgrooves. As shown in day-0 image of **Figure 3.5a**, there was no cells adhered on the ridges after the cell-seeding process. Cell seeded microgroove arrays were placed in the incubator for 3 days to form longitudinal tissues. **Figure 3.5a** shows the cell-seeding efficiency and tissue formation in PNIPAAm deposited microgrooves during the 3 day culture. After one day in culture, tightly packed cell clusters were observed in many microgrooves and by 3 days in culture longitudinal tissue fibers were visible in the majority of the grooves. Similar to two dimensional (2D) cell and protein adhesion experiments, the non-swollen state of the responsive polymer film increases cell adhesion. This contact between cells and the responsive film may increase the stability of the tissue constructs in the microgrooves.

Cell alignment within 3D culture platforms is a crucial element of recreating the tissue complexity of a number of tissues such as muscle.[33, 35] Alignment of the cells were previously achieved with either microfabricated templates[30-34] or patterning methods[35-39]. Herein, we analyzed orientation of the cells within the microgrooves after staining their F-actin fibers with phalloidin. **Figure 3.5b** illustrates cytoskeletal organization of the cells within longitudinal tissues after 3 days in culture. In the majority of the microgrooves, F-actin filaments in the cells were aligned along the direction of the grooves. Actin fiber intensity and organization show well oriented and interconnected cells within microtissues, suggesting that PNIPAAm deposited templates can be potentially useful to form tissue constructs with controlled alignment and cytoskeletal organization.

Retrieval of tissue constructs from PNIPAAm deposited microgrooves

Retrieval of longitudinal tissues is a desirable property of microfabricated culture templates. This study describes a temperature responsive strategy for tissue retrieval from PNIPAAm deposited PDMS microgrooves by exploiting swelling/deswelling property and hydrophilicity change of responsive polymer film on the substrate. As shown in **Figure 3.1c**, for the retrieval of micro

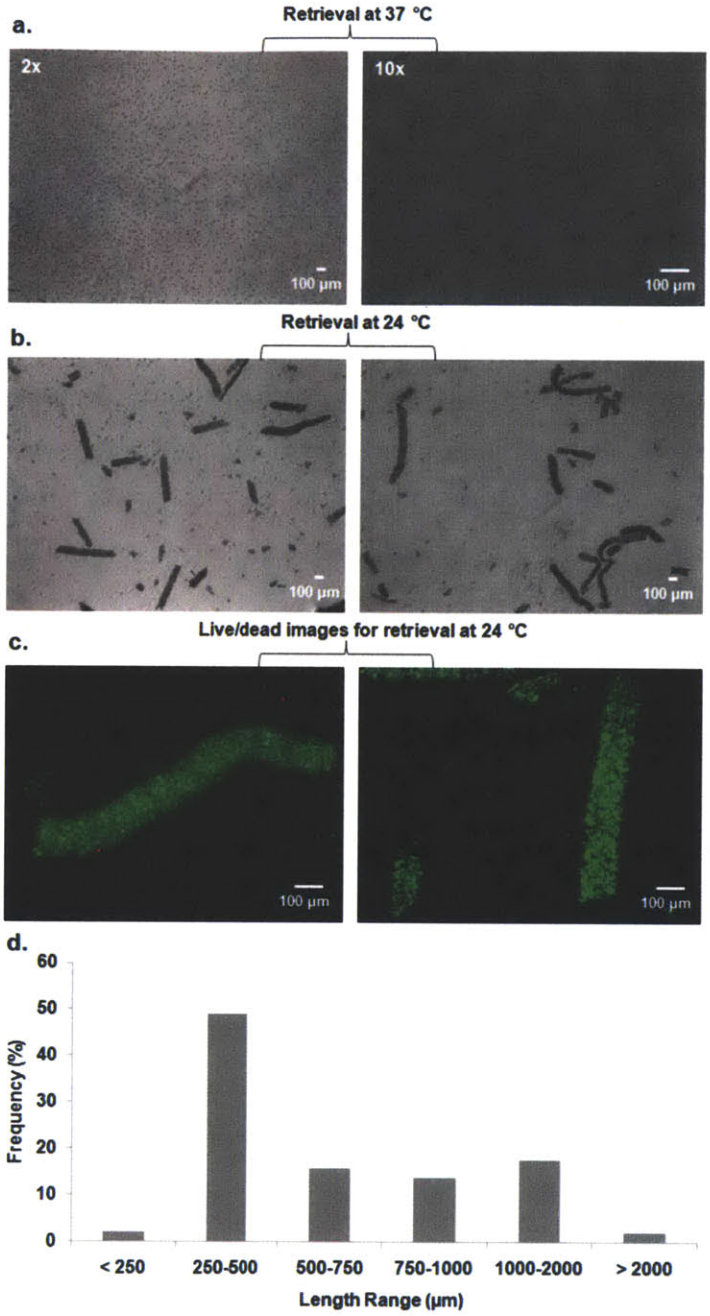

Figure 3.6. Retrieval of longitudinal tissue constructs from PNIPAAm coated microgrooves on a glass slide and frequency of length range of retrieved microtissues. a) Phase and live/dead images for control experiment at 37 °C show that only single cells were detached from PNIPAAm coated microgrooves. b) Low magnification (2x) phase contrast images of retrieved tissues from PNIPAAm microgrooves after incubation at 24 °C. c) Fluorescent images of tissue constructs with live/dead staining. d) Frequency of lengths of longitudinal tissues retrieved from PNIPAAm coated microgrooves at 24 °C.

tissues, glass slides were gently placed on the microgroove arrays, and the entire structures were flipped to initiate the detachment of tissue constructs through gravity. Inverted microgrooves were covered with PBS to keep PNIPAAm film in an aqueous environment. Retrieval experiments were performed at 24 °C and 37 °C. Microgroove arrays were incubated for 30 min at particular temperature while they were placed face down on a glass slide. After a 30 min incubation, excess solution was removed from the periphery and the microgroove arrays were gently detached from the glass surface as shown in **Figure 3.1c**.

When the retrieval experiment was performed at 37 °C, with PNIPAAm film on the surface in a hydrophilic and less swollen state, no tissue retrieval was observed from PNIPAAm deposited microgrooves (**Figure 3.6a**). In these experiments only a few individual cells were detached from the arrays as shown in **Figure 3.6a**. However, when the procedure was conducted at 24 °C while the PNIPAAm film was in a more hydrophilic and swollen state, microgrooves demonstrated a dramatic increase in retrieval of longitudinal tissues (**Figure 3.6b**). Furthermore, we observed high cell viability levels based live/dead staining images for retrieval experiments that were conducted at 24 °C (**Figure 3.6c**), suggesting that neither PNIPAAm film deposited on the substrate nor retrieval process did not adversely affect the cell viability.

Comparison between the results of control experiments at 37 °C and results of retrieval experiments at 24 °C and considering microgrooves flipped through gravity at both temperatures suggest that swelling and hydrophilicity change of PNIPAAm film on the substrate at two different temperatures is the main cause for the retrieval of the modular tissues. We hypothesize that higher hydrophilicity of the PNIPAAm film at 24 °C makes the surface undesirable for cell adhesion and initiates cell detachment and swelling of the PNIPAAm film at 24 °C compared to 37 °C changes the topography of the surface which can drive subsequent release of tissue constructs from the grooves. During retrieval experiments at 24 °C and at 37 °C, microgroove arrays were placed in an aqueous environment. Although the aqueous solution was removed before the detachment of the arrays from the glass surface, there was liquid remaining underneath the microgrooves. The detachment of the arrays from the deposition substrates may have initiated a liquid flow which may subsequently have caused hydrodynamic forces. We infer that release of singles cells at 37 °C was resulted from these hydrodynamic forces. These forces

may have disrupted the cells which were not well interconnected with tissue structures because of less cell-cell and cell-ECM contacts.

To characterize the uniformity of the retrieved modular tissues, the lengths of the retrieved tissue constructs were quantified. A wide distribution in the frequency of lengths of longitudinal tissues was observed, as shown in **Figure 3.6d**. This may be due to the hydrodynamic forces in aqueous environment occurred during the detachment of microgroove arrays from the deposition surface or due to less cell-cell and cell-ECM interactions. These modular tissues can be convenient models for cardiac tissues[37], myotubes[40], myocardium tissues[32], skeletal muscle tissues[34], and capillaries[20]. In further studies, using modular tissue engineering methods[41], it may be possible to assemble these modular tissue units into defined geometries to form more elaborate tissue constructs.

Harvesting tissue constructs from culture platforms with either digestive enzymes or mechanical scraping often causes undesirable effects on cells and their conditioned ECM.[19, 42, 43] PNIPAAm grafted culture substrates were previously used to form tissue structures and detach them from the culture surface by using switchable hydrophilicity/hydrophobicity at two different temperatures.[19, 20] However, previous coating method on microstructured substrates led to non-conformal PNIPAAm coatings.[19, 20] In this study, PNIPAAm coating with iCVD caused a conformal thin film on PDMS microgrooves which provided a desirable 3D microenvironment for structural organization of the cells to form tissue fibers. In addition, conformally coated rigid PDMS substrates provide an advantage over soft-lithographically fabricated PNIPAAm microstructures[21] in terms of stability under temperature changes because temperature dependent shape changing characteristics of soft-lithographically fabricated PNIPAAm microstructures apply mechanical forces on cell aggregates and may cause deformation on resulting tissue structures[21]. Furthermore, responsive polymer film exhibited a remarkable swelling change and an increased hydrophilicity at 24 °C compared to 37 °C. This swollen state and increased hydrophilicity of the polymer film caused subsequent retrieval of modular tissue constructs from the grooves. These properties suggest that PNIPAAm deposited PDMS microgrooves may be useful as 3D culture platforms.

3.4 Conclusions

In summary, conformal coating of PNIPAAm on the PDMS microgroove substrates is shown. We demonstrated that these responsive microgrooves can generate tissue fibers and enable their subsequent release in a temperature dependent manner. Temperature responsive film on the templates exhibited more swelling and higher hydrophilicity at room temperature compared to physiological temperature. Furthermore, the swollen state PNIPAAm film with increased hydrophilicity at room temperature initiated the retrieval of modular tissue constructs. This stimuli-responsive template can be potentially integrated with microfluidic devices and may become a versatile tool for various applications that require modular tissue formation and experimentation, such as tissue engineering and drug discovery.

3.5 References

[1] N. A. Peppas, R. Langer, Science 1994, 263, 1715.

[2] P. J. Hung, P. J. Lee, P. Sabounchi, N. Aghdam, R. Lin, L. P. Lee, Lab on a Chip 2005, 5, 44.

[3] M. S. Kim, J. H. Yeon, J. K. Park, Biomedical Microdevices 2007, 9, 25.

[4] N. N. Ye, J. H. Qin, W. W. Shi, X. Liu, B. C. Lin, Lab on a Chip 2007, 7, 1696.

[5] D. Huh, B. D. Matthews, A. Mammoto, M. Montoya-Zavala, H. Y. Hsin, D. E. Ingber, Science 2010, 328, 1662.

[6] J. N. Lee, C. Park, G. M. Whitesides, Analytical Chemistry 2003, 75, 6544.

[7] D. Wright, B. Rajalingam, J. M. Karp, S. Selvarasah, Y. B. Ling, J. Yeh, R. Langer, M. R. Dokmeci, A. Khademhosseini, Journal of Biomedical Materials Research Part A 2008, 85A, 530.

[8] G. Demirel, N. Malvadkar, M. C. Demirel, Thin Solid Films 2010, 518, 4252.

[9] G. O. Ince, G. Demirel, K. K. Gleason, M. C. Demirel, Soft Matter 2010, 6, 1635.

[10] M. E. Alf, A. Asatekin, M. C. Barr, S. H. Baxamusa, H. Chelawat, G. Ozaydin-Ince, C. D. Petruczok, R. Sreenivasan, W. E. Tenhaeff, N. J. Trujillo, S. Vaddiraju, J. J. Xu, K. K. Gleason, Advanced Materials 2010, 22, 1993.

[11] D. Ma, H. W. Chen, D. Y. Shi, Z. M. Li, J. F. Wang, Journal of Colloid and Interface Science 2009, 332, 85.

[12] E. L. Lee, H. A. von Recum, Journal of Biomedical Materials Research Part A 2010, 93A, 411.

[13] T. Okano, N. Yamada, M. Okuhara, H. Sakai, Y. Sakurai, Biomaterials 1995, 16, 297.

[14] H. E. Canavan, X. H. Cheng, D. J. Graham, B. D. Ratner, D. G. Castner, Langmuir 2005, 21, 1949.

[15] H. E. Canavan, X. H. Cheng, D. J. Graham, B. D. Ratner, D. G. Castner, Journal of Biomedical Materials Research Part A 2005, 75A, 1.

[16] A. Kushida, M. Yamato, A. Kikuchi, T. Okano, Journal of Biomedical Materials Research 2001, 54, 37.

[17] A. Kushida, M. Yamato, C. Konno, A. Kikuchi, Y. Sakurai, T. Okano, Journal of Biomedical Materials Research 1999, 45, 355.

[18] L. K. Ista, V. H. Perez-Luna, G. P. Lopez, Applied and Environmental Microbiology 1999, 65, 1603.

[19] B. C. Isenberg, Y. Tsuda, C. Williams, T. Shimizu, M. Yamato, T. Okano, J. Y. Wong, Biomaterials 2008, 29, 2565.

[20] Y. Tsuda, M. Yamato, A. Kikuchi, M. Watanabe, G. P. Chen, Y. Takahashi, T. Okano, Advanced Materials 2007, 19, 3633.

[21] H. Tekin, M. Anaya, M. D. Brigham, C. Nauman, R. Langer, A. Khademhosseini, Lab Chip 2010, 10, 2411.

[22] M. E. Alf, P. D. Godfrin, T. A. Hatton, K. K. Gleason, Macromolecular Rapid Communications 2010, 31, 2166.

[23] S. Sugiura, W. Imano, T. Takagi, K. Sakai, T. Kanamori, Biosensors & Bioelectronics 2009, 24, 1135.

[24] M. J. Lydon, T. W. Minett, B. J. Tighe, Biomaterials 1985, 6, 396.

[25] R. E. Baier, A. E. Meyer, J. R. Natiella, R. R. Natiella, J. M. Carter, Journal of Biomedical Materials Research 1984, 18, 337.

[26] J. M. Schakenraad, H. J. Busscher, C. R. H. Wildevuur, J. Arends, Journal of Biomedical Materials Research 1986, 20, 773.

[27] R. J. Klebe, K. L. Bentley, R. C. Schoen, Journal of Cellular Physiology 1981, 109, 481.

[28] D. K. Pettit, T. A. Horbett, A. S. Hoffman, Journal of Biomedical Materials Research 1992, 26, 1259.

[29] M. Yamato, C. Konno, A. Kushida, M. Hirose, M. Utsumi, A. Kikuchi, T. Okano, Biomaterials 2000, 21, 981.

[30] J. L. Charest, A. J. Garcia, W. P. King, Biomaterials 2007, 28, 2202.

[31] D. Motlagh, T. J. Hartman, T. A. Desai, B. Russell, Journal of Biomedical Materials Research Part A 2003, 67A, 148.

[32] P. Camelliti, J. O. Gallagher, P. Kohl, A. D. McCulloch, Nature Protocols 2006, 1, 1379.

[33] D. H. Kim, E. A. Lipke, P. Kim, R. Cheong, S. Thompson, M. Delannoy, K. Y. Suh, L. Tung, A. Levchenko, Proceedings of the National Academy of Sciences of the United States of America 2010, 107, 565.

[34] W. N. Bian, B. Liau, N. Badie, N. Bursac, Nature Protocols 2009, 4, 1522.

[35] H. Aubin, J. W. Nichol, C. B. Hutson, H. Bae, A. L. Sieminski, D. M. Cropek, P. Akhyari, A. Khademhosseini, Biomaterials 2010, 31, 6941.

[36] J. M. Karp, Y. Yeo, W. L. Geng, C. Cannizarro, K. Yan, D. S. Kohane, G. Vunjak-Novakovic, R. S. Langer, M. Radisic, Biomaterials 2006, 27, 4755.

[37] A. Khademhosseini, G. Eng, J. Yeh, P. A. Kucharczyk, R. Langer, G. Vunjak-Novakovic, M. Radisic, Biomedical Microdevices 2007, 9, 149.

[38] C. S. Chen, M. Mrksich, S. Huang, G. M. Whitesides, D. E. Ingber, Science 1997, 276, 1425.

[39] D. Mooney, L. Hansen, J. Vacanti, R. Langer, S. Farmer, D. Ingber, Journal of Cellular Physiology 1992, 151, 497.

[40] N. F. Huang, S. Patel, R. G. Thakar, J. Wu, B. S. Hsiao, B. Chu, R. J. Lee, S. Li, Nano Letters 2006, 6, 537.

[41] J. W. Nichol, A. Khademhosseini, Soft Matter 2009, 5, 1312.

[42] A. Kikuchi, T. Okano, Journal of Controlled Release 2005, 101, 69.

[43] H. A. Von Recum, T. Okano, S. W. Kim, P. S. Bernstein, Experimental Eye Research 1999, 69, 97.

Chapter 4: Responsive micromolds for controlling spatial distribution of multiple cell types in hydrogel microstructures

The content of this chapter has been published in the following journal article: H. Tekin, T. Tsinman, J.G. Sanchez, B.J. Jones, G. Camci-Unal, J.W. Nichol, R. Langer, A. Khademhosseini. Responsive micromolds for sequential patterning of hydrogel microstructures. *Journal of the American Chemical Society*, 2011. 133 (33): 12944–12947.

4.1 Introduction

This chapter introduces responsive micromolds to sequentially pattern hydrogel microstructures and control spatial distribution of multiple cell types within these structures. Hydrogels are readily engineered with tuned biodegradability, high permeability to oxygen or other soluble factors, and mechanical stability[1, 2] and are therefore ideal for tissue engineering[3] and drug delivery applications.[2] Micro- and nano-engineering methods have been used to fabricate shape-controlled micro- and nano-scale hydrogels to encapsulate living materials for tissue engineering and bioprocess applications[4-6] or chemicals for controlled drug delivery.[7, 8] Cell-laden hydrogels have been sequentially photopatterned to generate biomimetic microtissues.[9, 10] Multi-compartment hydrogels were also used to encapsulate and deliver drugs in a controlled manner.[11, 12] Traditionally, sequential patterning of hydrogels has relied on photolithographic methods, which are not applicable to a wide variety of polymers such as those that require thermal or ionic crosslinking.[6] Herein, we describe a simple method to sequentially pattern hydrogel microstructures by utilizing the temperature dependent shape change properties of poly(N-isopropylacrylamide) (PNIPAAm) based micromolds.

The shape of microgels can control the loading and release of the drugs[13] and the design of constructs for tissue engineering applications.[4-6, 14] Drugs can be encapsulated in multi-compartment microgels to control the release of drugs sequentially from different compartments.[11, 12] Sequentially patterned hydrogels have also been used to fabricate tissue constructs that mimic native tissue architecture.[9, 10] Microfluidic methods have been used to generate microparticles[15] or pattern microgels,[16, 17] though it is challenging to use these methods to fabricate sequentially patterned hydrogels with different shapes and the associated apparatus is

generally complex and requires multiple fabrication steps, limiting a high-throughput production. Therefore, a simple method to fabricate sequentially patterned microgels could be useful.

While photolithographic methods have been used to sequentially pattern multilayer hydrogel microstructures,[9, 10] they cannot be used with non-photocrosslinkable hydrogels. Furthermore, photoinitiators may cause cytotoxicity for applications where cells are encapsulated.[9] Micromolding is an alternative approach for forming hydrogel microstructures,[5, 6, 14] though the static nature of conventional micromolding templates inhibits sequential molding. Therefore, micromolding hydrogel microstructures with two or more spatially organized gel portions remains a challenge. This is because as one material gels there is no additional free space for subsequent gels. Herein, we exploited the thermoresponsiveness of PNIPAAm to create dynamic micromolds to overcome the static nature of conventional micromolding techniques. PNIPAAm is a temperature responsive polymer which exhibits a lower critical solution temperature (LCST) of ~32 °C.[18] PNIPAAm swells when the temperature is below its LCST and shrinks when the temperature is raised above. We utilized thermoresponsive behavior of dynamic micromolds to control spatial arrangement of multiple cell types within multicompartment hydrogel microstructures.

4.2 Materials and Methods

Materials

Agarose Type VII-A low gelling temperature, N-isopropylacrylamide (NIPAAm), N,N-methylene-bis-acrylamide (MBAAm), dimethyl sulfoxide (DMSO), photoinitiator 2-hydroxy-2-methylpropiophenone (PI), sodium hydroxide (NaOH), 3-(tri-methoxysilyl)-propyl-methacrylate (TMSPMA), Pluronic F127, and PKH26 red fluorescent cell linker kit were all purchased from Sigma-Aldrich Company (St. Louis, MO). Silicon elastomer and curing agent were obtained from Dow Corning Corporation (Midland, MI). Red polymer microspheres were supplied by Polysciences Company (Warrington, PA). Green polymer microspheres were purchased from Duke Scientific (Palo Alto, CA). Glass slides were purchased from VWR (West Chester, PA). Ethanol was supplied by Fisher Scientific (Fair Lawn, NJ). EBM-2 media for Human Umbilical Vein Endothelial Cells (HUVECs) and its components were purchased from Lonza Walkersville Inc. (Walkersville, MD). Dulbecco's Modified Eagle Medium (DMEM), Dulbecco's phosphate

buffered saline (PBS), calcein-AM and ethidium homodimer, fetal bovine serum (FBS), and penicillin streptomycin (Pen-strep) were all obtained from Gibco Invitrogen (Carlsbad, CA).

PDMS molds, PDMS slabs, and glass substrates

Silicon masters were fabricated by using standard SU-8 photolithography techniques and were used to generate poly(dimethylsiloxane) (PDMS) molds. A mixture of 1:10 of curing agent to silicon elastomer was poured on the master mold and cured for 2 h at 70 °C. Then, PDMS molds were cut into small rectangular shapes with a surface area of ~2.7 cm^2. PDMS molds had protruding patterns with shapes of stripes, circles, and squares. The depths of the stripes were ~150 μm and ~200 μm wide. The distance between two adjacent stripes was ~250 μm. The stripe PDMS molds were used to fabricate poly(N-isopropylacrylamide) (PNIPAAm) microgrooves. The depths of the cylindrical patterns were ~300 μm and their diameters were ~300 μm. Cylindrical PDMS molds were used to fabricate PNIPAAm circular microwells. The square shapes were ~300 μm on each side and ~300 μm deep. The square shaped PDMS molds were used to fabricate PNIPAAm square microwells. PDMS slabs were prepared by pouring 1:10 ratio of curing agent to silicon elastomer in polystyrene petri dishes and curing for 2 h at 70 °C. PDMS slabs were cut into rectangular shapes and immersed in a 1% (w/v) Pluronic solution in PBS for 3 h to prevent adhesion of gel precursors or cells to the PDMS slab during the formation of hydrogel microstructures. Pluronic-coated PDMS slabs were dried and stored at room temperature.

Glass slides were coated with TMSPMA to crosslink PNIPAAm to the glass surface as previously shown.[19] Glass slides were immersed in 10% (w/v) NaOH in deionized water for 12 h, and then washed with deionized water and ethanol 3 times. After cleaning, the glass slides were dried at room temperature and were subsequently treated with TMSPMA at 70 °C for 24 h. Treated slides were then rinsed with ethanol 3 times and dried at room temperature.

Fabrication of PNIPAAm micromolds

The prepolymer solution to fabricate PNIPAAm micromolds was created by mixing NIPAAm, MBAAm, DMSO, deionized water, and PI in the weight ratios of 2.18 : 0.12 : 3 : 1 : 0.15. These weight ratios were previously used to fabricate thermo-responsive microwell structures.[19] PNIPAAm prepolymer solution was stirred overnight at room temperature. The photoinitiator

was added shortly before the fabrication step. As previously reported,[19] PNIPAAm micromolds were generated with a soft lithographic method. PDMS molds were treated with plasma (PDC-001, Harric Plasma) for 1 min on high power to obtain a hydrophilic surface. Afterwards, the prepolymer solution was poured on a PDMS mold and a TMSPMA coated glass slide was immediately placed on the PDMS mold, then exposed to ultraviolet (UV) light. PNIPAAm microstructures were crosslinked with UV light of 320–500 nm wavelength at an intensity of 4 mW/cm^2 for 30 s using the OmniCure Series2000 (EXFO, Mississauga, Canada). Resulting PNIPAAm micromolds were fabricated with varying shapes such as microgrooves, circular microwells, and square microwells. The PNIPAAm micromolds were placed in 70% ethanol solution to rinse off unreacted chemicals, subsequently washed with PBS, and maintained in PBS until needed.

Responsiveness test

The responsiveness tests for PNIPAAm microstructures were conducted at 4 °C, 24 °C and 37 °C to visualize and quantify the response of microstructures under temperature changes. PNIPAAm micromolds were first subjected to 4 °C for 15 min and images were taken with an inverted microscope (Nikon Eclipse TE2000-U). Microstructures were subsequently placed at ambient temperature of 24 °C for 15 min. After taking images at 24 °C, microstructures were kept at 37 °C for 30 min, after which images were taken of all microstructures. Three samples of PNIPAAm microgroove arrays (n = 3) were fabricated; 3 images were taken of each; each image contained 3 single grooves. Three samples for each microwell type (circular or square) (n = 3) were fabricated; 9 images were taken of each sample. Each image contained one single microwell. To quantify the responsiveness of PNIPAAm micromolds, the top-view surface area of each pattern (microgroove, circular microwell, square microwell) was measured with Spot Advanced software (Spot Imaging Solutions, Sterling Heights, MI). The surface area of each pattern at each temperature was displayed as the mean value with standard deviation.

Sequential micromolding of hydrogel microstructures

Agarose solutions were prepared by heating low gelling temperature agarose until it was dissolved in PBS. For experiments in which microbeads were used, 2% (w/v) agarose in PBS was prepared at over 65 °C. Green (1.2 μm diameter) and red (2 μm diameter) microbeads were

mixed with dissolved agarose with volume ratios of 2% (v/v) and 4% (v/v), respectively. PNIPAAm micromolds were kept at 24 °C for 15 min before the experiments. To pattern the first gel, 100 μl of agarose precursor containing green microbeads was pipetted onto a PNIPAAm micromold at 24 °C and immediately a PDMS slab was pressed onto the micromold. Subsequently, the entire structure was moved to 4 °C for 15 min for rapid gelling. After 15 min, the PDMS slab was removed and the micromold containing the first patterned gel was placed at 37 °C for 30 min to allow the PNIPAAm microstructure to shrink. Then, 50-60 μl of agarose precursor containing red microbeads was pipetted on the micromold at 37 °C and a new PDMS slab was pressed onto the micromold. The entire structure was then kept at 37 °C for 30 min to crosslink the second gel. The PDMS slab was then removed and the micromold containing the two patterned microgels was immersed in PBS. Sequentially patterned hydrogels within the micromolds were imaged with an inverted fluorescent microscope (Nikon Eclipse TE2000-U). Hydrogel microstructures were harvested from the micromolds by gently flowing PBS over the surfaces of the micromolds with a pipette. Recovered microgels were then imaged with an inverted fluorescent microscope.

Cell culture

NIH-3T3 fibroblasts and human hepatoblastoma, HepG2, cells were cultured in medium containing 89% DMEM, 10% FBS, and 1% Pen-strep. HUVECs were cultured in 2% FBS supplemented EBM-2 media containing all the components from the supplement kit. All cell types were passaged every 3 days and maintained at 37 °C in a 5% CO_2 humidified incubator.

Cell encapsulation

For cell encapsulation experiments, 4% (w/v) agarose was prepared by heating low gelling temperature agarose until dissolved in PBS. Agarose solution was kept in an oven at 70 °C until used. 3T3 fibroblasts and HepG2 cells were labeled with PKH26 (red) membrane stain by following the manufacturer's protocol. 3T3 fibroblasts (red), HepG2 cells (red), and green fluorescent protein (GFP) labeled HUVECs were prepared in their culture media at a density of 40 x 10^6 cells/ml. Prior to cell encapsulation, PNIPAAm micromolds were kept at room temperature (24 °C) for 15 min. Cell suspensions were mixed with 4% (w/v) agarose solutions with a 1:1 volume ratio to give the final cell concentration of 20 x 10^6 cells/ml. 100 μl of the

hydrogel precursor containing 3T3 fibroblasts (red) was pipetted onto the microgroove and 100 µl of gel precursor containing HepG2 cells (red) was pipetted onto both circular and square microwells at 24 °C and PDMS slabs were immediately pressed onto the micromolds. All structures were subsequently moved to 4 °C for 15 min to induce rapid gelling. After 15 min, PDMS slabs were removed and micromolds were placed at 37 °C for 30 min. Subsequently, 50-60 µl of gel precursor containing GFP-HUVECs were spread on micromolds at 37 °C and new PDMS slabs were pressed onto the micromolds, which were then kept at 37 °C for 30 min to allow the second gel to crosslink. After 30 min, PDMS slabs were removed and PNIPAAm micromolds containing cell-laden microgels were immersed in culture media containing culture mediums of 3T3 fibroblasts–HepG2 cells and HUVECs with a 1:1 volume ratio. The resulting cell-laden hydrogel microstructures within the micromolds were imaged with an inverted fluorescent microscope (Nikon Eclipse TE2000-U).

For cell viability experiments, cell suspensions of 3T3 fibroblasts and HepG2 cells were mixed with 4% (w/v) agarose solutions with a 1:1 volume ratio to reach a final cell concentration of 20 x 10^6 cells/ml. After keeping PNIPAAm microstructures at 24 °C for 15 min, 100 µl of hydrogel precursor containing 3T3 fibroblasts was spread on the microgroove and 100 µl of gel precursor containing HepG2 cells was spread on both circular and square microwells at room temperature and PDMS slabs were subsequently pressed onto the micromolds. The entire structures were then moved to 4 °C for rapid gelling. After 15 min, PDMS slabs were removed and micromolds containing the cell-laden microgels were immersed in culture medium and maintained at 37 °C in a 5% CO_2 humidified incubator for 3 days.

Live/dead staining

For live/dead evaluation, micromolds were covered with a solution of 2 mM of calcein-AM and 4 mM of ethidium homodimer in PBS and incubated for 15 min at 37 °C. Calcein-AM caused green fluorescent staining in live cells while the homodimer was expressed in dead cells with red fluorescent color. Images for live/dead staining were taken with an inverted fluorescent microscope (Nikon Eclipse TE2000-U).

Statistical analysis

Data regarding the responsiveness test was shown with a mean value and a standard deviation (±sd). Statistical analysis was done with a paired student's *t*-test by considering $p < 0.05$ as significant.

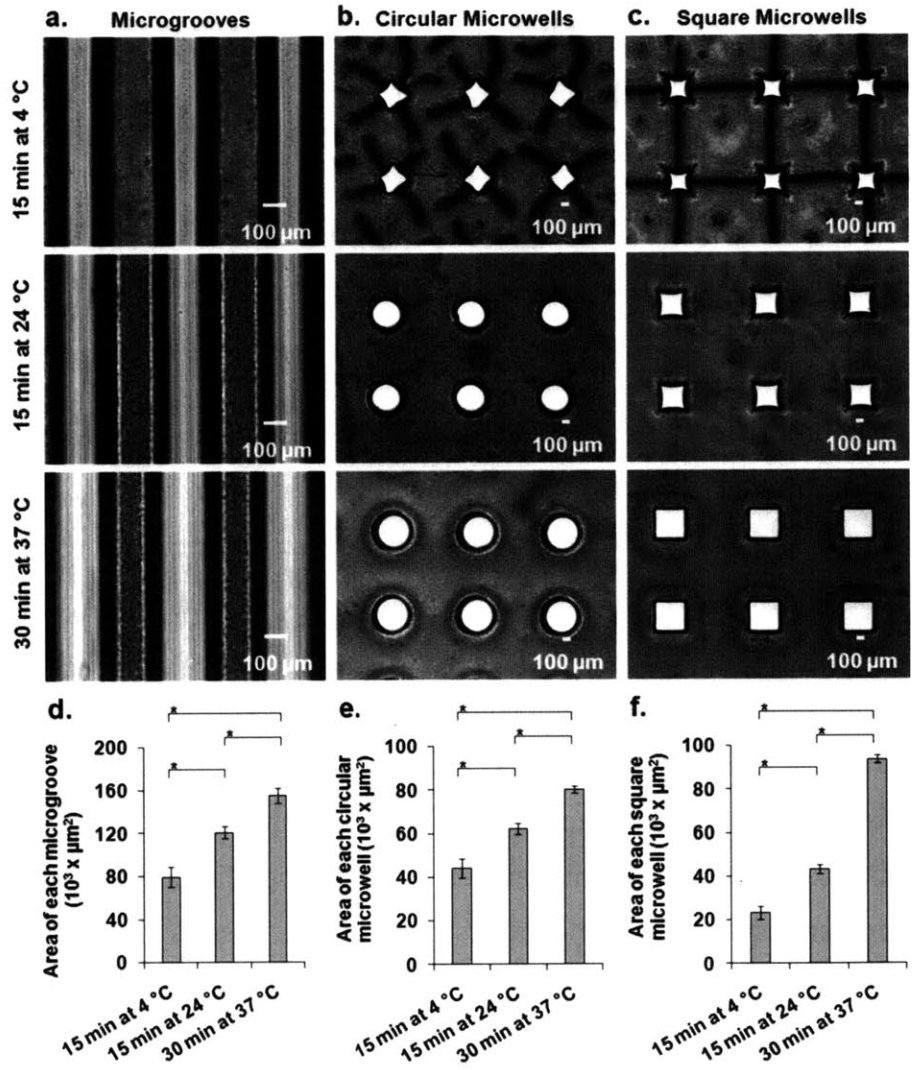

Figure 4.1. Shape responsiveness of PNIPAAm micromolds at three different temperatures. Time lapse images for a) microgrooves, b) circular microwells, and c) square microwells. Corresponding responsiveness plot based on top-viewed surface areas for d) microgrooves, e) circular microwells, and f) square microwells. * indicates a statistically significant difference in variance ($p < 0.05$).

4.3 Results and Discussion

By using a soft lithographic method,[19] we fabricated PNIPAAm micromolds with various patterns, such as microgrooves, as well as circular and square microwells. We subjected these structures to different temperatures (4 °C, 24 °C and 37 °C) to test the responsiveness. After 15 min of incubation at 4 °C, microstructured PNIPAAm stripes swelled significantly (**Figure 4.1a**). After raising the temperature from 4 °C to 24 °C, the space within the PNIPAAm stripes significantly increased within 15 min as the gels shrank (**Figure 4.1a,d**). The space within the PNIPAAm stripes further expanded (**Figure 4.1a,d**) within 30 min after changing the temperature from 24 °C to 37 °C. We also analyzed the temperature dependent shape change of circular microwells. When circular microwells were subjected to the same experimental procedure, swelling of PNIPAAm caused circular microwells to lose their circularity at 4 °C (**Figure 4.1b**). Within 15 min after changing the temperature from 4 °C to 24 °C, microwells had returned to their original circular shapes with significantly increased surface area (**Figure 4.1b,e**). Similarly, microwells retained their circularity while increasing their surface area significantly (**Figure 4.1b,e**) within 30 min following a temperature increase from 24 °C to 37 °C. Square microwell arrays were also tested in a similar manner, exhibiting non-square microwell shapes at 4 °C with reduced surface area (**Figure 4.1c**). The microwells began to return to their square shapes with a significant change in surface area (**Figure 4.1c,f**) within 15 min after changing the temperature from 4 °C to 24 °C. Microwell size increased further (**Figure 4.1c,f**) within 30 min following a temperature increase from 24 °C to 37 °C. Taken together these results show that PNIPAAm micromolds exhibited significant changes in the patterned areas at different temperatures. Therefore, these micromolds possess sufficient shape changing behavior for sequential patterning of hydrogels at different temperatures.

We demonstrated the capability of responsive micromolds for fabrication of multi-compartment hydrogels by generating sequentially patterned microstructures of agarose. Agarose is a thermo-responsive polysaccharide[20] which can be tailored to be gelled or melted at different temperatures.[21] The mechanical stiffness of agarose can be altered by varying the gelling temperature, prepolymer concentration, or curing time.[21, 22] Agarose has previously been used in various applications such as cell encapsulation,[20, 23] hydrogel microfluidics,[21] and drug delivery.[24, 25] Agarose is also biocompatible for *in vivo* applications.[26] We therefore fabricated sequentially

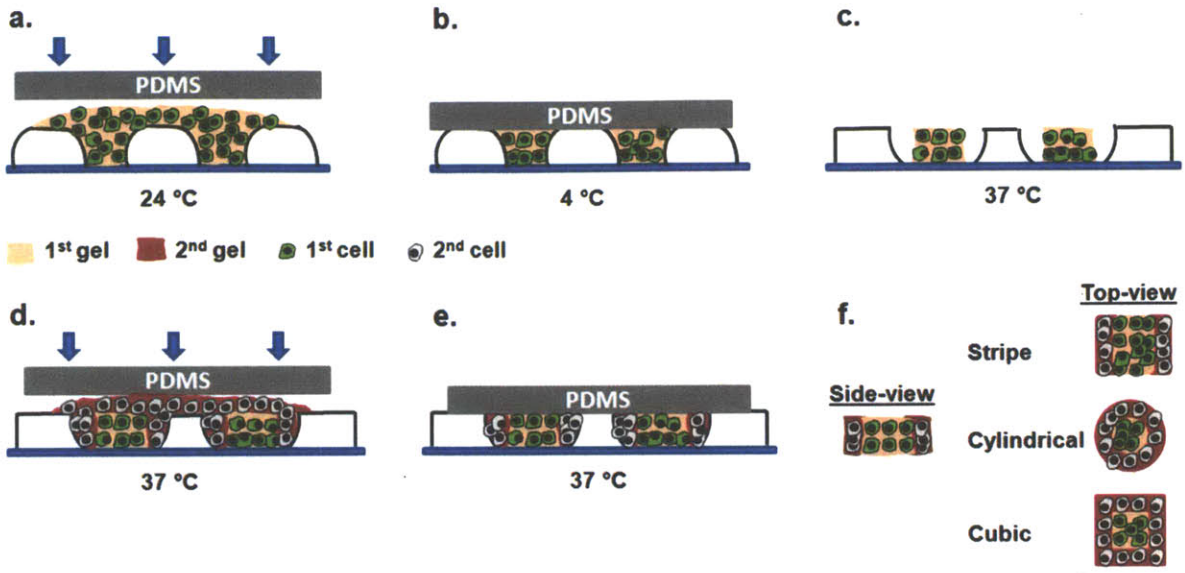

Figure 4.2. Schematic diagram of sequential patterning of hydrogel microstructures with responsive micromolds. Either fluorescent microbeads or cells (3T3 fibroblasts, HepG2 cells and HUVECs) were encapsulated within agarose microgels during fabrication process. a) The first gel precursor with encapsulated cells or microbeads was put on a responsive micromold and molded with a PDMS slab at 24 °C. b) 15 min incubation at 4 °C for crosslinking the first gel. c) 30 min incubation at 37 °C to allow responsive micromolds to shrink. d) The second gel precursor with encapsulated cells or microbeads was put on a responsive micromold and molded with a PDMS slab at 37 °C. e) 30 min incubation at 37 °C for crosslinking the second gel. f) Side and top views of resulting hydrogel microstructures

patterned agarose microstructures for potential use in biotechnological applications. To generate multi-compartment agarose microstructures, we molded agarose at two different temperatures by exploiting the temperature dependent shape changing properties of PNIPAAm based micromolds.

The schematic for sequential patterning of hydrogel microstructures is shown in **Figure 4.2**. After fabrication, responsive micromolds were first kept at 24 °C for 15 min to reach their ambient temperature shape. In our process, the prepolymer of the first gel was then placed onto a responsive micromold and molded with a flat PDMS substrate at 24 °C. The molded gel was then placed at 4 °C for 15 min to induce rapid gelling. Then, the responsive micromold

containing the first crosslinked gel was placed at 37 °C for 30 min to allow the micromold to expand, resulting in more free space. The second gel solution was then placed on the micromold and immediately pressed with a new PDMS slab at 37 °C and crosslinked for 30 min. As the micromolds have already maximized their free spaces during the first incubation at 37 °C due to

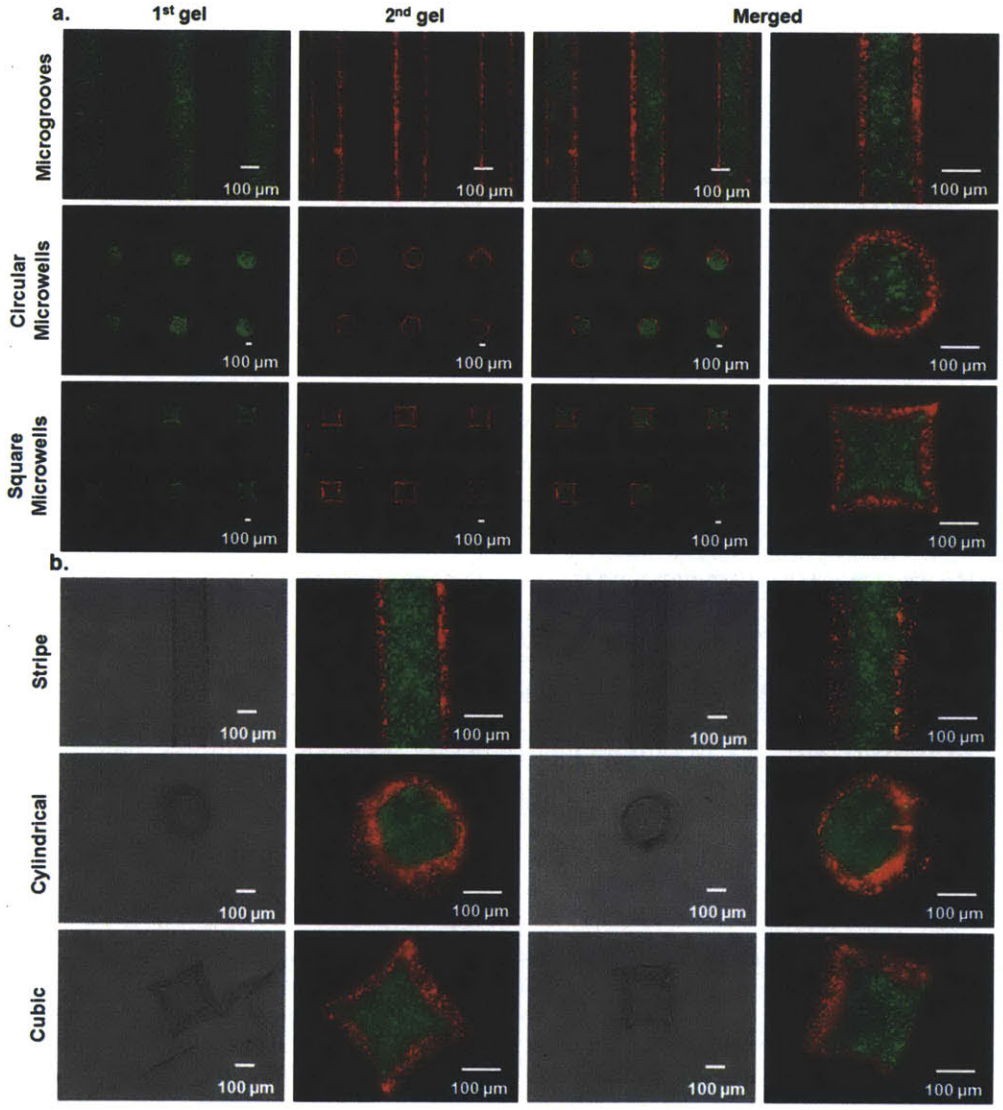

Figure 4.3. Fabrication of multicompartment hydrogels by using dynamic micromolds and their retrieval from the molds. a) Fluorescent images of sequentially molded microgels within responsive microgrooves, circular microwells, and square microwells. Green microbeads were encapsulated within the first gels and red microbeads were encapsulated within the second gels. b) Hydrogel microstructures were recovered from responsive micromolds. Phase contrast and fluorescent images for stripe microgels, cylindrical microgels, and cubic microgels.

PNIPAAm shrinking, the second incubation at 37 °C did not cause a further significant expansion in patterned areas of the micromolds. Three different sequentially patterned hydrogel microstructures were obtained with this process, particularly stripe microgels from microgroove molds, cylindrical microgels from circular microwell molds, and cubic microgels from square micromolds.

To model the encapsulation of organic materials, we encapsulated green fluorescent microbeads (1.2 μm) within the first gel and red fluorescent microbeads (2 μm) within the second gel. The first crosslinked gel roughly possessed the shape of the microgroove patterns at 24 °C and the second gel was spatially aligned parallel to the first gel by filling the free space that resulted from PNIPAAm contraction at 37 °C (**Figure 4.3a**). The resulting microstructures within the microgrooves were multi-compartment stripe microgels. For circular microwells, the first crosslinked gel had the similar circular shape of microwells at 24 °C and the second gel was molded around the first gel by keeping the free space that resulted from PNIPAAm shrinking at 37 °C (**Figure 4.3a**). Multi-compartment cylindrical microgels were fabricated by using the circular microwell molds. For square microwells, the first molded gel had a similar square-like shape of the microwells at 24 °C and second gel was spatially immobilized around the first gel pattern by obtaining a square shape at 37 °C (**Figure 4.3a**). Interestingly, the shapes of the first gels were similar to the shapes of all micromold patterns at 24 °C, suggesting that 15 min incubation at 4 °C to crosslink the first gels did not significantly affect their shape.

Resulting hydrogel microstructures were recovered from micromolds by gently flowing PBS over the micromold surfaces with a pipette. As shown in **Figure 4.3b**, stripe microgels were recovered from microgrooves and conserved their shapes and multi-compartmental structures. Multi-compartmental cylindrical microgels were also harvested from circular microwells and conserved their cylindrical geometry (**Figure 4.3b**). Harvested microgels from square microwells exhibited cubic geometry with two layers (**Figure 4.3b**). For all hydrogel microstructures, the second layer was patterned around the first gel. Therefore, this sequential micromolding process may be useful for encapsulating drugs or other organic functional materials within microgels to generate multi-compartment drug carriers or functional multi-layer microstructures.

Native tissues contain multiple spatially organized cell types within a three dimensional (3D) microenvironment.[6, 17, 27] Heterotypic cell-cell interactions and cell-matrix interactions play an

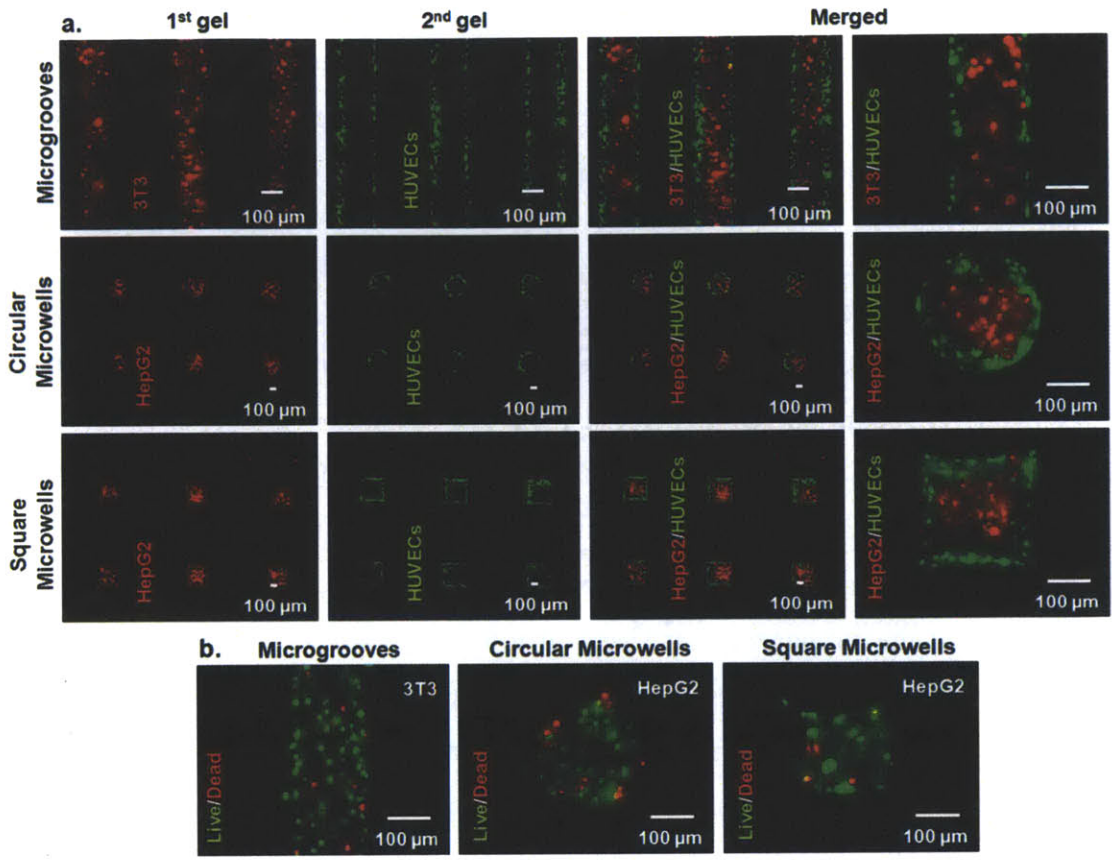

Figure 4.4. Living materials were encapsulated in agarose microgels. a) Cell encapsulated microgels were sequentially patterned with responsive micromolds. For microgrooves, agarose precursor containing 3T3 fibroblasts (red) was patterned as the first gel and gel precursor containing GFP-HUVECs was patterned as the second gel. For circular and square microwells, agarose prepolymer containing HepG2 cells (red) was patterned as the first gel and the second gel contained GFP-HUVECs. b) Fluorescent microscopy images for live/dead experiment. Microgels containing 3T3 fibroblasts were encapsulated within microgrooves while HepG2-laden microgels were within circular and square microwells.

important role in fabricating functional tissue constructs.[14, 17, 28] 3D microenvironments can be engineered with biocompatible or biodegradable hydrogels. The presented sequential micromolding technique can replicate the biological complexity of native tissues by arranging the orientation of different cell types within hydrogel microstructures. To showcase this method for tissue engineering applications, cells were encapsulated within hydrogel microstructures (20

x 10^6 cells/ml) (**Figure 4.4a**). 3T3 fibroblasts were used as one model cell type and human umbilical vein endothelial cells HUVECs were chosen as the second cell type due to their relevance in engineered vascularized tissues. 3T3 fibroblasts (red) were encapsulated in agarose molded as the first gel within microgrooves. Subsequently, GFP labeled HUVECs (green) were separately mixed with agarose which was then molded as the second gel. The second gel was finely patterned around the first gel which resulted in a stripe tissue construct containing two spatially organized cell types (**Figure 4.4a**). These cell-laden stripe microgels could be useful as models for cardiac, skeletal muscle, myoblast, and neural tissues.

For circular and square microwells, we used HepG2 cells as the first cell type and HUVECs as the second cell type. Co-culturing hepatocytes with endothelial cells resulted in an improved hepatic functionality.[28] An agarose solution containing HepG2 cells (red) was first molded within both circular and square microwells. The second gels containing GFP-HUVECs (green) were subsequently molded around the first gels. The second gels containing HUVECs were patterned around the first gels which produced circular and square shaped tissue constructs containing two spatially oriented cell types (**Figure 4.4a**). After 3 days of incubation, high cell-viability levels were observed, qualitatively suggesting that the hydrogel patterning process, the agarose precursor, and the PNIPAAm micromolds did not cause an adverse effect on cell viability (**Figure 4.4b**). These cell-laden hydrogel microstructures could be used as models of hepatic tissues. Other cell types could be substituted for 3T3 fibroblasts, HepG2 cells, and HUVECs to obtain different tissue models. These cell-laden modular tissues can further be assembled to obtain larger tissue constructs retaining the controlled microarchitecture and cell placement by using modular tissue engineering methods.[29] Furthermore, mixing agarose with proteins such as collagen can induce cell spreading,[30, 31] which could be potentially useful for fabricating vascularized tissues with our micromolding method.

For microbead or cell experiments, we observed that some excess prepolymer solutions were adsorbed within the hydrogel structure of micromolds. We also observed that wrapping of the second gel over the first gel may occur with non-flat PDMS slabs or by using the second gel precursor over desired volume (60 μl). It should also be noted that our micromolding method may require further refinements to fabricate smaller hydrogel microstructures. For example,

different PNIPAAm concentrations may be required to control the swelling/deswelling behavior of the micromold.

4.4 Conclusions

We have described a simple method, called dynamic micromolding, to sequentially pattern hydrogel microstructures by using the thermo-responsive PNIPAAm-based micromolds. The patterned surface areas of responsive micromolds increased with increased temperature. This feature was exploited to sequentially mold microgels containing two distinct layers. This technique can encapsulate different organic materials into different layers of microgels for drug delivery or functional microparticle applications. Furthermore, this method can encapsulate living materials to create biomimetic modular tissue constructs with spatially organized different cell types in a single hydrogel microstructure. In summary, these responsive micromolds could be a versatile tool in several fields, including tissue engineering, drug delivery, diagnostics, drug discovery, and 3D cell culture systems.

4.5 References

[1] R. Langer, N. A. Peppas, AIChE Journal 2003, 49, 2990.

[2] N. A. Peppas, J. Z. Hilt, A. Khademhosseini, R. Langer, Advanced Materials 2006, 18, 1345.

[3] R. Langer, J. P. Vacanti, Science 1993, 260, 920.

[4] A. P. McGuigan, M. V. Sefton, Proceedings of the National Academy of Sciences of the United States of America 2006, 103, 11461.

[5] G. T. Franzesi, B. Ni, Y. B. Ling, A. Khademhosseini, Journal of the American Chemical Society 2006, 128, 15064.

[6] M. D. Tang, A. P. Golden, J. Tien, Journal of the American Chemical Society 2003, 125, 12988.

[7] A. S. Hoffman, Advanced Drug Delivery Reviews 2002, 54, 3.

[8] J. Y. Kelly, J. M. DeSimone, Journal of the American Chemical Society 2008, 130, 5438.

[9] V. A. Liu, S. N. Bhatia, Biomedical Microdevices 2002, 4, 257.

[10] Y. A. Du, M. Ghodousi, H. Qi, N. Haas, W. Q. Xiao, A. Khademhosseini, Biotechnology and Bioengineering 2011, 108, 1693.

[11] Y. J. An, J. A. Hubbell, Journal of Controlled Release 2000, 64, 205.

[12] P. F. Kiser, G. Wilson, D. Needham, Journal of Controlled Release 2000, 68, 9.

[13] D. A. Edwards, J. Hanes, G. Caponetti, J. Hrkach, A. BenJebria, M. L. Eskew, J. Mintzes, D. Deaver, N. Lotan, R. Langer, Science 1997, 276, 1868.

[14] J. Yeh, Y. B. Ling, J. M. Karp, J. Gantz, A. Chandawarkar, G. Eng, J. Blumling, R. Langer, A. Khademhosseini, Biomaterials 2006, 27, 5391.

[15] W. J. Jeong, J. Y. Kim, J. Choo, E. K. Lee, C. S. Han, D. J. Beebe, G. H. Seong, S. H. Lee, Langmuir 2005, 21, 3738.

[16] S. Chung, R. Sudo, P. J. Mack, C. R. Wan, V. Vickerman, R. D. Kamm, Lab on a Chip 2009, 9, 269.

[17] C. P. Huang, J. Lu, H. Seon, A. P. Lee, L. A. Flanagan, H. Y. Kim, A. J. Putnam, N. L. Jeon, Lab on a Chip 2009, 9, 1740.

[18] C. D. H. Alarcon, S. Pennadam, C. Alexander, Chemical Society Reviews 2005, 34, 276.

[19] H. Tekin, M. Anaya, M. D. Brigham, C. Nauman, R. Langer, A. Khademhosseini, Lab on a Chip 2010, 10, 2411.

[20] H. Uludag, P. De Vos, P. A. Tresco, Advanced Drug Delivery Reviews 2000, 42, 29.

[21] Y. Ling, J. Rubin, Y. Deng, C. Huang, U. Demirci, J. M. Karp, A. Khademhosseini, Lab on a Chip 2007, 7, 756.

[22] P. Aymard, D. R. Martin, K. Plucknett, T. J. Foster, A. H. Clark, I. T. Norton, Biopolymers 2001, 59, 131.

[23] K. S. Jones, M. V. Sefton, R. M. Gorczynski, Transplantation 2004, 78, 1454.

[24] B. O. Haglund, S. M. Upadrashta, S. H. Neau, M. A. Cutrera, Drug Development and Industrial Pharmacy 1994, 20, 947.

[25] J. Y. Wang, Z. H. Wang, J. Gao, L. Wang, Z. Y. Yang, D. L. Kong, Z. M. Yang, Journal of Materials Chemistry 2009, 19, 7892.

[26] B. Rahfoth, J. Weisser, F. Sternkopf, T. Aigner, K. von der Mark, R. Brauer, Osteoarthritis and Cartilage 1998, 6, 50.

[27] C. B. Weinberg, E. Bell, Science 1986, 231, 397.

[28] S. N. Bhatia, U. J. Balis, M. L. Yarmush, M. Toner, Faseb Journal 1999, 13, 1883.

[29] J. W. Nichol, A. Khademhosseini, Soft Matter 2009, 5, 1312.

[30] A. Batorsky, J. H. Liao, A. W. Lund, G. E. Plopper, J. P. Stegemann, Biotechnology and Bioengineering 2005, 92, 492.

[31] T. A. Ulrich, A. Jain, K. Tanner, J. L. MacKay, S. Kumar, Biomaterials 2010, 31, 1875.

Chapter 5: Controlling spatial organization of multiple cell types in defined 3D geometries

Some parts of this chapter have been published in the following journal article: H. Tekin, J.G. Sanchez, C. Landeros, K. Dubbin, R. Langer, A. Khademhosseini. "Controlling spatial organization of multiple cell types in defined 3D geometries". *Advanced Materials*, 2012, *In Press*. (DOI: 10.1002/adma.201201805)

5.1 Introduction

This chapter introduces a simple method to pattern multiple cell types in a spatially controlled manner within predefined microenvironments. Spatial distribution of cells and interactions between neighboring cells in native microenvironments are of fundamental importance in determining cell fate decisions, such as differentiation, migration, and growth.[1-7] These interactions also serve an important role in developmental biology, organ development, tissue hemostasis, and cancer.[8-10] All these processes occur in various complex architectural organizations. Controlling the spatial distribution of different cell types in defined geometries can replicate these intricate native organizations, which can lead to useful models for several fields.

Native tissues are made of complex architectural organizations of multiple cell types. Parenchymal and non-parenchymal cells generate homotypic and heterotypic cell interactions which all regulate tissue and organ functions.[5,6,10] Tissue geometry also takes a role in cell fate decision and overall functions of an organ.[1,4,7,10] Spatial and geometrical distribution of different cells is also crucial in embryonic development.[9,11,12] Interplay between different spatially organized germ layers[9] and interactions of stem cells and surrounding stromal cells in defined microenvironments regulate stem cell differentiation into particular phenotypes; all of these associations eventually lead to organogenesis and tissue specification.[11,12] In addition, the intricate interactions between epithelial and mesenchymal layers are of importance in creating tissue architectures and organ development.[10] Tissue complexity can also be found in the tumor microenvironment in which heterotypic interactions between various spatially arranged cell types

regulate tumor growth, invasion, and metastasis.[8] Mimicking these complex cell-cell interactions *in vitro* can thus be used to understand the processes involved in developmental biology, tissue homeostasis and pathologies such as cancer or be applied to tissue engineering and regenerative medicine.

Microfluidic devices have been previously utilized to replicate such complex cell-cell interactions in defined microenvironments, though it is challenging to use these devices to pattern multiple cell types with different spatial arrangements, and the associated device fabrication and cell seeding process are complex and tedious, inhibiting the high-throughput production.[13-15] Stencils[12,16] and micromechanical substrates[2] were also utilized to pattern multiple cell types, but these methods require subsequent manipulations and change of substrates at each step which is cumbersome and challenging to generate different shapes of patterns. In another approach, cell membranes were modified to promote their attachment to different cells to form cell aggregates,[3] though it is challenging to control the geometry of the tissues and spatial distribution of multiple cell types by using this method. Microstructures with different geometries were used to create microtissues of one cell type.[17-19] The static nature of the microstructures inhibits sequential patterning of multiple cell types within a single geometry. Given previous efforts, a simple method to control spatial distributions of multiple cell types within defined microenvironments would be highly useful.

Herein, we introduce a simple patterning method to control spatial arrangements of multiple cell types in defined geometries by utilizing the shape changing properties of poly(N-isopropylacrylamide) (PNIPAAm)-based dynamic microstructures. PNIPAAm is a thermoresponsive polymer possessing a lower critical solution temperature (LCST) of ~32 °C which goes to swollen state below LCST and turns to shrunken state above LCST.[20,21] PNIPAAm has been previously used to coat cell culture platforms and to fabricate hydrogel-based templates, largely with the purpose of generating cell based tissue constructs.[21] In one of our earlier studies, we have fabricated PNIPAAm-based microwells in order to develop harvestable microtissues.[22] In a later study, we have shown the first time use of thermoresponsive micromolds for fabricating multicompartment hydrogels of non-photocrosslinkable materials, which has previously been challenging by using conventional static micromolding techniques and photolithographic methods.[23] These hydrogels have also been

shown to encapsulate either different particles or multiple cell types within different compartments.[23] However, it is challenging to control the proximity between different cells and the resulting cell-cell interactions within hydrogel systems. Controlling cell-cell interactions in defined microenvironments can better recapitulate multicellular organizations. In this study, we utilized PNIPAAm-based dynamic microwells to pattern multiple cell types in a spatially controlled manner to obtain multi-layered aggregates with controlled cell-cell interactions.

5.2 Materials and Methods

Materials

N-isopropylacrylamide (NIPAAm), N,N-methylene-bis-acrylamide (MBAAm), dimethyl sulfoxide (DMSO), photoinitiator 2-hydroxy-2-methylpropiophenone (PI), sodium hydroxide (NaOH), 3-(tri-methoxysilyl)-propyl-methacrylate (TMSPMA), were all obtained from Sigma-Aldrich Company (St. Louis, MO). Curing agent and silicon elastomer were supplied by Dow Corning Corporation (Midland, MI). Glass slides were supplied by VWR (West Chester, PA). Ethanol was purchased from Fisher Scientific (Fair Lawn, NJ). EBM-2 media for Human Umbilical Vein Endothelial Cells (HUVECs) and its supplementary components were supplied by Lonza Walkersville Inc. (Walkersville, MD). Dulbecco's phosphate buffered saline (PBS), Dulbecco's Modified Eagle Medium (DMEM), penicillin streptomycin (Pen-strep), fetal bovine serum (FBS), and CellTracker™ Green CMFDA , and CellTracker™ Red CMTPX were all purchased from Life Technologies (Carlsbad, CA).

PDMS micromolds and glass slides

Silicon wafers with microwell patterns were fabricated using SU-8 photolithography and resulting wafers were used to fabricate poly(dimethylsiloxane) (PDMS) molds. Elastomer and curing agent were mixed with a 10:1 weight ratio. The mixture was then poured onto silicon wafers and kept at 70 °C for 2 h until cured. PDMS molds with circular and square protruding patterns were detached from the silicon wafers and sliced into rectangular shapes with surface areas of ~3.2 cm^2. The diameter and depth of circular micromolds were ~250-270 μm. These circular micromolds were used to fabricate PNIPAAm-based circular microwells. The depth of square micromolds was ~300 μm and their dimensions on each side were ~275-320 μm. Square micromolds were used to generate PNIPAAm-based square microwells.

Glass slides were placed in 10% (w/v) NaOH in deionized water for 8 h. Glass slides were then washed with deionized water and ethanol 3 times. After drying at ambient temperature, glass slides were stacked into a beaker and 3 ml of TMSPMA were pipetted onto the glass slides and allowed to flow through via capillary effect. Glass slides were kept at 70 °C overnight to initiate the coating process. Finally, TMSPMA-coated glass slides were rinsed with ethanol 3 times and dried at ambient temperature. Coated glass slides were kept at room temperature until microwell fabrication.

Fabrication of dynamic microwells

PNIPAAm precursor solutions were generated by mixing NIPAAm, MBAAm, DMSO, deionized water, and PI in the weight ratios of 2.18 : 0.12 : 3 : 1 : 0.15. Prepolymer solutions were mixed by stirring overnight at ambient temperature. Photo-initiator was added to the prepolymer solution before microwell fabrication. PNIPAAm-based dynamic microwells were fabricated with a soft-lithographic technique. Prepolymer solution was pipetted onto a PDMS mold and a TMSPMA coated glass slide was immediately pressed over the solution. The setup was then exposed to ultra-violet (UV) light with 320–500 nm wavelength at an intensity of 4 mW/cm^2 for 30 s using the OmniCure Series2000 (EXFO, Mississauga, Canada) to crosslink the hydrogel microstructures. PNIPAAm microwells with circular and square shapes were generated by this method. Microwells were immersed in 70% ethanol to wash unreacted chemicals, rinsed with PBS 3 times, and kept in PBS.

Responsiveness test

The responsiveness of the dynamic microwells was tested at 24 °C and 37 °C. For this test, three samples (n=3) of microwell arrays for each circular and square microwell structures were placed in PBS. Microwells were first kept at ambient temperature (24 °C) for 30 min, at which point images of microwells were taken with an inverted microscope (Nikon Eclipse TE2000-U). The microwell arrays were then immediately placed at 37 °C for a total of 2 hours, and images were taken every 5 min for the first 30 min of incubation at 37 °C. For the following 30 min incubation period at 37 °C, images were taken every 10 min. The last microwell images were taken after the final hour of incubation at 37 °C. An image showing 6 individual microwells was taken of each sample for both circular and square microwell structures at each time point. The

responsiveness of each pattern was quantified by measuring the top-view surface area of the pattern with Spot Advanced software (Spot Imaging Solutions, Sterling Heights, MI). Pattern areas at each temperature and time point were represented as the mean value with a standard deviation.

Cell culture

Human hepatoblastoma, HepG2, cells and NIH-3T3 fibroblasts were cultured in medium which was a mixture of 89% DMEM, 10% FBS, and 1% Pen-strep. HUVECs were cultured in EBM-2 media supplemented with 2% FBS and all the components of the EGM-2 bullet kit. All cell types were incubated at 37 °C in a 5% CO_2 humidified incubator. Passaging of all cell types was conducted every 3 days.

Spatially controlled patterning of two different cell types

HepG2 cells were labeled with red CMTPX cell tracker and 3T3 fibroblasts were labeled with green CMFDA cell tracker according to the manufacturer's protocol. HUVECs were already pre-labeled with green fluorescent protein (GFP). Cell suspensions were prepared in corresponding culture mediums. Microwell structures were placed in 6-well plates, rinsed with 70% ethanol, and washed with PBS 3 times. Each microwell array was then kept in 4 ml of PBS in a 6-well plate at room temperature for 30 min to allow microwells to reach their pattern areas at 24 °C. For experiments with circular microwells, 200 µl of HepG2 (red) cell suspension with a density of 10 x 10^6 cells/ml was evenly seeded on the microwells at ambient temperature. For square microwells, 200 µl of HepG2 (red) cell suspension with a density of 12 x 10^6 cells/ml was seeded on the microwells. All microwell arrays were immediately washed with PBS 3 times to rinse off cells that were not docked into the microwells. Microwells containing HepG2s (red) were then immersed in 4 ml of culture medium and subsequently placed at 37 °C for 2h. This incubation at 37 °C allowed the PNIPAAm structure to shrink resulting in a larger microwell area and more space for seeding of the second cell type. After the incubation at 37 °C, 200 µl of either 3T3 fibroblast (green) cell suspension or GFP-HUVEC cell suspension, each having a density of 5 x 10^6 cells/ml, was evenly seeded onto the circular microwells. For square microwells, 200 µl of either 3T3 fibroblast (green) cell suspension or GFP-HUVEC cell suspension, each having a density of 6 x 10^6 cells/ml, was seeded onto microwells. All microwell

arrays were rinsed with PBS 3 times to wash cells that were not docked into microwells. For experiments with HepG2-HUVECs, microwells were immersed in 4 ml of medium which was a mixture of HepG2 medium and HUVEC medium with a 1:1 volume ratio. For HepG2-3T3 experiments, microwells were immersed in 4 ml of HepG2-3T3 medium. All microwells were then placed at 37 °C in a 5% CO_2 humidified incubator.

For the quantification of the cell seeding process, each microwell type (circular or square) contained three samples (n=3) for each experiment (HepG2-HUVECs or HepG2-3T3s). After seeding the second cell type, images of the microwells containing different cell types were taken with an inverted fluorescent microscope (Nikon Eclipse TE2000-U). Images of the first seeded cell type (HepG2) were taken first, and then images of the second seeded cell type (HUVECs or 3T3s) were taken for each sample. An image of each microwell sample was taken for each cell type. Each image contained 6 individual microwells and showed the pattern areas of one cell type. Pattern areas of different cell types for each experiment were measured by using Spot Advanced software and represented as a mean value with a standard deviation.

Circular and square microwells seeded with HepG2s and HUVECs were incubated for 3 days to observe the changes in the morphology of the cells and in the resulting microtissues. Images of each HepG2 and HUVEC layer for each microwell type were taken at day 1 and day 3 with an inverted fluorescent microscope. Experiments with HepG2s and 3T3 fibroblasts were incubated for 3 days and only day 1 images were taken.

Harvesting of resulting microtissues from microwells

Retrieval experiments were only conducted for microwells seeded with HepG2s and HUVECs. After 3 days of culture, the resulting microtissues were harvested from both circular and square microwells by gently flowing PBS over the microwell surfaces with a pipette. Retrieved tissues were imaged with an inverted fluorescent microscope. It was also observed that microwell structures may disengage from glass substrates at day 3 which may help the tissue harvesting process by leaving microtissues on glass substrates. These tissues could be easily detached from the glass substrates by gently pipetting with PBS.

Statistical analysis

All data were demonstrated as a mean ± standard deviation (sd). Statistical analysis for responsiveness tests was done with paired t-test whereas all other statistical analyses were performed with one-way ANOVA followed by Bonferroni post-hoc test with GraphPad Prism 5.04 (GraphPad Software, San Diego, USA) by considering **p < 0.01 and ***p < 0.001.

5.3 Results and Discussion

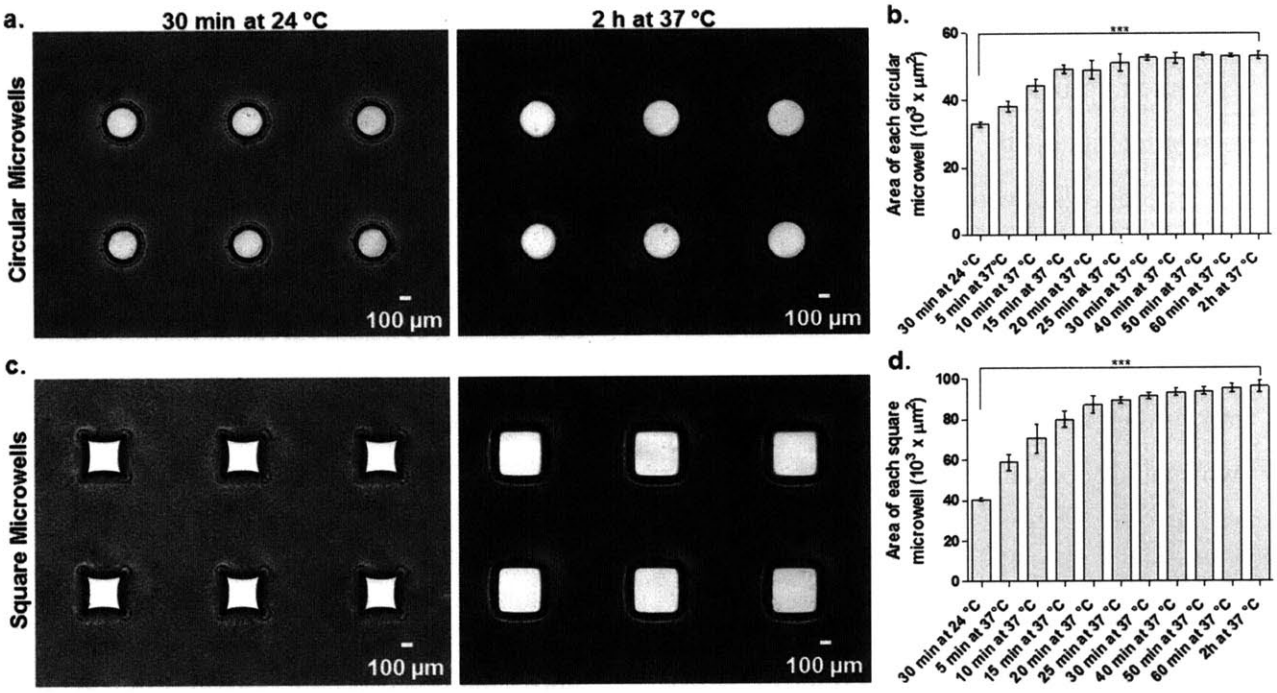

Figure 5.1. Temperature-dependent shape change properties of dynamic microwells. (a) Time lapse images and (b) corresponding responsiveness plot for circular microwells (n=3). (c) Time lapse images and (d) responsiveness plot for square microwells (n=3). Both microwell types were first incubated at 24 °C and then moved to 37 °C. During the incubation period at 37 °C, images of both microwell types were taken every 5 min for the first 30 min incubation period, every 10 min for the second 30 min incubation period, and the last images were taken at the 2 h time point. The responsiveness is represented with change in surface areas of microwells. Error bars: ± sd and *** shows statistically significant difference (p < 0.001).

Dynamic microwells with circular and square shapes were fabricated using a soft lithographic technique. To test their temperature dependent shape change properties, these dynamic

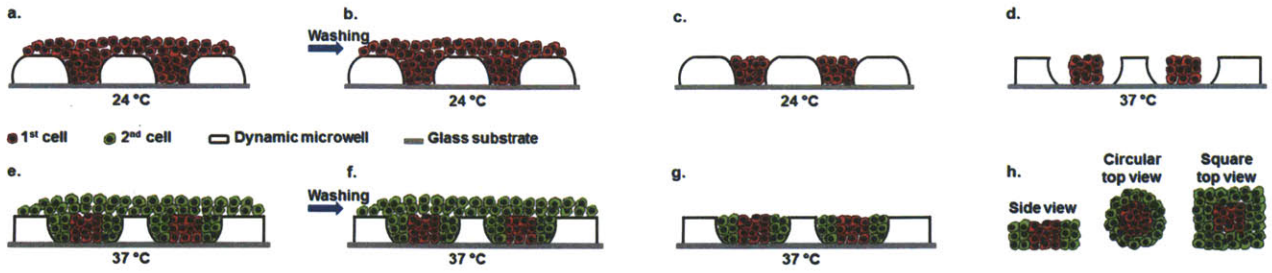

Figure 5.2. Schematic diagram of spatially controlled patterning of two different cell types with dynamic microwells. (a) Seeding the first cell type (red) at 24 °C when microwell structures were at swollen state. (b) Washing microwells to rinse off undocked cells on microwell surfaces. (c) Undocked cells were washed off the microwell surfaces. (d) Incubation at 37 °C to allow microwell structures to shrink, resulting in more free space for the second cell type. (e) Seeding the second cell type (green) within microwells. (f) Subsequently washing microwells to rinse off undocked cells on the surface. (g) Two cell types were spatially distributed within microwells and further incubated at 37 °C. (h) Side and top views of the resulting microtissues containing two spatially organized cell types.

microwells were subjected to different incubation times at both 24 °C and 37 °C. After 30 min of incubation at 24 °C, circular microwells swelled and retained their circularity (**Figure 5.1a**). After increasing the temperature from 24 °C to 37°C, circular microwells significantly increased their surface areas within 2 h and conserved their circularity (**Figure 5.1a,b**). The overall time response of circular microwells to the temperature rise from 24 °C to 37 °C showed a gradual increase in surface areas (**Figure 5.1b**). The thermoresponsiveness of square microwells were also analyzed in the same manner. After 30 min of incubation at 24 °C, square microwells swelled and exhibited square-like shapes (**Figure 5.1c**). After the temperature was raised from 24 °C to 37 °C, square microwells returned to their original square shapes with significantly increased surface areas within 2 h (**Figure 5.1c,d**). Similar to circular microwells, surface areas of square microwells gradually increased in response to incubation at 37 °C with different time intervals (**Figure 5.1d**). In light of these results, dynamic microwells demonstrate significant changes in surface areas at two different temperatures by conserving their geometries, facilitating the spatial patterning of multiple cell types at different temperatures.

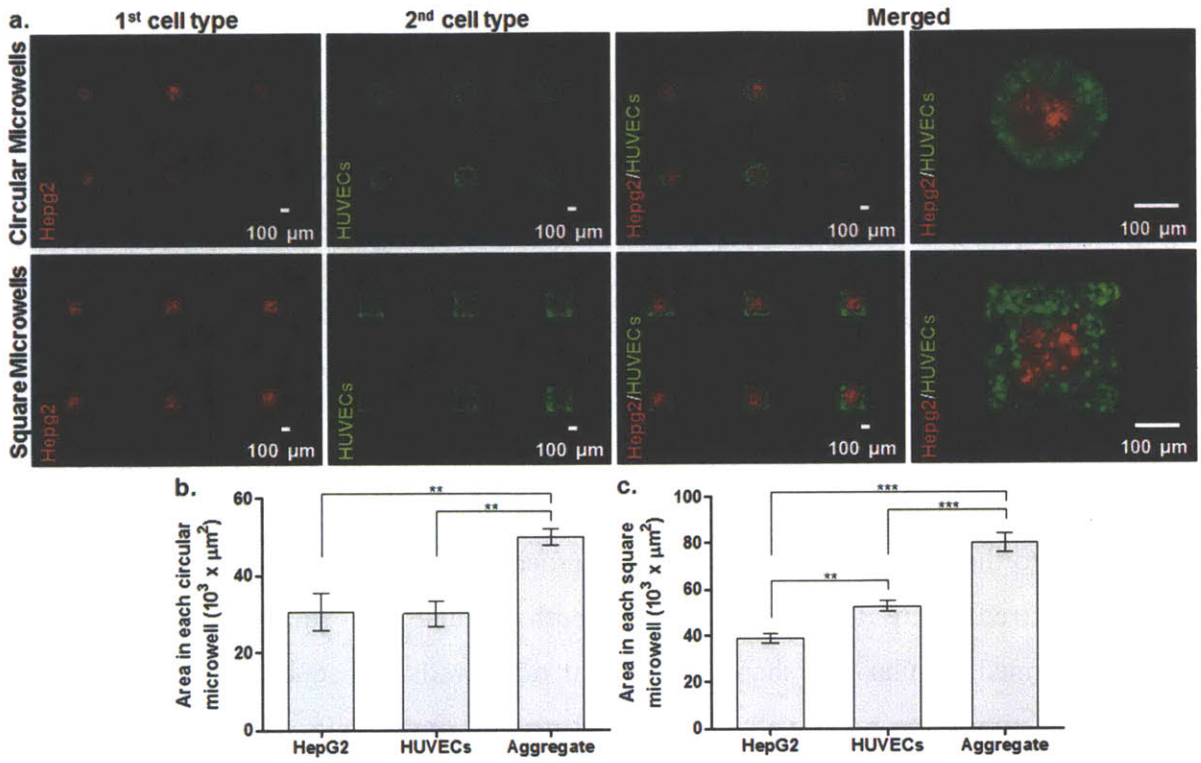

Figure 5.3. Spatially controlled patterning of HepG2 cells (red) and GFP-HUVECs (green) within dynamic circular and square microwells. (a) HepG2 cells were the first patterned cell type in both circular and square microwells. GFP-HUVECs were patterned as the second cell type and spatially organized around HepG2 aggregates by filling the free space that resulted from microwell expansion at 37 °C. Merged images show that spatial distribution of two cell types was controlled in a single geometry, either circular or square. Areas of both cell types and overall aggregates were measured and plotted for (b) circular microwells (n=3) (c) square microwells (n=3). (Error bars: ± sd and statistical differences: **p < 0.01; ***p < 0.001).

We showed the capability of these dynamic microwells to control spatial organization of multiple cell types in defined microenvironments by patterning two different cell types for potential use in various applications, such as developmental biology, cancer, and tissue engineering. **Figure 5.2** illustrates the experimental procedure to pattern two different cell types with dynamic microwells. After fabrication, microwells were placed at 24 °C for 30 min to allow them to reach their ambient temperature areas. A cell suspension of the first cell type was then seeded onto the microwells at 24 °C and immediately washed with phosphate buffered saline

(PBS) to rinse off undocked cells. Cell-seeded microwells were then incubated at 37 °C for 2 h to allow microwells to shrink, resulting in more free space. A cell solution of the second cell type was then seeded onto the microwells at 37 °C and undocked cells were immediately rinsed off by washing with PBS. Microwells containing two different spatially patterned cell types were then placed at 37 °C for further incubation. By using this patterning process, two different cell types were spatially organized in a single geometry, either circular or square.

Human hepatoblastoma, HepG2, cells having parenchymal characteristics, were chosen as the first cell type due to their relevance in tumor models[24] and tissue engineering.[22,25] Human umbilical vein endothelial cells (HUVECs) are non-parenchymal and were selected as the second cell type due to their relevance in the cancer microenvironment[8] and tissue vascularization.[26] HepG2 cells (red) were first seeded within both circular and square microwells. HepG2 aggregates formed circular-like shapes in circular microwells and square-like shapes in square microwells by filling the microwell surfaces that resulted from PNIPAAm swelling at ambient temperature (**Figure 5.3a**). After the incubation at 37 °C, green fluorescent protein (GFP)-labeled HUVECs were then seeded on both circular and square microwells. GFP-HUVECs were patterned around HepG2 aggregates in both microwell types by filling the free space that resulted from PNIPAAm expansion at 37 °C (**Figure 5.3a**). The resulting aggregates in circular microwells had two different spatially organized cell types in circular geometries (**Figure 5.3a**). HepG2 cells possessed surface areas similar to GFP-HUVECs in circular microwells (**Figure 5.3b**). Small amounts of GFP-HUVECs overlapped around HepG2 cells. Surface areas of the resulting circular aggregates were significantly larger than that of either HepG2 cells or GFP-HUVECs (**Figure 5.3b**). The resulting microtissues in square microwells had two spatially distributed cell types in square geometries (**Figure 5.3a**). GFP-HUVECs occupied significantly more space than HepG2 cells in square microwells (**Figure 5.3c**). Surface area of the resulting square microtissues was significantly larger than that of either HepG2 cells or GFP-HUVECs. Similar to circular microwells, few GFP-HUVECs overlapped around HepG2 cells in square microwells. To showcase that other non-parenchymal cells can be patterned, 3T3 fibroblasts were substituted for GFP-HUVECs as the second cell type. Fibroblasts (3T3 cells) are non-parenchymal and relevant to both tumor microenvironment[8] and tissue engineering.[2,5] By using the same patterning method, HepG2 cells (red) were first patterned within both circular and square microwells. The resulting HepG2 aggregates formed circular shapes in circular

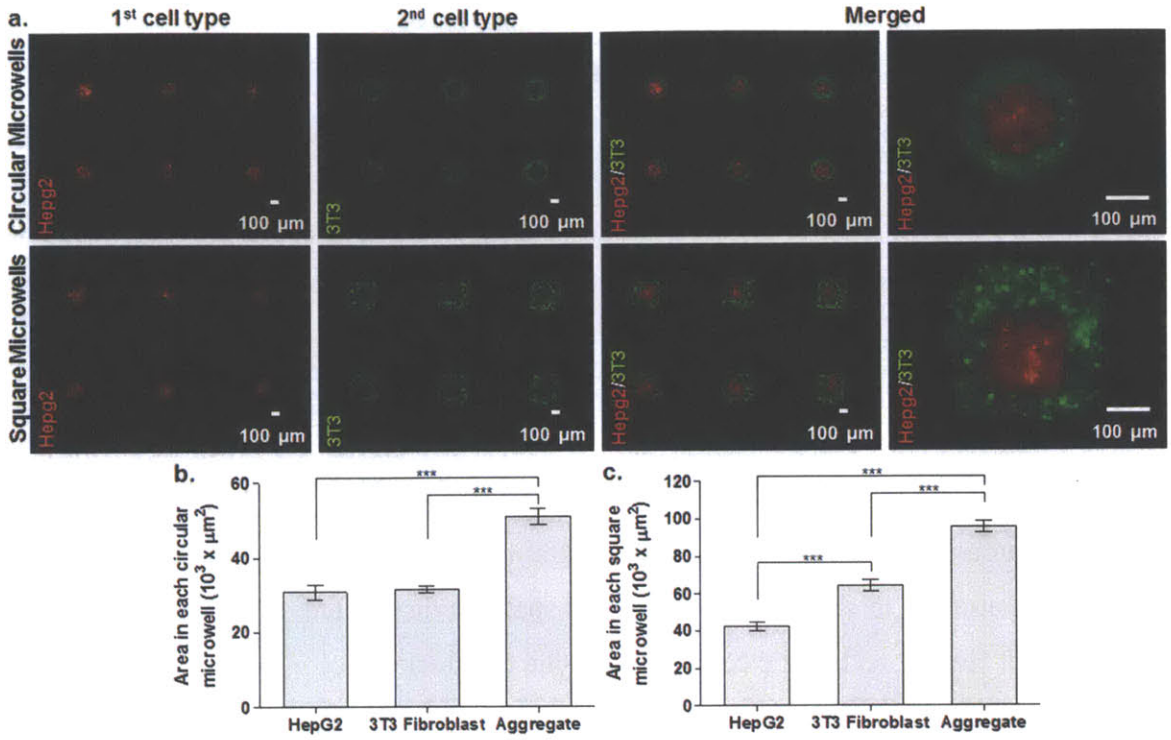

Figure 5.4. Spatially controlled patterning of HepG2 cells (red) and 3T3 fibroblasts (green) in dynamic circular and square microwells. (a) HepG2 cells were the first patterned cell type in both microwell types, and after incubation at 37 °C, 3T3 fibroblasts were patterned as the second cell type. Fibroblasts (3T3 cells) were seeded around the HepG2 aggregates by filling the free space that resulted from polymer shrinking and microwell expansion at 37 °C. Merged images demonstrate that spatial distribution of two cell types was controlled within a single circular or square geometry. Areas of both HepG2 and 3T3 fibroblast layers and overall aggregates were shown in corresponding plots for (b) circular microwells (n=3) (c) square microwells (n=3). (Error bars: ± sd and statistical difference: ***$p < 0.001$).

microwells and square-like shapes in square microwells (**Figure 5.4a**). After incubation at 37 °C, 3T3 fibroblasts (green) were patterned around HepG2 aggregates within both microwell types (**Figure 5.4a**). Surface areas of HepG2 cells and 3T3 fibroblasts were similar for circular microwells. The resulting aggregates in circular microwells exhibited significantly larger surface areas than that of either HepG2 cells or 3T3 fibroblasts (**Figure 5.4b**). For square microwells, 3T3 fibroblasts occupied remarkably more space than HepG2 cells and the resulting microtissues

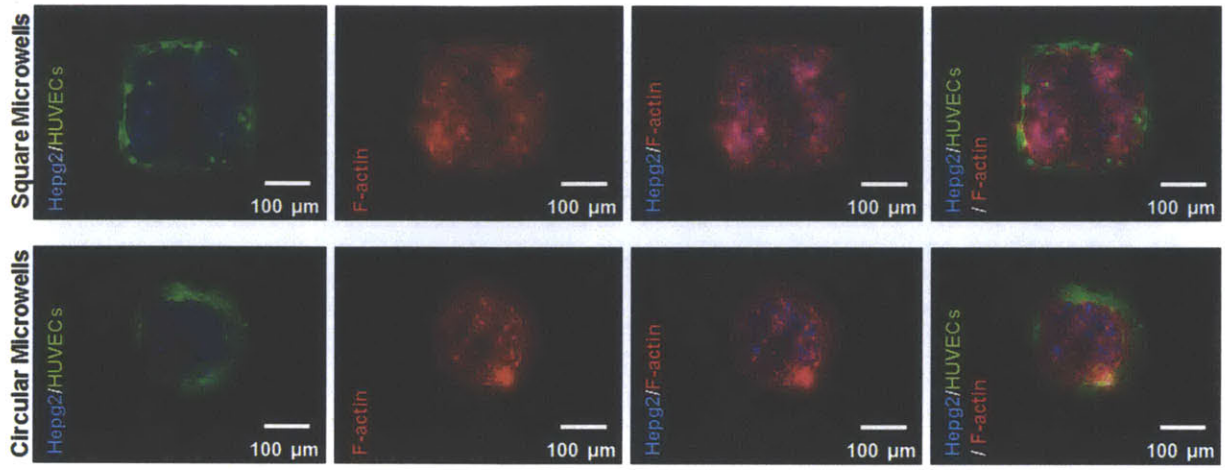

Figure 5.5. Circular and square microwells containing HepG2 cells and GFP-HUVECs were stained with Phalloidin to show F-actin fibers of spatially distributed cells at day 1. F-actin was shown with red. HepG2 cells were colored with blue cell tracker.

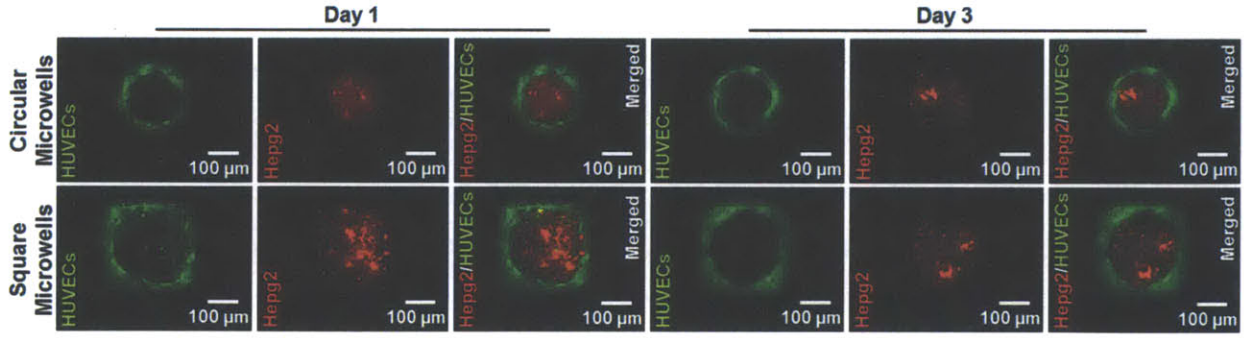

Figure 5.6. Microwells containing HepG2 cells (red) and GFP-HUVECs (green) were cultured for 3 days to observe the morphology of cells. Images of both HepG2 and GFP-HUVECs layers were taken at day 1 and day 3 for both circular and square microwells. HepG2 and GFP-HUVECs layers were shown in different images and their merged images were given for each microwell. Day 1 images show that GFP-HUVECs started spreading and generating an endothelial network around HepG2 aggregates. Within 3 days, GFP-HUVECs formed dense endothelial networks around HepG2 layers. (Day 1 and day 3 images are independent from each other for both microwell types).

kept significantly more space than either HepG2 cells or 3T3 fibroblasts (**Figure 5.4c**). Similar to experiments with GFP-HUVECs, few 3T3 fibroblasts overlapped around HepG2 cells in both circular and square microwells. These results demonstrate that dynamic microwells are potentially useful for controlling the spatial organization of multiple cell types in defined microenvironments.

Microwells containing HepG2 cells and GFP-HUVECs were incubated for 3 days to observe the morphological changes of patterned cells. Cytoskeletal organization of HepG2 cells and HUVECs has been assessed at day 1 by staining their F-actin fibers (**Figure 5.5**). F-actin staining for HUVECs in both circular and square microwells showed that HUVECs spread around HepG2 aggregates by following the geometry (either circular or square) of HepG2 aggregates after one day of incubation. Within 1 day, GFP-HUVECs were located more towards the sides of circular and square microwells without overlapping HepG2 aggregates. GFP-HUVECs also started spreading and forming endothelial networks around HepG2 aggregates in both microwell types after 1 day of incubation (**Figure 5.6**). At day 3, GFP-HUVECs had formed endothelial networks around HepG2 aggregates within both circular and square microwells (**Figure 5.6**). For circular microwells, the shapes of HepG2 aggregates, endothelial networks, and composite aggregates conserved their circularity at day 3. Within square microwells, both endothelial network of GFP-HUVECs and HepG2 aggregates started to become circular at day 3 (**Figure 5.6**). On the other hand, 3T3 fibroblasts started overlapping over HepG2 aggregates in circular and square microwells after 1 day of incubation (**Figure 5.7**). Cytoskeletal organization of F-actin fibers of 3T3 fibroblasts has also revealed the overlap of 3T3 fibroblasts over HepG2 microtissues at day 1 (**Figure 5.8**). It was observed that fibroblasts (3T3 cells) overlapped more over HepG2 cells at day 3 (data not shown). These results could be attributed to interactions between different cell types within different geometries, suggesting that dynamic microwells could potentially control the interplay between multiple spatially arranged cell types.

Cell-cell interactions were assessed by staining multi-layered microtissues with anti-cadherin antibodies. HepG2 cells were tagged with blue color and seeded within square microwells. By using the presented method, GFP-HUVECs were patterned around HepG2 cells. After 1 day of incubation, microtissues were double immunostained with anti-VE cadherin and anti-E cadherin

antibodies (**Figure 5.9**). Anti-VE cadherin showed the homotypic cell-cell interactions between HUVECs while anti-E cadherin both demonstrated the homotypic cell-cell interactions between

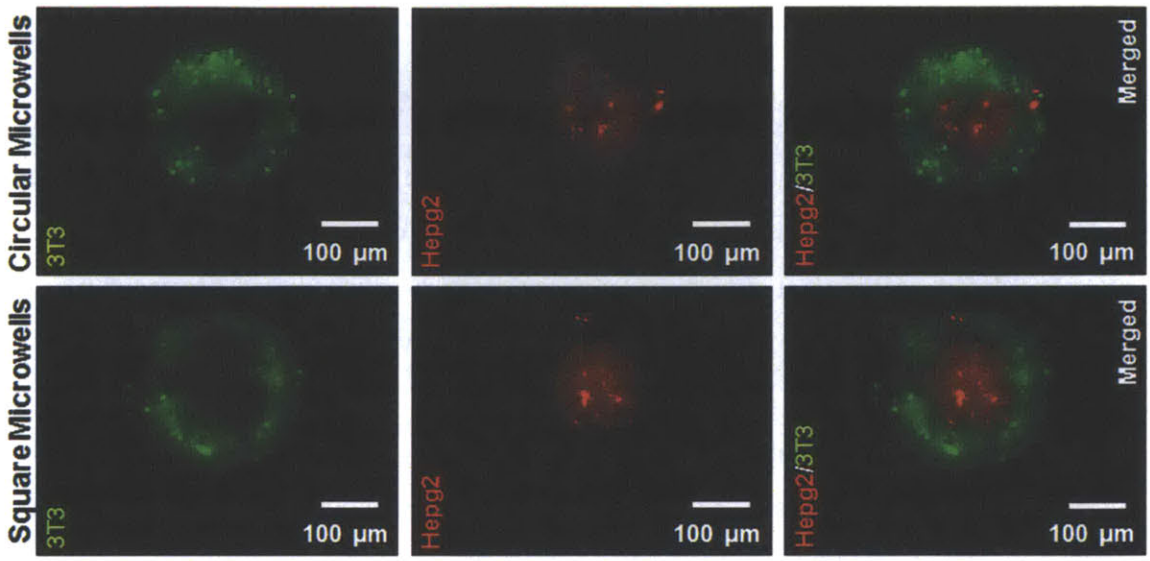

Figure 5.7. Microwells containing HepG2 cells and 3T3 fibroblasts were cultured and imaged at day 1 to observe cell morphology. Fibroblasts (3T3 cells) started to overlap onto HepG2 aggregates in both circular and square microwells.

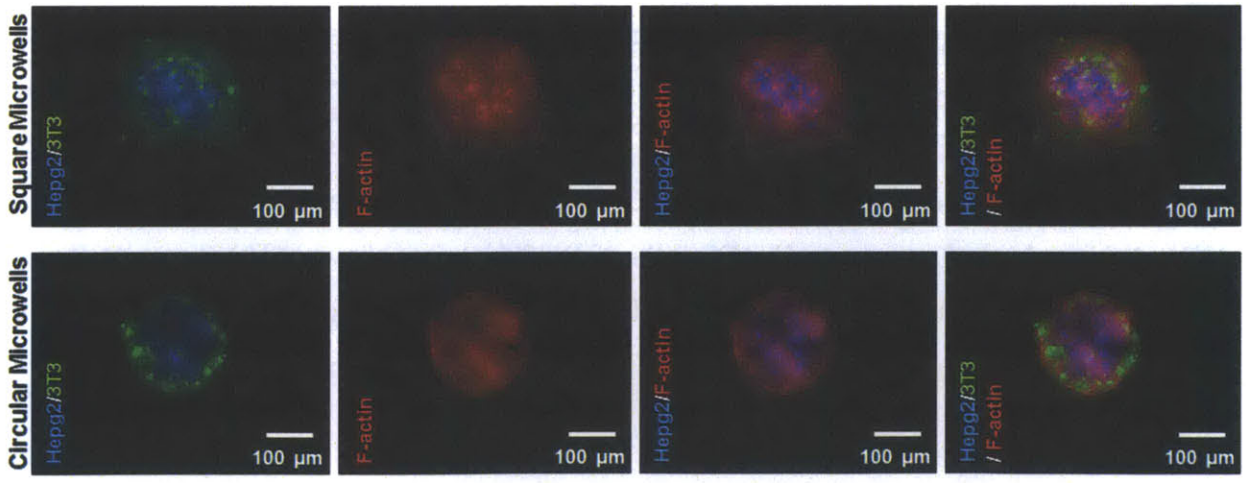

Figure 5.8. F-actin (red) staining for circular and square microwells containing spatially organized HepG2 cells and 3T3 fibroblasts at day-1. HepG2 cells were stained with blue cell tracker and fibroblasts were colored with green cell tracker.

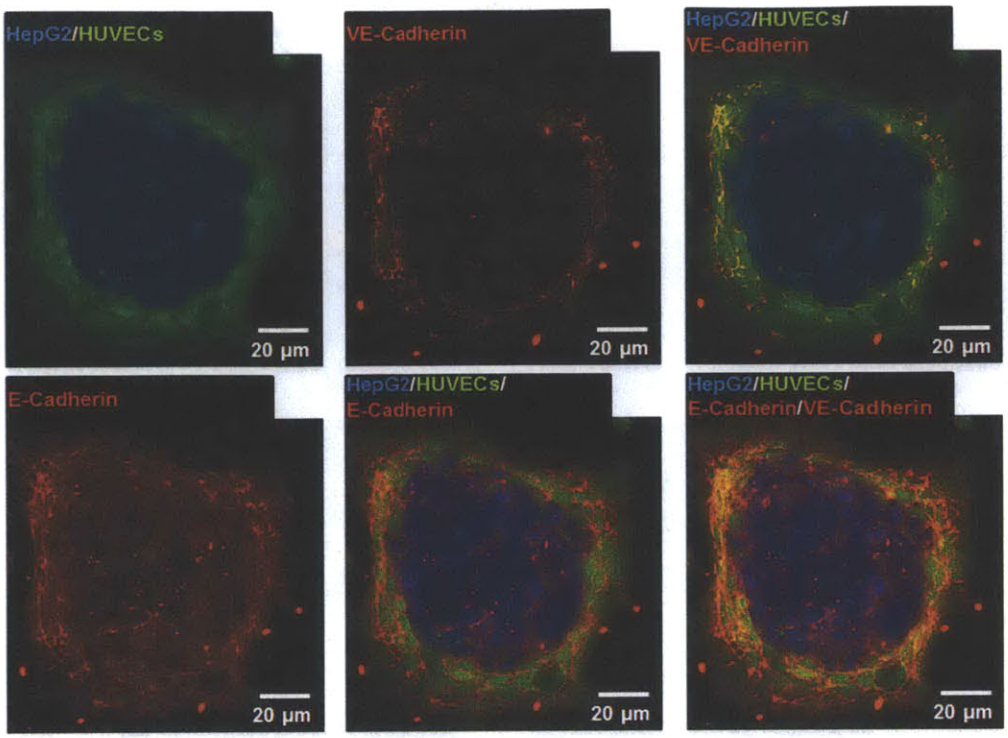

Figure 5.9. Microtissues containing spatially organized HepG2 cells (blue) and GFP-HUVECs (green) were double immunostained with anti-VE cadherin and anti-E cadherin to show cell-cell interactions. Images were taken with a confocal microscopy. VE-cadherin staining (red) showed cell-cell interactions between HUVECs around HepG2 cells. E-cadherin staining (far-red) exhibited cell-cell contacts between HepG2-HepG2, HepG2-HUVECs, and HUVECs-HUVECs.

HepG2 cells, homotypic cell-cell interactions between HUVECs, and heterotypic cell-cell interactions between HepG2 cells and HUVECs. Furthermore, some other microtissues were only stained with anti-N cadherin antibody at day 1 and imaged at a higher magnification (**Figure 5.10**). Anti-N cadherin staining exhibited the heterotypic interactions between HepG2 cells and HUVECs at the boundary of HepG2 and HUVEC layers. It also showed the homotypic cell-cell interactions between HepG2 cells within HepG2 layer. Thus, spatially controlled patterning of two different cell types by using dynamic microwells can produce microtissues with controlled homotypic and heterotypic cell-cell interactions.

The resulting microtissues can be recovered from microwells by gently flowing PBS over the surface of the microwells. Microwells may also detach from the substrates at day 3, which may

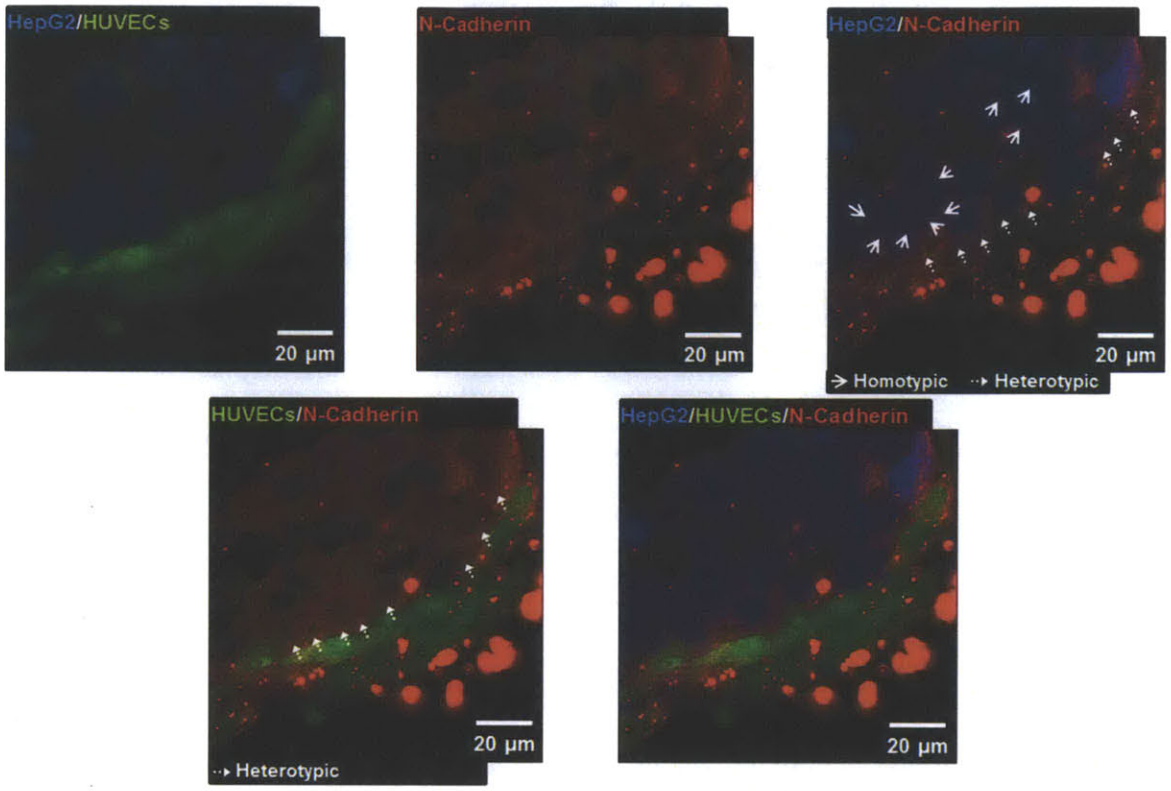

Figure 5.10. Microtissues of spatially organized HepG2 cells (blue) and GFP-HUVECs (green) were only immunostained with anti-N cadherin. Images were obtained by using a confocal microscopy at a high magnification. N-Cadherin staining (red) demonstrated heterotypic cell-cell interactions between HepG2 cells and HUVECs at the boundary of two layers as well as homotypic interplay between HepG2 cells.

ease the retrieval of the resulting microtissues. Aggregates containing HepG2 cells and GFP-HUVECs were recovered from both circular and square microwells (**Figure 5.11**). After retrieval from microwells, aggregates conserved their multi-layered structures containing HepG2 cells and GFP-HUVECs at different layers (**Figure 5.11**).

Cell concentrations in this study were optimized for the microwell sizes and shapes used. For different sizes and shapes of microwells and different applications, cell concentrations and seeding process may need further refinements. Furthermore, microwells with different thermoresponsive behaviors or with different dimensions could be fabricated by changing PNIPAAm prepolymer solutions or by using micromolds with different dimensions. Using

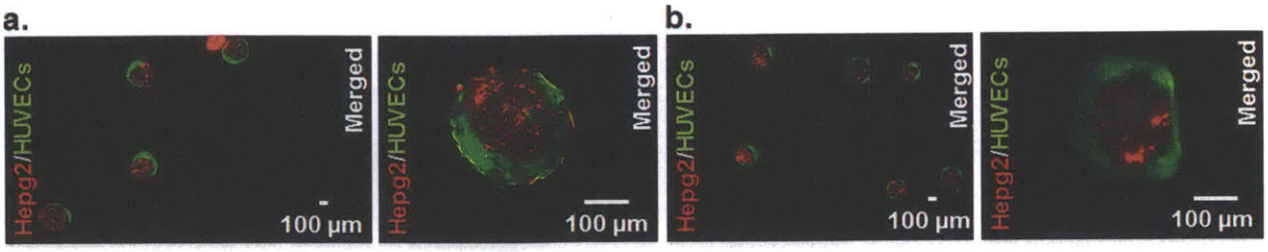

Figure 5.11. The resulting microtissues containing HepG2 cells and GFP-HUVECs were recovered from (a) circular microwells and (b) square microwells at day 3.

higher concentrations of the second cell type and insufficient washing steps may cause the second cell type to wrap over the first cell type. It was observed that after seeding the first cell type, small agitations and improper washing may cause the detachment of aggregates of the first cell type from microwells. This may lead to the formation of aggregates of the second cell type within the corresponding microwells. Stability of the cells could be improved by using adhesion proteins within microwells in future applications.

Different cell types could be substituted for the cells used in this study. One could pattern multiple cell types within different geometries in a spatially controlled manner to study early stages of development and tissue morphogenesis. It could also be possible to study cancer dynamics, such as metastasis and angiogenesis, by patterning their associated cell types with native spatial organizations. Another potential application could be to fabricate microtissues with native biological complexities for use in regenerative medicine and drug discovery. Furthermore, by using modular tissue engineering methods,[27] the resulting microtissues retrieved from microwells could be assembled into complex architectures with spatially controlled cell placement.

5.4 Conclusions

In summary, we described a simple method to control the spatial distributions of multiple cell types in predefined geometries. Dynamic microwells possess shape changing properties at different temperatures due to the thermoresponsiveness of PNIPAAm. This feature was exploited to pattern multiple cell types at different temperatures. Biologically relevant cell types were spatially patterned within dynamic circular and square microwells. The second cell type was

spatially arranged around the first cell type in a defined microenvironment. The ability to control spatial organization of various cell types in defined microenvironments can be used to replicate different native biological complexities containing intricate cell-cell interactions, such as those found in development, cancer, and tissues. Thus, the presented method could potentially be useful in a number of fields, including tissue engineering, developmental biology, cancer biology, and drug discovery.

5.5 References

[1] C. M. Nelson, M. M. VanDuijn, J. L. Inman, D. A. Fletcher, M. J. Bissell, Science 2006, 314, 298.

[2] E. E. Hui, S. N. Bhatia, Proceedings of the National Academy of Sciences of the United States of America 2007, 104, 5722.

[3] Z. J. Gartner, C. R. Bertozzi, Proceedings of the National Academy of Sciences of the United States of America 2009, 106, 4606.

[4] C. S. Chen, M. Mrksich, S. Huang, G. M. Whitesides, D. E. Ingber, Science 1997, 276, 1425.

[5] S. N. Bhatia, M. L. Yarmush, M. Toner, Journal of Biomedical Materials Research 1997, 34, 189.

[6] S. N. Bhatia, U. J. Balis, M. L. Yarmush, M. Toner, Faseb Journal 1999, 13, 1883.

[7] C. M. Nelson, R. P. Jean, J. L. Tan, W. F. Liu, N. J. Sniadecki, A. A. Spector, C. S. Chen, Proceedings of the National Academy of Sciences of the United States of America 2005, 102, 11594.

[8] D. Hanahan, R. A. Weinberg, Cell 2011, 144, 646.

[9] L. H. Li, T. Xie, Annual Review of Cell and Developmental Biology, Vol. 21, 2005, 605.

[10] C. M. Nelson, M. J. Bissell, Annual Review of Cell and Developmental Biology, Vol. 22, 2006, 287.

[11] J. Rossant, P. P. L. Tam, Development 2009, 136, 701.

[12] Y.-C. Toh, K. Blagovic, H. Yu, J. Voldman, Integrative Biology 2011, 3, 1179.

[13] D. T. Chiu, N. L. Jeon, S. Huang, R. S. Kane, C. J. Wargo, I. S. Choi, D. E. Ingber, G. M. Whitesides, Proceedings of the National Academy of Sciences of the United States of America 2000, 97, 2408.

[14] J. Tien, C. M. Nelson, C. S. Chen, Proceedings of the National Academy of Sciences of the United States of America 2002, 99, 1758.

[15] Y.-s. Torisawa, B. Mosadegh, G. D. Luker, M. Morell, K. S. O'Shea, S. Takayama, Integrative Biology 2009, 1, 649.

[16] S. Jinno, H. C. Moeller, C. L. Chen, B. Rajalingam, B. G. Chung, M. R. Dokmeci, A. Khademhosseini, Journal of Biomedical Materials Research Part A 2008, 86A, 278.

[17] J. M. Karp, J. Yeh, G. Eng, J. Fukuda, J. Blumling, K.-Y. Suh, J. Cheng, A. Mahdavi, J. Borenstein, R. Langer, A. Khademhosseini, Lab on a Chip 2007, 7, 786.

[18] A. Khademhosseini, R. Langer, J. Borenstein, J. P. Vacanti, Proceedings of the National Academy of Sciences of the United States of America 2006, 103, 2480.

[19] B. Yuan, Y. Li, D. Wang, Y. Xie, Y. Liu, L. Cui, F. Tu, H. Li, H. Ji, W. Zhang, X. Jiang, Advanced Functional Materials 2010, 20, 3715.

[20] H. Tekin, G. Ozaydin-Ince, T. Tsinman, K. K. Gleason, R. Langer, A. Khademhosseini, M. C. Demirel, Langmuir 2011, 27, 5671.

[21] H. Tekin, J. G. Sanchez, T. Tsinman, R. Langer, A. Khademhosseini, Aiche Journal 2011, 57, 3249.

[22] H. Tekin, M. Anaya, M. D. Brigham, C. Nauman, R. Langer, A. Khademhosseini, Lab on a Chip 2010, 10, 2411.

[23] H. Tekin, T. Tsinman, J. G. Sanchez, B. J. Jones, G. Camci-Unal, J. W. Nichol, R. Langer, A. Khademhosseini, Journal of the American Chemical Society 2011, 133, 12944.

[24] B. Smrekar, L. Wightman, M. F. Wolschek, C. Lichtenberger, R. Ruzicka, M. Ogris, W. Rodl, M. Kursa, E. Wagner, R. Kircheis, Gene Therapy 2003, 10, 1079.

[25] V. A. Liu, S. N. Bhatia, Biomedical Microdevices 2002, 4, 257.

[26] J. Rouwkema, N. C. Rivron, C. A. van Blitterswijk, Trends in Biotechnology 2008, 26, 434.

[27] J. W. Nichol, A. Khademhosseini, Soft Matter 2009, 5, 1312.

Chapter 6: Summary and Outlook

6.1 Summary

Living systems are complex multicellular communities. Recreating physiological systems in outside environment can be greatly useful for a wide variety of applications in life sciences, such as those in tissue engineering, regenerative medicine, drug discovery, cancer biology, and developmental biology. Replicating these systems require methods utilizing precise and versatile engineering tools. This thesis focuses on developing methods to recapitulate multicellular organizations in a geometrically and spatially controlled manner. The first part of the thesis aimed to fabricate thermoresponsive platforms to generate spherical and striped microtissues of single cell types and to initiate their further retrieval in a controlled manner. The second part of the thesis intended to develop techniques to control spatial organization of multiple cell types either in a microgel or in a scaffold-free microenvironment.

A versatile technique based on a thermoresponsive template was developed to form cell aggregates with spherical geometries in stable microenvironments and harvest them in a controlled manner. Circular microwells were fabricated from photocrosslinkable poly(N-isopropylacrylamide) (PNIPAAm) by using a soft-lithographic method. Microwells possessed temperature dependent shape changing properties. Increasing temperature results in increased microwell areas due to the shrinking of PNIPAAm structure. It was shown that microwells with different responsiveness characteristics can be fabricated by changing crosslinker amount in prepolymer solutions. A model cell type which is relevant to tissue engineering, cancer biology, and drug discovery was used to generate cell spheroids. As fabrication method facilitated the glass bottomed microwell structures which are adherent to cells, spheroids were stably formed within microwells. Furthermore, cell adherent substrates can ease high-throughput experimentation on microtissues in microwells. As cells are the same type, homotypic cell-cell interactions can occur in cell aggregates. Temperature dependent shape change property of microwells was exploited to retrieve microtissues in a controlled manner for further use.

Another generic tool was developed to be able to generate striped microtissues which are relevant to physiological tissues, such as muscle and cardiac. Poly(dimethylsiloxane) (PDMS) was chosen to fabricate microgroove substrates due to its biocompatibility, elasticity, gas

permeability, and wide use in microfluidic devices. Initiated chemical vapor deposition (iCVD) method was utilized to conformally coat microgrooves with PNIPAAm without changing their groove geometry. PNIPAAm film which was covalently crosslinked on microgrooves responded to temperature decrease by swelling and becoming more hydrophilic. PNIPAAm coated substrates demonstrated reversible hydrophilicity for quick temperature changes. Cell adhesion on coated substrates was higher at physiological temperature due to decreased hydrophilicity. Coated surfaces became less cell-adherent when temperature was decreased to room temperature. Physiologically relevant single type cells were seeded when microgrooves were more hydrophilic. Incubation at physiological temperature facilitated the cell adhesion on microgrooves and led to stable formation of tissues. As microgrooves were coated in a conformal manner, the geometry of microtissues was preserved as stripe. Increased swelling and hydrophilicity of templates at ambient temperature were exploited to harvest striped microtissues for potentially further use in different applications requiring physiologically relevant single cell type stripe tissues with homotypic cell-cell interactions.

Thermoresponsive platforms were further exploited to recreate physiological complexity in a hydrogel based microtissues to create a suitable microenvironment for cell-matrix interactions. Non-photocrosslinkable polymers were previously not commonly used to form multilayered microgels due to the limited fabrication methods which inhibit the use of these materials for biological applications. In this part of the thesis, dynamic micromolding method was developed to fabricate multicompartment microgels made of non-photocrosslinkable materials. Dynamic micromolds were fabricated with various geometries such as circular, square, and grooves. These molds showed temperature dependent shape change properties which were exploited to sequentially pattern different layers of microgels at two different temperatures. Physiologically relevant different cell types were encapsulated into different compartments of geometrically controlled hydrogels. Particles other than cells were shown to be encapsulated as well. Stripe microgels containing two cell types with different spatial orientations were fabricated as models stripe tissues with cell-matrix interactions. Circular and square microgels were also fabricated to encapsulate physiologically relevant two cell types in a spatially controlled manner to potentially replicate complexity of native tissues in regards to cell-matrix interactions and intricate multicellular organizations.

In the last part of the thesis, a versatile method was developed to control spatial orientation of multiple cell types in defined microenvironments. Multicellular systems are made of intricate organizations of multiple cell types which are spatially distributed in defined microenvironments. Interactions between various cell types in native microenvironments regulate cell fate, differentiation, tissue and organ development, and cancer. Recapitulating these complexities could be used to create developmental models, specific tissues, cancer models, and disease models for drug discovery. However, it has been challenging to spatially arrange multiple cell types in defined microenvironments using previous methods. The presented method in the last part of this thesis utilized PNIPAAm-based dynamic microwells. These microwells demonstrated shape changes at two different temperatures. Parenchymal and non-parenchymal cell types were chosen in a physiologically relevant manner. The first cell type was parenchymal and patterned in microwells at room temperature, and then the second cell type which was non-parenchymal immobilized around the first ones at physiological temperature occupying the free space resulted from PNIPAAm shrinking. Geometry of multicellular organization was conserved in circular and square microwells. It was also shown that different non-parenchymal cell types (human umbilical vein endothelial cells (HUVECs) or 3T3 fibroblasts) give different responses after patterned around the same parenchymal cell type (human hepatoblastoma (HepG2) cells). The multicellular complexity led to homotypic cell-cell interactions between same cell types and heterotypic cell-cell interactions between different cell types. The presented method can be highly useful for applications in tissue engineering, regenerative medicine, drug discovery, cancer biology, and developmental biology.

6.2 Outlook

The structural and functional complexity of living systems results from the spatial distribution of multiple cell types and their reciprocal interactions with each other and the surrounding extracellular matrix (ECM) in a three-dimensional (3D) fashion. Recapitulating these complexities require engineering principles possessing precise tools to control orientation of cells and their interactions with various cell types and ECM materials in well-defined 3D geometries. The methods developed in this thesis are versatile and can fabricate biomimetic microtissues with controlled spatial and geometrical arrangements of multiple cells and materials within 3D microenvironments. These microscale multicellular organizations can produce controlled cell-cell and cell-matrix interactions in a physiologically relevant manner. The

specifications of these techniques make them highly useful for several disciplines, including tissue engineering, regenerative medicine, cancer biology, drug discovery, and developmental biology.

Thermoresponsive microwells can be utilized to study cancer dynamics in a high-throughput manner. Cancer cells, such as those originated from breast, liver, kidney, and lung, can form spheroids within microwells. Various ECM molecules, soluble factors, and drug candidates could be printed on these microtissues to screen their effects on certain dynamics of cancer, such as tumor growth, cell differentiation, and metastasis. As responsive microwells are glass-bottomed, cells will attach and form stable tissues within microwells which will not be disturbed by high-throughput manipulation. Microtissues would further be analyzed in molecular level for gene expression studies after being retrieved from the templates by using shape changing behavior of microwells. Harvested tumor tissues could also be encapsulated within biomaterials to fabricate 3D tumor models. One can utilize these microwells to culture embryonic stem cells and further form embryonic bodies to control cell differentiation into particular phenotypes. Cells attached on adhesive substrates will enable high-throughput screening of the effects of growth factors and ECM molecules on embryonic development. Temperature dependent shape changes of microwells will enable the retrieval of embryonic bodies for further molecular biology experiments. Responsive microwells may also be integrated with microfluidic channels to first form spheroids of single cell types, and then test the effects of different concentrations of drugs, chemicals, ECM molecules, and soluble factors on microtissues by generating concentration gradients. As microtissues are easily harvestable from microwells, various experiments can further be run on microtissues to analyze the effects of tested materials. Another application is that single cell types, such as from liver (hepatocytes) and pancreas (beta cells), can be cultured in responsive microwells to form functional organoids. As microwells have adhesive substrates, the effects of different biological molecules on the functions of microtissues, such as albumin for hepatocytes and insulin for beta cells, can be tested in a high-throughput fashion. These microtissues may further be recovered from the substrates and be encapsulated within 3D biomaterials to generate functional organ-specific tissues for implantation or *in vitro* use.

Some native tissues have cells oriented like stripes, such as those in cardiac and muscular tissues. Cells associated with these tissues can easily be seeded within conformally PNIPAAm coated microgrooves at ambient temperature and attach on the substrates at physiological temperature. Cells could be elongated towards the channel direction by mimicking the physiological alignment of cells in cardiac and muscle tissue microenvironment. As microgrooves are PDMS-based, they can be integrated with microfluidic devices which will enable high-throughput experimentation on tissues for drug discovery and cell biology and cell-based biosensors. If experiments are processed at physiological temperature, tissues will be stable in microchannels which will ease the flow of solutions containing molecules, such as drugs, chemicals, and ECM compositions. Immunochemistry on tissues may be formed when they are attached to the microgrooves. Microtissues can also be harvested at ambient temperature for further experiments to analyze the results of tested materials. Striped tissues may be patterned on biomaterials at room temperature or be assembled to fabricate larger tissue constructs mimicking native cell alignment, cell-cell and cell-matrix interactions. To fabricate contractile cardiac tissues in thermoresponsive microgrooves, electrodes may be inserted within channels to electrically excite cells. Both biomimetic alignment of cells throughout the channels and electrical stimulation will initiate the formation of beating cardiac organoids. These functional tissues could also be integrated with microfluidic devices for drug discovery and cardiac based bio-sensors. Functional organoids can easily be harvested and either assembled or encapsulated in 3D materials to produce functional cardiac tissue constructs for regenerative therapeutics. Application of same techniques on muscle cells will generate particular muscular tissues as well.

Living systems contain a wide variety of cells organized in a 3D matrix. Recreating the different ECM microenvironments requires the use of various materials for cell encapsulation. With the dynamic micromolding method presented in this thesis, one will be able to use different kinds of materials to encapsulate various biological entities in a spatially controlled arrangement which will lead to the development of suitable microenvironments for cell-matrix interactions and cell-matrix mechanics. Dynamic microgroove molds can be used to fabricate multicompartment stripe microgels encapsulating cardiac cells in one compartment and endothelial cells into another layer in a spatially controlled manner which may lead to a biomimetic cardiac organoid. Biomaterials could be selected with mechanical properties closed native cardiac tissue. Not only one type of materials but also two different types of materials could be sequentially patterned to

form one structure. ECM molecules, such as collagen, fibronectin, laminin, and elastin, and their compositions could be used to fabricate multicompartment stripe constructs for recapitulating native cardiac tissues. Incorporating ECM molecules into polysaccharides can initiate the spreading and elongation of cardiac cells and endothelial cells within a 3D matrix which would better mimic the vascular fiber structure of native cardiac tissue. These microtissues can be electrically stimulated to develop beating cardiac tissue fibers. One could also encapsulate conductive materials into a 3D matrix to improve electrical and mechanical properties of tissue fibers. Similar procedures could be employed to fabricate stripe muscular tissues with 3D arrangement of cells in a matrix. Cylindrical and cubic multilayered microgels encapsulating physiologically relevant two different cell types can be fabricated by using dynamic circular and square micromolds to mimic other native tissue architectures. For example, hepatocytes and endothelial cells could be arranged in different compartments of a microgel to recapitulate microarchitecture in a liver lobule. These microgels could be made of materials which are present in the liver, such as collagens, laminin, and fibronectin. Another application would be to encapsulate bone and cartilage associated cell types in biomaterials replicating the native ECM properties and cell-matrix interactions. One could also encapsulate mesenchymal stem cells and epithelial cells into different materials to study mesenchymal tissue development for different cell-matrix interactions in defined microenvironments. Various compositions of materials would be used to mimic the mechanical properties of different native tissues and their cell-matrix interactions. All of these stripe, cylindrical, and cubic multicompartment microtissues could be assembled to fabricate complex structures mimicking native tissues which would be useful for regenerative medicine. Another application for the use of dynamic micromolding is fabricating tumor models. Cancer cells, such as those associated with liver and breast cancers, and other cell types in the same microenvironment can be encapsulated in different compartments of microgels made of materials which have mechanical properties similar to ECM in tumor microenvironments. As such these microscale tumor models mimicking cell-matrix interactions of associated cancer tissues will be beneficial for drug discovery.

Multicellular complexity in physiological systems results in cell-cell interactions between various cell types which control several biological activities, such as cell fate, differentiation, and overall functions of a tissue. Recreating such complexities in defined microenvironments is possible with spatially controlled patterning of multiple cell types by using dynamic microwells.

Resulting geometrical patterns of various cell populations will be useful to study cell-cell interactions to find out cell-signaling pathways for different biological dynamics and to fabricate complex microtissues with controlled cell-cell interactions. For example, one can first pattern tumor cells associated with the cancer in different organs, such as breast, liver, kidney, and brain, and then immobilize another cell type present in tumor microenvironment, such as endothelial cells, fibroblasts, and stromal cells, around the first patterned tumor tissue to replicate the heterotypic cell-cell interactions in defined microenvironments. Such tumor microtissues could be used as models to investigate fundamental circuitry of cell-cell signaling in tumor microenvironment which controls tumor growth, invasion, and metastasis. These tumor models will also be useful for high-throughput drug discovery. As microwell substrates are adhesive to cells, tissues will be stable under mechanical stress which may occur during high-throughput manipulation. The effects of ECM molecules and soluble factors on different tumor tissues can be screened by printing associated molecules on the microtissues. It is also possible to pattern cancer associated cells in different geometries of microwells to study geometrical effect on cell-cell interactions regulating the cancer dynamics. Thus, recapitulating the complexity of tumor microenvironment in a 3D manner could replace the animal models which take a considerable cost and time. Such *in vitro* models may decrease the time spent on drug discovery.

Another area of interest to study is underlying heterotypic cell-cell interactions controlling the developmental stages of human embryo which have not been fully elucidated. Differentiated cell types associated with three germ layers (mesoderm, endoderm, and ectoderm) can be spatially patterned within defined 3D geometries to study reciprocal interactions between two different germ layers. By engineering hydrogel-based microwells, it may be possible to sequentially pattern three germ layers with a spatial organization in the same 3D microenvironment. The presented technique will enable one to study the effects of pattern geometry and the size of the overall pattern on the heterotypic interactions between different germ layers. The effects of growth factors and ECM molecules on the interactions between spatially organized germ layers could be studied in a high-throughput manner. One can also employ the spatially controlled cell-patterning technique to investigate the heterotypic interactions between mesenchymal cells and epithelial cells within defined microenvironments. Understanding the interplay between these cells will elucidate the underlying cell-signaling pathways regulating the development of tissue architectures and functions of native tissues. Thus, employing the patterning technique to study

developmental biology will be useful for understanding the embryonic development, tissue morphogenesis, and be helpful to produce particular cell types by controlling the differentiation of embryonic stem cells.

Homotypic (between parenchymal and parenchymal) and heterotypic (between parenchymal and non-parenchymal) cell-cell interactions regulate functions of organs. Such interactions and 3D tissue architecture can be replicated by patterning the associated cell types with dynamic microwells. It may also be possible to fabricate the static layers in responsive microwells to create more complex patterns. For example, hepatocytes can first be patterned in microwells, and another liver associated cell type can be spatially distributed around the first cell type, and if one wants to create a space between the first layer and second layer of tissues, during fabrication of microwells before patterning cells it may be possible to put a layer static polymer not responsive to temperature. In the future, refining the hydrogel structure of dynamic microwells and integrating static layers may allow replicating the native tissue architectures in a more elaborated manner. Biomimetic microtissues produced with the presented technique would be useful for regenerative medicine and for studying geometry dependent intricate interplay between various cell types regulating the organ-specific functions.